Center for Medical Physics and Biomedical Engineering
Medical University of Vienna

Austrian Society for Biomedical Engineering (ÖGBMT)

11th VIENNA INTERNATIONAL WORKSHOP ON FUNCTIONAL ELECTRICAL STIMULATION

in the frame of
3 - Länder - Tagung D - A - CH (BMT 2013)

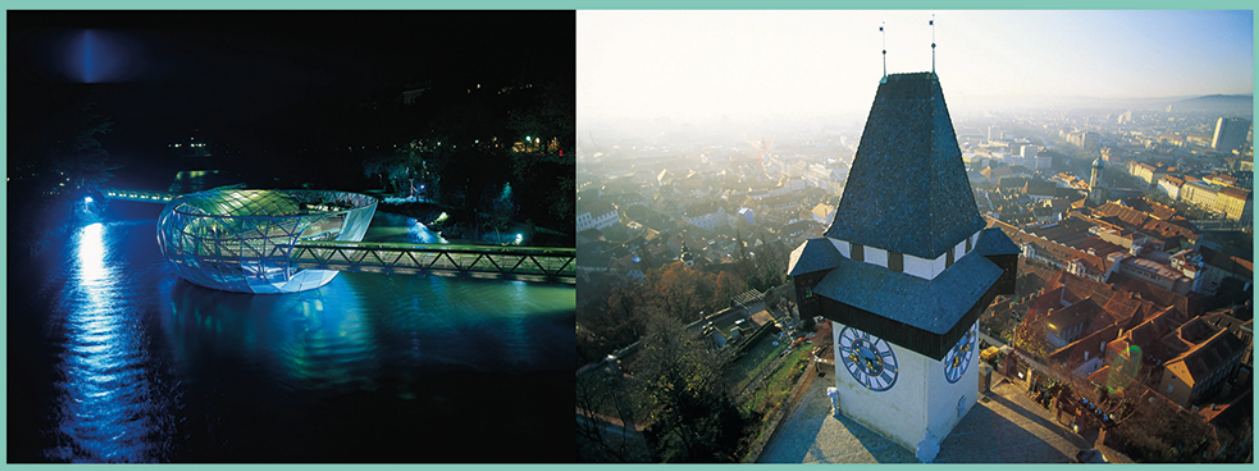

Graz, Austria September 18th - 21th, 2013

PROCEEDINGS

ISBN 978-3-900928-11-7

MED-EL

MED-EL Hörimplantatsysteme

Der Standard in Hörqualität, Benutzerfreundlichkeit und Zuverlässigkeit

BONEBRIDGE™
Knochenleitungs-Implantatsystem
Das weltweit erste aktive Knochenleitungs-Implantatsystem für Schallleitungs- und kombiniertem Hörverlust.

VIBRANT SOUNDBRIDGE®
Mittelohr-Implantatsystem
Die weltweit erfolgreichste Lösung für Innenohrschwerhörigkeit, Schallleitungs- oder kombiniertem Hörverlust.

MAESTRO®
Cochlea-Implantatsystem
Jetzt mit RONDO, dem ersten CI Single-Unit Prozessor. Bei hochgradigem bis völligem Innenohrhörverlust.

EAS®
Hörimplantatsystem
Kombinierte elektrisch-akustische Stimulation in der zweiten Generation. Die ideale Lösung bei partiellem Hörverlust.

hearLIFE

Nähere Infos im hearLIFE Care Center

hearlife.cc

MED-EL Deutschland GmbH · Moosstr. 7/2. OG · 82319 Starnberg · Tel. gebührenfrei 0800 0077030

medel.de

Proceedings

of the

11th Vienna International Workshop on Functional Electrical Stimulation

in the frame of

3-Länder-Tagung D-A-CH (BMT 2013)

Graz, Austria
September 18th-21st, 2013

Edited by

Manfred Bijak
Hermann Scharfetter
Winfried Mayr
Melitta Pichler

Published by

Center for Medical Physics and Biomedical Engineering
Medical University of Vienna, Vienna Medical School
AKH 4L
Waehringer Guertel 18-20
A-1090 Vienna
Austria

Tel.: +43-1-40400-1984
Fax: +43-1-40400-3988

http://www.fesworkshop.org
ISBN 978-3-900928-11-7

Scientific Committee

Christine AZEVEDO-COSTE
Tadej BAJD
Rik BERKELMANS
Manfred BIJAK
Humberto CERREL BAZO
Alberto CLIQUET JR.
Simon DANNER
Glen DAVIS
Simona FERRANTE
Paolo GARGIULO
Werner GIRSCH
Thordur HELGASON
Christian HOFER
Ursula HOFSTOETTER
Kenneth HUNT
Jonathan JARVIS
Roman KAMNIK
Klaus Peter KOCH
Matthias KRENN
Hermann LANMUELLER
Thomas MANDL
Johannes MARTINEK
Winfried MAYR
Karen MINASSIAN
Milos POPOVIC
Dietmar RAFOLT
Frank RATTAY
Janez ROZMAN
Ruediger RUPP
Michael RUSSOLD
Stefan SAUERMANN
Mohamad SAWAN
Thomas SCHAUER
Martin SCHÜTTLER
Thomas STIEGLITZ
Paul TAYLOR
Rune THORSEN

Table of Contents

Spinal Cord Stimulation

FES Gait

FES Control

FES and Nerve

The conducting and processing capabilities of the human lumbar cord network and "spinal brain"

Emeritus Professor Dr. Milan R. Dimitrijevic. M.D., Ph.D.

Baylor College of Medicine. Houston. TX, USA
Principal Investigator of Foundation for Movement Recovery, Oslo. Norway
Founder of "Vienna Program for Movement Recovery", Vienna, Austria
Founder of University Institute for Clinical Neurophysiology. Ljubljana, Slovenia

lepasrna@hotmail.com

The spinal cord is part of the Central Nervous System-present in all vertebrates and for nearly two centuries, extensively studied for its anatomical, physiological and biological characteristics [1]. In the lecture we shall review the present status of neurophysiology in sensorimotor processes of the human lumbar cord involved in motor control when deprived from motor control, partially deprived and fully integrated. We shall explore the hypothesis that human lumbar cord isolated from brain control can respond to external sustained electrical epidural spinal cord stimulation with variety of tonic and rhythmical activity resembling "brain at the human lumbar cord" or in other words "spinal brain". In addition, we shall address significance of the spinal brain capabilities for interpretation of complex descending input to the supplementary spinal brain in order to generate functional Movement, initiated and controlled by the main brain. We shall also discuss role of spinal brain processing function for modification of altered motor control in neurological conditions.

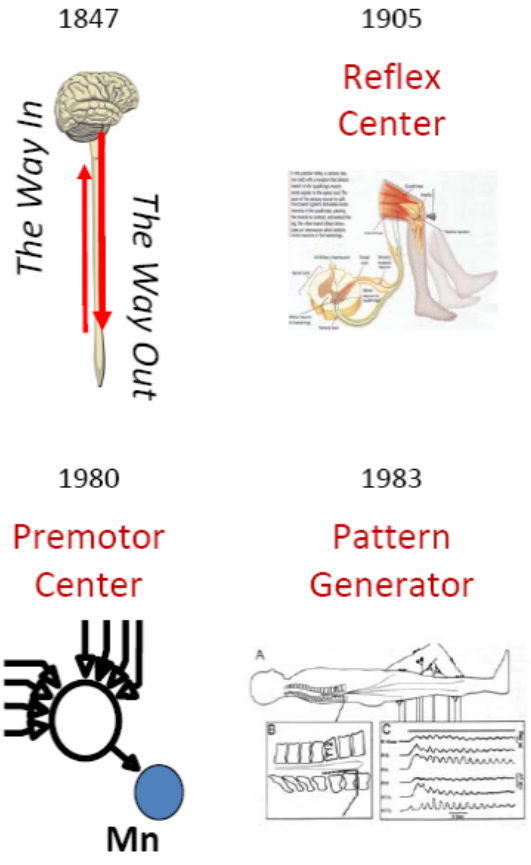

Figure 1: Concepts of spinal function

Figure 2 consist of following sketches:
1847: **The Way in and The Way out** sketch made after, Charles Bell's book published 1847 [2].
1905: Reflex center made after C. S. Sherrington's book **The Integrative Action on the Nervous System**, [3].
1980: Premotor center, made after A. Lundberg, **Multisensory control of spinal reflex pathways** [4].
1985: Pattern generator, made after S. Grillner, **Neurobiological bases of rhythmic motor acts in vertebrates** [5].

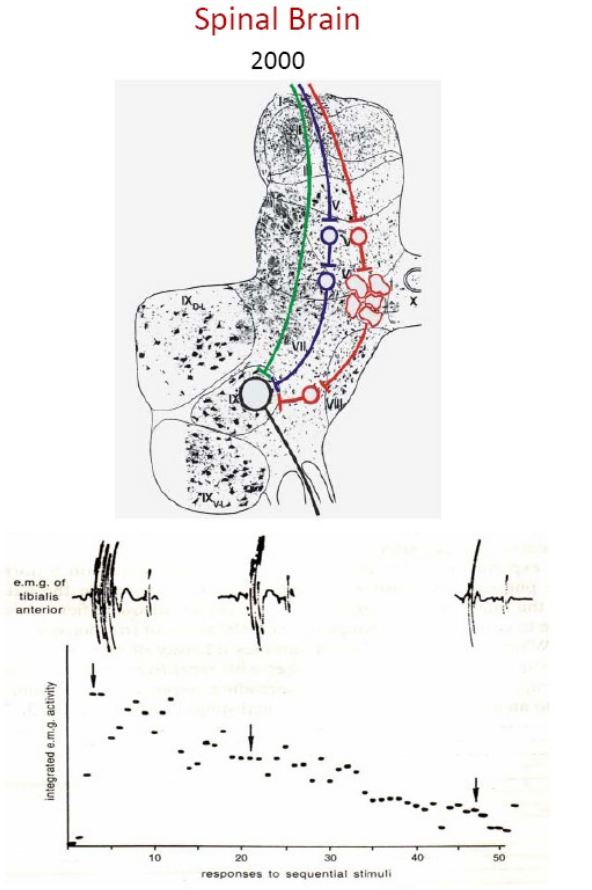

Figure 2:
Studies of repetitive lower limb withdrawal, flexor reflexes

Figure 2 relates to studies of repetitive lower limb withdrawal, flexor reflexes as shown at the bottom Figure 2 and resulting habituation of withdrawal reflex [6]. Dependence of output from the rate of spinal reflex responses and technological advancement in the epidural spinal cord stimulation of lumbar posterior structures contribute to the studies of systematic posterior roots lumbar stimulation motor responses by frequency from 0,2 to 100 Hz [7]. Sketch of Figure 2 label "Spinal Brain 2000" illustrates testing spinal reflex mono, polysynaptic and pattern responses of the lumbar cord reflex activity in humans with complete disconnection from brain motor control. These studies lead to development of the concept on spinal brain. We are using term "Spinal Brain" for lumbar network capable to interpret descending and peripheral inputs to the lumbar network and respond with the dynamic configurations of interneuron subpopulation in order to generate, while responding to afferent inputs of different parameters [in our case electrical stimuli of different strength, frequency], to different inputs or motor tasks "natural volleys" [in latter when partial or complete brain-spinal cord connectivity exist].

Conclusion 1

Regular and stochastic afferent input of spinal cord reflex can evoke different behaviour of evoked reflex activity-patterns to repetition and can modify patterns of spinal cord responses.

"The neural circuitry of the spinal cord is capable of solving some of the most complex problems in motor control. A key issue in motor control is how sensory inputs direct and inform motor output - this is the sensory-motor process. It has, for over a century, is known that the intrinsic circuitry of vertebrate spinal cord is sufficient to control many kinds of behaviourally important motor activities" [8].

Illustrations 3a, 3b, 3c, 3d summarizes our studies in human motor behaviour of lumbar cord evoked by different strengths or different frequencies of sustained electrical stimulation the large afferents of posterior lumbar roots. In all this studied subjects lumbar cord spinal reflexes have been preserved in complete absence of brain motor control by accidental spinal cord injury from cranial above lumbar cord segments.

Figure 3a is EMG recording from lower limb by surface electrodes from Quadriceps, Hamstring, Tibialis Anterior, Triceps Surae muscle groups. Multisite, epidural stimulation of lumbar posterior roots with train stimulation and stimulus strength from 3, to 5 V. Figure 3a is an illustration of motor behaviour evoked by constant 25 Hz train of stimuli and alteration of stimulus strength. Figure 3c illustrates the set up for EMG recording and spinal cord stimulation. Figures 3a and 3c show data from [7], Figure 3b rhythmical and tonic EMG activity of paralyzed lower limbs induced by spinal cord stimulation (SCS). Applying continuous tonic spinal cord stimulation to a single anatomical site by using constant stimulus strength and changing frequency to 31 and 21 Hz, induces rhythmical responses, and only by changing stimulation frequency to 16 and 10 Hz, rhythmical muscle activity turns to a tonic one. Thus motor behaviour can be converted from rhythmical to tonic EMG activity by changing stimulus frequency as single control parameter. Figure 3d shows goniometer traces covering the first movements induced by SCS at different frequencies [8].

Conclusion 2

Alteration of frequency of spinal cord stimulation within narrow RANGE and constant strength CAN EVOKE TWO STRIKINGLY DIFFERENT functional movement modalities: tonic and rhythmical activity.

In addition to dependence on a variety of outputs in the lumbar cord to a variety of parameters of stimuli used for external control and within range of frequency from 0.2-30.0 Hz responding with locked stimulus response there are also other factors which can modify elicited spinal reflex response. This is state-dependent modulation of spinal reflexes (see Figure 4). State dependent modulation of transmission through spinal reflex pathways can be used to reveal details about the organization of spinal interneuron into functional circuits [10].

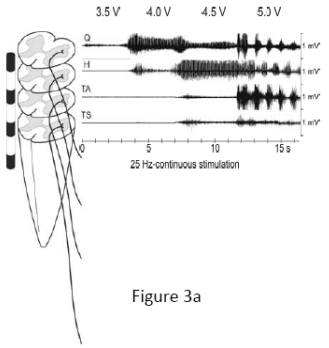

Figure 3a

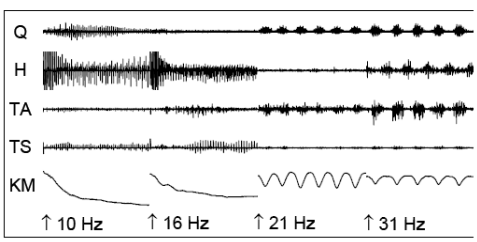

Figure 3b

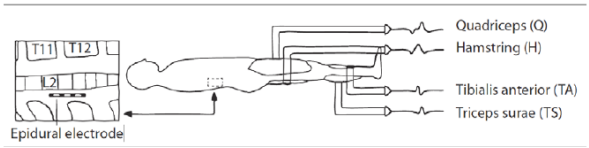

Figure 3c

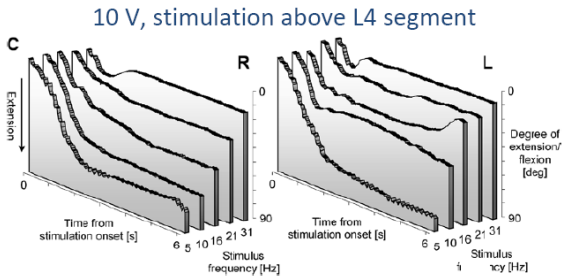

Figure 3d

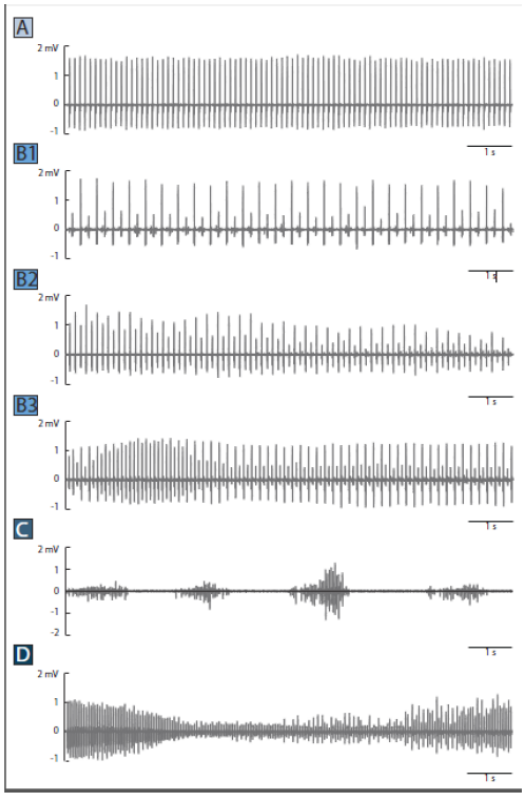

Figure 4

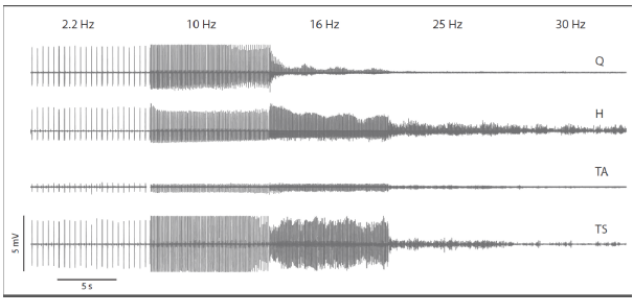

Figure 5

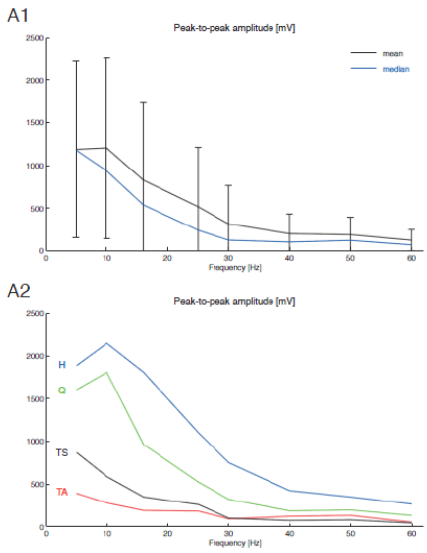

Figure 6

Figure 4 shows 4 different categories of the dynamic of peak to peak amplitude of stimulus locked response. A-shows constant amplitude responses in quadriceps with 10 Hz stimulation . B1-B3, are recording with alternating response amplitude , the two amplitudes can be relatively constant. C-shows rhythmical activity in tibial anterior at 25 Hz. D-illustrate a recording where the amplitude change slowly over time (dynamic, 25 Hz quadriceps).

Figure 5 shows EMG recordings of SCS at different frequencies and constant intensity (common threshold) from: Q-quadriceps, H-hamstrings, TA-tibial anterior, TS-triceps surae. Our hypothesis is that dynamics of this stimulus-time locked responses should revel information about the configuration of the lumbar spinal cord network.

Figure 6-A1 documents a monotonic decrease of peak-to-peak amplitudes with increasing stimulation frequency, in Figure 6-A2 the different muscle groups split up and reveal different features of the thigh and leg muscle groups.

Conclusion 3

There are stimulus locked responses with additional state-depend modulation. Both of them can contribute to exploration of organization of spinal interneuron. These two factors are suggesting further sophistication of external control of afferents. Different lower limbs proximal and distal muscle groups do not respond same on same externally controlled input.

This extended abstract reviews of sensory-motor processes of the human lumbar cord deprived of brain motor control demonstrate that is possible with external control of afferents elicit functional movement in paralyzed lower limbs. Moreover, we can expect further development from tool development for patho-physiological studies of spinal cord injury and as well by substituting, enhancing with external control of afferents completely or partially lost supraspinal, brain, motor control. This is shown in below Figure 7 and Figure 8.

Figure 7 compares intact and injured spinal cord in macro and micro anatomy and sketches conducting neurophysiology with listing cellular therapies under development for cure of defect (neurobiological efforts to cure paralysis).

Figure 8 illustrates Biomedical Engineering possibilities which are coming from neurophysiological studies of motor

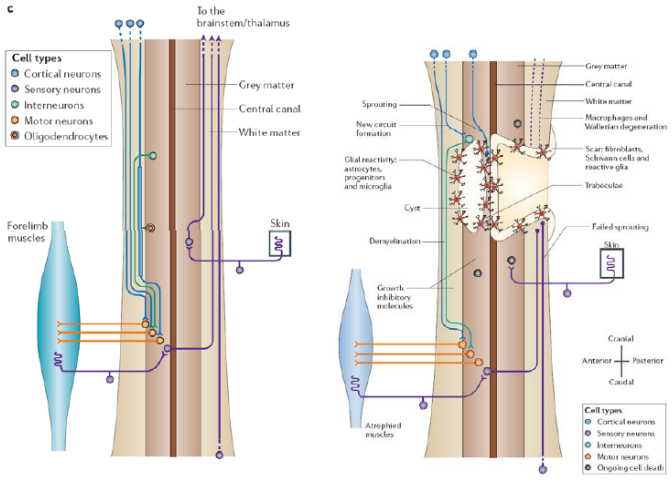

Figure 7

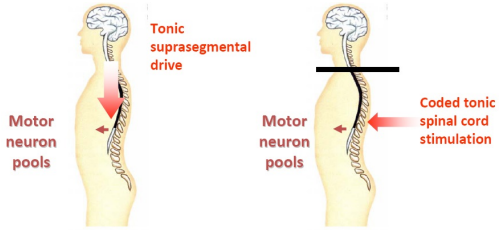

Figure 8

control in humans by recruiting integrating residual non-injured motor structures by adaptation technological generators with processing functions of the Central Nervous System motor structures.

Ultimately both approaches should be part of treatment program since external control of afferents without neurobiological background will have limited option for restorative procedures. Moreover, neurobiology without functional neurocontrol also will be extremely limited in restoration procedures. Thus structures and functions are essential, but in the same time we should not neglect when we do have structure, residual and not injured, then shall apply principles of human neurosciences of motor control.

Shown measurements of processing capabilities of human lumbar cord and finding that profile of spinal cord input is setting up configuration of subpopulation of interneurons and their heterogeneity Figures 3a, 3b, 3c, 3d, 4 and 5, suggest that we can advanced knowledge of network configuration by computational neurosciences, modelling of neuronal system studies and design of devices for interaction with spinal cord network. These hybrid approach of technical and biological sciences support missing developmental genetical properties in today biological approaches of implanted tissue as shown in Figure7.

Let us finish this extended abstract by acknowledging two large, recent research projects. The first is named **The Brain Initiative** and promises new tools for brain research that will become available for next generations. The second project is **The Blue Brain Project** whose goal is to simulate and record synaptic activity. From both, we expect to advance our knowledge about the contribution of sub-cellular, cellular and neuronal circuits to the configuration of interneuron subpopulation and their interaction. Presenting model of human lumbar spinal brain it is in a way simplified model of large brain capable to respond to different profiles of input with variety of motor pattern activities. Thus by studying human spinal brain motor behaviour it is possibility to learn orders and variability in interneuronal microcircuits function pertinent for understanding of the human brain behaviour of

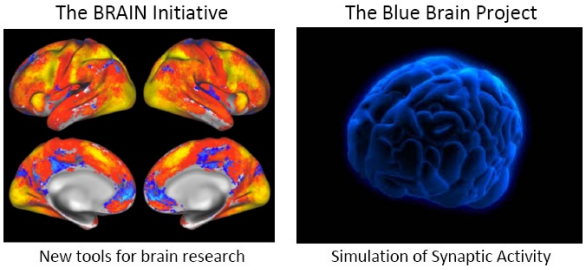

Figure 9

variety of vast numbers of neurons dynamic interaction of the subpopulations.

This lecture can be example how it is possible in humans to collect data from large population of lumbar networks of patients with chronic spinal cord injury during their treatment of augmentation of lumbar motor control by spinal cord stimulation. Analysis of data with defined method clinical and research design provides significant new insight to interactions within network of central nervous system while generating motor behaviour. In another words all our horizons are helped with all the collective research occurring today as we continue to search at the source by Brain Initiative, by Computer analyses of synaptic activity of Blue Brain Project or by neurophysiological analysis of human lumbar processor under external afferent control.

Acknowledgement

This report on human motor control and role of "spinal brain" in interpretation of peripheral and central inputs to the lumbar cord is result of joint effort of researchers of the Vienna Program for Movement Recovery. Many thanks to Drs. Winfried Mayr, Frank Rattay, Karen Minassian, Bernhard Jilge, Ilse Persy, Ursula Hofstoetter, Simon Danner and Mathias Krenn.
Special for funding support to the Vienna Science and Technology Fund (WWTF), Vienna, Austria, the Wings-for-Life Spinal Cord Research Foundation (WfL), Salzburg, Austria and the Foundation for Movement Recovery, Oslo, Norway.

Bibliography

[1] Robert E. Burke, *Spinal cord*, Scolarpedia. 2006.
[2] Charles Bell, 1847, Reprinted book/1847 by Futura Publishing Company, Mount Kisco. New York 1974
[3] C. S. Sherrington, *The Integrative Action on the Nervous System*, New Haven, 1906
[4] Lundberg A.: Multisensory control of spinal reflex pathways, *Progress in Brain Research*, Vol. 50, pp: 11-28. 1979.
[5] Grillner, S: Neurobiological bases of rhythmic motor acts in vertebrates, *Science*. 228, pp. 143-149, 1985.
[6] Dimitrijevic, MR, et al: Habituation :Effect of regular and stochastic stimulation, *J. Neurol Neurosurg Psychiatry* 35. 234-242, 1972.
[7] Dimitrijevic, MR, et al: Evidence for Spinal Central Pattern Generator in Humans, *Annals of the New York Academy of Sciences*, Vol. 860, pp 360-376, 1998.
[8] Poppele, R and Bosco, G: Sophisticated spinal contributions to motor control, *Trends in Neurosciences*, Vol.26 (5), May 2003
[9] Jilge, B, et al: Initiating extension of the lower limbs in subjects with complete spinal cord injury by epidural lumbar cord stimulation, *Exp Brain Res*, 154, pp. 308-326, 2004
[10] Burke, RE: The use of state-dependent modulation of spinal reflexes as a tool to investigate the organization of spinal interneurons, *Exp Brain Res*,. 128, pp. 263-277, 1999.

First Results with a Prototype of a new Cochlear Implant Electrode featuring Shape Memory Effect

Majdani O[1], Lenarz T[1], Pawsey, N[2], Risi F[2], Sedlmayr G.[3], Rau T[1]

[1]Dept. of Otolaryngology, Hannover Medical School, Germany
[2]Cochlear Ltd., Sydney, Australia
[3]G.RAU GmbH & Co. KG, Pforzheim, Germany

Majdani.Omid@MH-Hannover.DE

Abstract: *In Cochlear Implant surgery an electrode is being introduced into the inner ear for electronic stimulation of the cochlear nerve. Cochlear nerve is positioned in the central axis of the inner ear (modiolus). In residual hearing preservation Cochlear Implant surgery very thin and straight electrodes are used, which get a intracochlear position far lateral. To reduce the distance between the contacts of the electrodes and the cochlear nerve and to be able to get a longer intracochlear position of the electrode, enabling the stimulation of merve nerve fibres, we developed the concept of a new electrode, which can be inserted in straight form and will move to the peri-modiolar position due to the integrated Memory Shape Inlay (Nitiniol).*

Keywords: cochlear implant, electrode, memory shape, Nitinol, residual hearing preservation

Introduction

Cochlear implants (CI) replace the function of the auditory sensory cells (hair cells) in the cochlea. For this, an electrode carrier is implanted into the cochlea for electrical stimulation. The indication range has expanded in recent years from profound deafness to moderate to severe hearing loss. These patients can hardly hear despite the best hearing aids, however with cochlear implants these patients can improve their hearing and understanding significantly.

However, these patients do not want to give up their residual hearing. The development of the electrode carrier for CIs therefore focused in recent years on structure-preserving electrodes. These are typically made much thinner in diameter than conventional electrode carrier and in a straight configuration. These electrodes typically are positioned at the lateral wall of the cochlea. Since the auditory nerve, however, extends centrally along the axis of cochlea, the transmission path for the electrical stimuli at the interface between electrode contact and auditory nerve spreads when the electrode is positioned at the lateral wall. This can in principle caused various problems, such as degradation of the frequency selectivity and results in increased power requirements. Another disadvantage of the lateral wall positioning of the straight electrodes is the shorter insertion depth in the cochlea compared to perimodiolar positioned electrodes due to the spiral shape of the cochlea. So far, however, no electrode carrier has been developed, which combines structure preservation and perimodiolar positioning of the electrode. The aim of this project was therefore to modify an existing and clinically established electrode for residual hearing preservation (Hybrid L electrode, Cochlear Ltd., Sydney, Australia) such that it keeps its preservation characteristics and will end up in a perimodiolar position. For this purpose the suitability of an inlay made of Nitinol, a shape memory material, was examined. Insertion of the straight electrode into the cochlea followed by recovery of a pre-curved shape by activation of the shape memory effect at body temperature would result in the contacts being closer to the cochlear nerve in the modiolus and the insertion depth being extended. Therefore potentially more nerve fibers of the auditory nerve could be stimulated.

Methods

As a starting point for the CAD-based design of the new CI electrode the geometry of an avarage human cochlear (Cochlear Ltd.) was used. Through the transparent plastic model a simple evaluation of the functionality of the prototypes produced could be visualized. The geometry of the nitinol wires has therefore been designed to direct the electrode into a perimodiolar position at the end of the insertion process.

First Nitinol wires with different diameters were provided by the company G.RAU GmbH & Co. KG (Pforzheim). Experiments have determined that a 0.12 mm Nitinol-wires could develop sufficient forces to achieve the final perimodiolar postion after activation of the shape memory effect. As the shape of the Hybrid L electrode is tapered from 0.4mm to 0.25mm toward the tip of the electrode, a tapered shape of the Nitinol-inlay has been chosen form 0.12mm to 0.08 mm over a length of the last 5mm. The proposed transformation temperature for the memory shape behavior was defined at 37 ° C in the finished part. As not only the Nitinol wire, but also the whole electrode with its components (e.g. silicone carrier and Platinum-Iridum wires and contacts) need to be shaped, the degree of shape recovery and transformation temperature for the electrode differed from the data for the Nitinol wire only. An iterative process for finding the best shape and alloy for the Nitinol Inlay has been followed.

For the correct cutting of the shape memory wires, a laser-cutting method was used to prevent deformation of the cutting area.

In order not to increase the overall rigidity of the electrode carrier by the additional Nitinol inlay, and retain the structure preservation characteristics of the electrode, the stiffener of the conventional Hybrid L electrode has been removed and replaced by the shape memory inlay.

Experiments were performed in a plastic cochlear model immersed in a temperature-controlled water bath. The temperature of the water bath was varied between 20°C and 45°C. A USB camera was used for documentation.

Results

An initial version of the Nitinol inlay showed a good ability of the electrode to recover its curved shape above the transformation temperature. However in this experimental setup the electrodes using Nitinol inlays with transformation temperature at 37° began curling before insertion. Cooling the electrodes with ice spray beforehand did not prevent this issue. Therefore it could be concluded that a higher transition temperature was necessary to prevent premature curling (Image 1).

With the next iteration of inlay with an elevated transformation temperature, this premature curling effect did not occur. This series of prototypes was able to be straightened effectively at room temperature, thus providing a sufficient starting point for insertion. However, the thermal characterization demonstrated an incomplete recovery of the electrode curved shape at 37° C. Only when heated up to approximately 43°C could full curvature be achieved.

Discussion

By replacing the stiffener of a conventional Hybrid L electrode with a shape memory actuator made of Nitinol, a perimodiolar position within the cochlea could be achieved with an initially straight electrode. More experimentation is required to optimize the material parameters. For clinical use, the influence of additional heat sources in surgical field (e.g. surgical lighting) is currently being investigated.

Acknowledgement

What the project funded by the German Federal Ministry of Education and Research. The project number is 0832 01EZ And. responsibility for the contents of this publication lies with the authors.

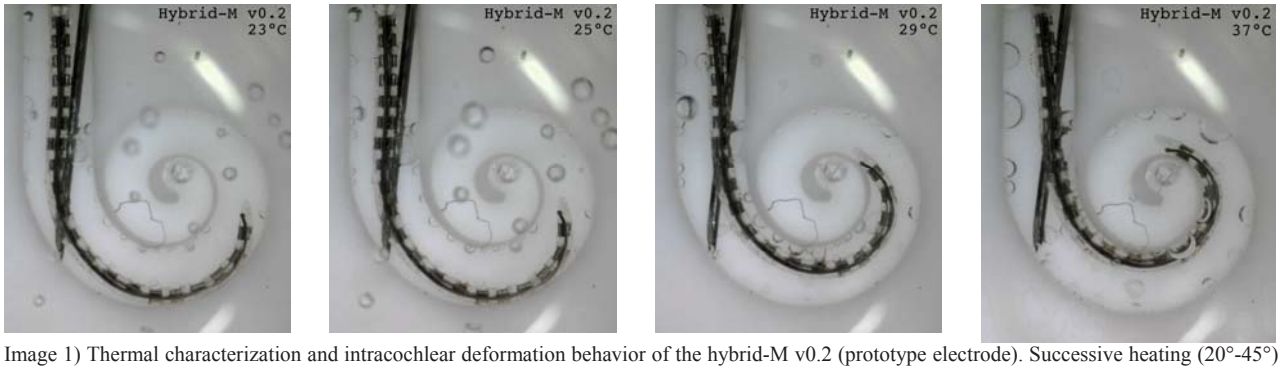

Image 1) Thermal characterization and intracochlear deformation behavior of the hybrid-M v0.2 (prototype electrode). Successive heating (20°-45°) was applied in a water bath. A substantial curvature at the tip is visible at 23 ° C. However, the desired intracochlear movement of the electrode from the outer wall to the inner wall has been reached at 37°C. In addition to the positioning of the electrode in close proximity to the nerve cells in the central axis (modiolus) of the cochlea, the insertion depth is increased as a side effect by the activation of the shape memory effect.

Laser-structured ceramic adapters for reliable assembly of flexible thin-film electrodes

E. Fiedler[1,2], J.S. Ordonez[1,2], T. Stieglitz[1,2]

[1]Laboratory for Biomedical Microtechnology, Department of Microsystems Engineering – IMTEK, University of Freiburg, Germany

[2]Bernstein Center Freiburg, University of Freiburg

fiedler@imtek.de

Abstract: *The assembly of flexible thin-film nerve electrodes, which is necessary for the connection with external data acquisition devices, often turns out to be a very time-consuming, sensitive fabrication step requiring a lot of manual skills. Here a new concept is presented, which allows a reliable, robust connection of commercial Nano Omnetics connectors to thin-film nerve electrodes. A laser-structured ceramic-adapter was fabricated, to which a polyimide-based nerve electrode could easily be soldered. Despite relieving the pressure of the connector pads of the thin-film electrode, the ceramic-substrate offers the further advantage that it is adjustable to individual electrode designs. However the technology is not restricted to the application and generally can be applied for electrical connection of thin-film devices.*

Keywords: *ceramic-adapter, laser-structuring, assembly, thin-film electrode*

Introduction

In neurosciences, flexible thin-film nerve electrodes are used for recording nerve signals as well as for stimulating the neurons. The devices are not always totally implanted but sometimes get transcutaneously connected to an external acquisition data system. The assembly of connectors to the miniaturized nerve electrodes is always a critical fabrication step. On the one hand the electrodes often show high pin densities, which require precise soldering of small connectors to the pads, and on the other hand a robust connection between the connectors and the thin-film electrodes is necessary to avoid breakage while connecting and unplugging the electrode device to recording and stimulation equipment.

Until now, the electrical connection of polyimide-based electrodes was performed using methods like MicroFlex Interconnection [1, 2] or directly soldering the connector pins to the metal pads embedded in the polyimide substrate [3]. Both demand precise serial treatment of every single connector pin, which is very time-consuming and the miniaturization depends on operator skills.

We have optimized and parallelized the assembly technique to electrically connect polyimide-based nerve electrodes. The devices are now more robust during handling and the total interconnect width is reduced compared to previous designs.

Methods

A HTCC-substrate (High Temperature Co-fired Ceramic-substrate) was laser-structured with through-holes, whose pitches and diameters were adjusted to those of the connectors (Nano Omnetics connectors (NPD series), Omnetics Connector Corp., Minneapolis, MN, USA). The pins of the connectors were embedded in the substrate with solder, whereby a mechanical and electrical connection was generated. Grinding the ceramic ensured a flat substrate surface with isolated metal pads. The conjunction of the ceramics and the connecters formed a robust adaptor to which the polyimide-based electrode could get connected by soldering. The polyimide around the contact pads acted as good solder stop, preventing shortcuts.

Production of the ceramic adapters is based on the technology described in [4]: An Al_2O_3 tape (HTCC 44000 by ESL Europe, Reading, England) was laser-structured with a Nd:YAG-Laser (λ = 1064 nm, CAB GmbH, Karlsruhe, Germany). Two layers of the HTCC green alumina tapes (tape thickness of 200 µm) were laminated with a pressure of 27 MPa at 70°C to achieve an adequate ceramic thickness. The substrate design was created with a CAD-software. Perimeters, solder pads and through-holes were arranged in a way to match the dimensions of the Omnetics connectors. Thereby a sinter shrinkage of 16.7 % was considered. Laser structuring was performed using different parameters for pads, through-holes and perimeters. While the perimeters and through-holes completely penetrated the Al_2O_3 tape, the pads, concentrically to the through-holes, only penetrate half of the tape, forming round gaps (see Figure 1 a).

Once the green bodies were lasered, they were sintered at 1500°C to a 96 % Al_2O_3 ceramic. Pt/Au paste (5837-G, ESL Europe) was applied with a squeegee to the substrate, filling the pad gaps. To prevent the through-holes of being filled with paste, they were exposed to vacuum. The paste was fired at 1000°C. Overlapping metallisation was removed by grinding the ceramic substrate to ensure insulation of the pad gaps. The Omnetics connectors were plugged in the through-holes (see left connector of Figure 1 b). The pins were manually trimmed to the substrates thickness and then soldered to it with solder (see right connector of Figure 1 b). The substrate was again grinded to get rid of the overlapping solder and connector pins and to obtain a flat substrate surface with isolated metal pads (Figure 1 c). The polyimide-based electrodes were fabricated like described in [5]. They were aligned to the

pads of the ceramic substrate under a light microscope. The connection of the adapter to the thin-film electrode could be performed by simply moving the solder-iron with solder over the connector pads. The polyimide thereby acted as good solder stop. For additional stabilisation of the interfaces between Omnetics connectors and substrate as well as polyimide-based electrode and substrate and to isolate the solder pins, the adapter was finally sealed with epoxy. Figure 1 d shows a completely assembled polyimide-based electrode.

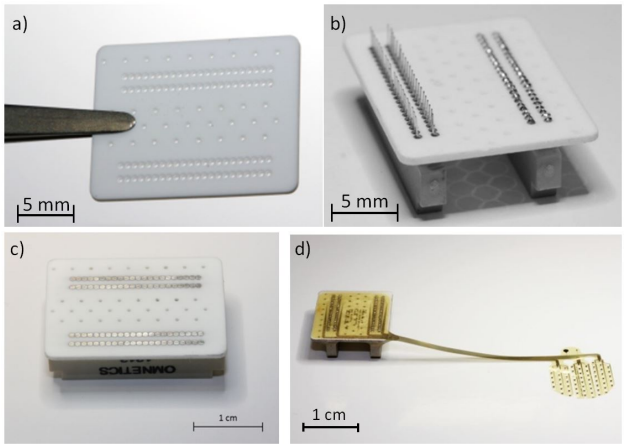

Figure 1: (a) Laser-structured and sintered Al_2O_3-substrate; (b) Omnetics connector plugged in ceramic substrate (left) and with pins trimmed and soldered to the metalized substrate (right); (c) Completed ceramic adapter with grinded surface and isolated pads; (d) Assembled polyimide-based electrode with epoxy-sealed ceramic adapter.

Results

Five adapters with a ceramic thickness of 330 µm and two Omnetics connectors with 44 pins each and pitches of 635 µm were fabricated. A polyimide-based thin-film electrode was soldered to each of the adaptors. The electrodes were characterized electrochemically to functionally prove a stable electrical connection between the Omnetics plugs and the electrode sites. Even after multiple plugging of mating plugs over a year the connection was not affected at all. Apart of the reliable electrical connection the adapter enabled good handling of the 10 µm thin flexible electrode devices.

Discussion

The ceramic adapter offers a new possibility of assembling flexible thin-film electrodes. The possibility of quasi simultaneously soldering the connector pads makes the assembly uncomplicated and time-saving.
Plugging and unplugging Omnetics connectors require relatively high forces in comparison to the small connector dimensions. The ceramic substrate, however, offers a stable connection of the flexible thin-film electrodes to the connectors. This allows testing of the electrical connection, i.e. plugging mating connectors, even before the devices are sealed with epoxy. Eventually, failed solder joints can be detected and re-soldered to increase the yield of the device.

The design of the ceramics is adjustable to very different connectors and thin-film devices. Furthermore it is possible to integrate circuit paths in the ceramics and to structure it on both sides. This makes the application field very expansible.
In near future, it is planned to realize a modular assembly of an ECoG (electrocorticography) electrode (Figure 2). Thanks to the ceramic adapter it is possible to minimize the width of the cable by stacking various polyimide-based electrodes.

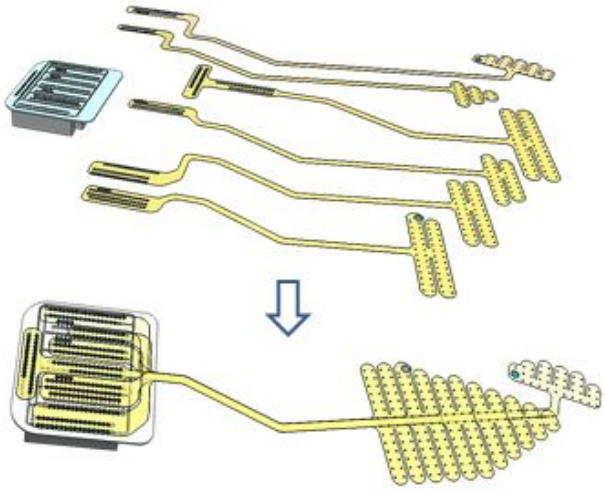

Figure 2: Sketch of a modular assembly of an ECoG electrode. The ceramic adapter allows stacking of various thin-film electrodes whereas holding the cable width very small.

Depending on the application, it is not obligatory to use HTCC-technology. LTCC-technology (Low Temperature Co-fired Ceramic-technology) might work as well and could make the fabrication of the ceramic substrates more cost- and time-saving.

Acknowledgement

This work was supported by the German Federal Ministry of Education and research (BMBF grant 01GQ0830).

Bibliography

[1] Beutel, H. et. al.: Microflex: A New Technique for Hybrid Integration for Microsystems, *Conf. Proc. IEEE Micro Electro Mechanical Systems,* pp. 306-311, 1998.
[2] Schuettler, M. et. al.: Multichannel neural cuff electrodes with integrated multiplexer circuit, *Conf. Proc. IEEE Microtechnol. Med. Biol.,* pp. 624-629, 2000.
[3] Rubehn, B. et. al.: A MEMS-based flexible multichannel ECoG-electrode array, *Journal of Neural Engineering*, vol. 6, 2009
[4] Ordonez, J. et. al.: A 232-channel retinal vision prosthesis with a miniaturized hermetic package, *Conf. Proc. IEEE Eng. Med. Biol. Soc.,* pp. 2796-2799, 2012
[5] Boretius, T. et. al.: A transverse intrafascicular multichannel electrode (TIME) to interface with the peripheral nerve, *Biosens. Bioeletron*, 26 (1), pp. 62–69, 2010

TOWARDS THE DEVELOPMENT OF IMPLANTABLE CONNECTORS WITH HIGH CONTACT NUMBER

Schuettler M[12], Huegle S[13], Ordonez JS[12], Stieglitz T[12]

[1]Laboratory for Biomedical Microtechnology, Department of Microsystem Engineering -IMTEK, University of Freiburg, Germany
[2]CorTec GmbH, Germany [3]Z-Laser GmbH, Germany

schuettler@ieee.org

Abstract: *A novel concept of fabrication electrical connectors for joining implantable electrode arrays and implantable electronic units is introduced. Although the concept potentially permits the realisation of some 10 channels per connector, a simple prototype with only 5 channels was fabricated to begin with and its electro-mechanical specifications were determined.*

Keywords: *Active implantable medical devices, connector, lead, contact, fabrication process*

Introduction

Modern active implantable devices such as spinal cord stimulator for treatment of chronic pain provide up to 32 channels for electrical stimulation (e.g. *Precision Spectra*™ by Boston Scientific). In order to ease the implantation procedure and to allow replacement of defective components of the system, reversible connectors that allow for joining electrode and implantable pulse generator (IPG) during surgery are widely used.

Today, the dominating technology for building connectors with 4..8 channels utilizes a male connector part which is located at the end section of the electrode lead and a female part which is located in the header of the IPG. The male part consists of an array of metal rings of an outer diameter very similar to the lead diameter. The female part is an alternating arrangement of a ring-shaped guided metal spring (electrical contact) and an elastomer gasket, which insulating adjacent electrical contacts against each other. The number of contacts is limited by the maximum force that must be applied during insertion of the male part. With each additional channel the friction during insertion increases caused by the additional spring and gasket. With increasing friction, the risk of kinking the lead during insertion rises. A less tight gasket would lead to reduced friction but would also compromise the electrical insulation between two adjacent contacts and result in increased cross talk at the electrodes. State of the art is an insulation resistance of ≥250 kOhm (1.96 mm centre-centre-distance of contacts) and insertion forces of ≤1.4 N per channel for 1.3 mm diameter leads [1]. Note: Connectors for implantable cardiac pacemakers (e.g. IS-4) or defibrillators (e.g. DF-4) are usually larger in diameter and contact distance, require higher insertion forces while providing a lower insulation resistance, e.g. ≥100 kOhm.

Usually, not more than 8 spring/gasket elements are used per connector. As a consequence, a 16-channel lead requires a 16 to 2x 8 adapter cable (splitter).

Future implanted devices might utilize electrode arrays with a higher channel count. Currently, there are no connector systems commercially available that can cope with 64+ electrical channels as required e.g. for the upcoming devices class of implantable brain computer interfaces (BCIs). In the study presented here, we investigate a novel connector technology with the potential of providing a channel number sufficient for BCIs.

Methods

The male part of the connector is fabricated from a 96% Al_2O_3 substrate (0.635 mm thick). Laser-milling is used to give the substrate the shape of a comb. Weld pads, integrated tracks and contact pads are deposited on the comb by screen-printing and firing of 7.5 µm thick PtAu. A 16.2 µm layer of electrically insulating overglaze is deposited by screen printing, covering the tracks. By using a thermosonic wire bonder loaded with 25 µm diameter wire, the contact pads receive a number (~15) of gold studs piling up to a height of 100 µm. A design sketch of a five-channel male connector is shown figure 1.

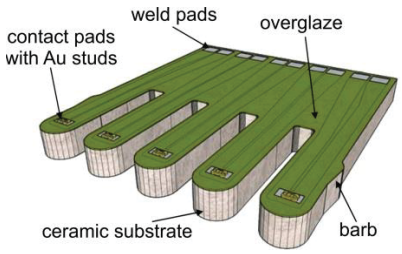

Figure 1: Sketch of 5-way connector (male part).
Note: Each contact pad is wired to two weld pads, permitting a four wire contact resistance measurement.

The female part of the connector consists of silicone rubber with integrated laser-patterned 12.5 µm thin platinum foil [2]. The silicone rubber body is the counter-part to the male comb-like connector, insulating the fingers against each other and elastically supporting the platinum contact foil. The body fabricated from three layers of laser-patterned rubber foil, attached to each other by plasma-bonding. The first layer is glued to a 0.635 mm ceramic substrate as shown in figure 2. The prototype design of a 5-way connector had a centre-centre distance between two adjacent fingers of 2.0 mm, a finger length of 4.5 mm and a finger width of 1.0 mm. The female connector had a total size of 13.5 x 12.0 1.6 mm³ (L x W x H).

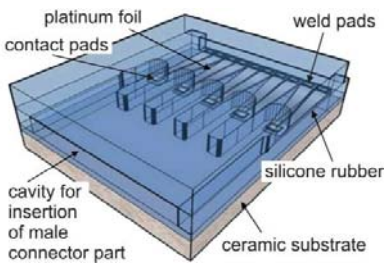

Figure **2**: Sketch of 5-way connector (female part).
Note: Each contact pad is wired to two weld pads, permitting a four wire contact resistance measurement.

A bond-pull tester was used to measure insertion and extraction forces as well as the force to break-off a single contact finger. Using 4-wire measurements, the contact resistance was determined and in combination with motorized mechanics, the durability (insertion/extraction cycles without contact breakage) was investigated. The maximum current per channel was verified using a current-controlled laboratory power supply. While the measurements described above were carried out in ambient atmosphere, the AC-insulation resistance of the connector was measured at 1 kHz in soaking tests, immersed in saline at 37°C.

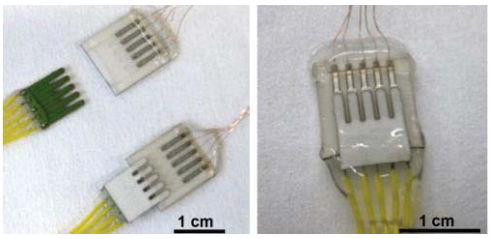

Figure **3**: Left: Open connection and insertion step (male part turned upside-down). Right: Inserted connector. Note: This prototype does not allow for 4-wire measurements.

Results

Figure 3 shows a photograph of the connector prototype with wires soldered to it. The results of the electromechanical characterisation are listed in table 1.

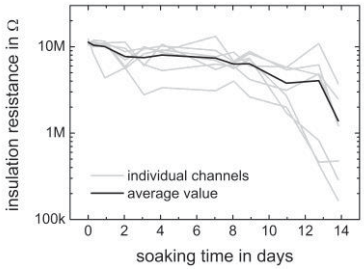

Figure **4**: Insulation resistance between two adjacent channels within a connector as function of soaking time.

The contact resistance is the resistance of the actual electrical contact (gold studs pushing against platinum foil) while the feed-through resistance is the electrical resistance between weld pads of the male and female connector parts. Practical aspects prevented us from successfully measuring the insertion force reliable, it is similar to the extraction force, though. The insulation resistance between two adjacent contacts within a connector unfortunately decreases with time of soaking in saline. Figure 4 provides an impression on the nature of the resistance change.

Table **1**: Specifications of implant connector prototype.

Specification	Value
Number of channels	5
Max current / channel	2 A*
Contact resistance	< 4.5 mΩ
Feed-through resistance	< 500 mΩ
Reliability	> 500 000 cycles
Extraction force	~ 4 N
Contact finger damage force	> 8 N
Size (L xW x H)	13.5 x 12 x 1.6 mm³
Insulation resistance	
dry	> 11 MΩ
after 1 week soaking	> 3.1 MΩ
after 2 weeks soaking	> 166 kΩ

* limited by power supply, not by connector

Discussion

Different to the state of the art, the new concept does not utilize contacts in-line with the electrode lead. For the sake of (potentially) more contacts per lead, a more bulky connector was designed which still might be suitable for common surgical techniques like subcutaneous tunnelling. The prototype of our new connector concept has the potential of being miniaturized without changing the manufacturing technology to at least half of the size in area. However, with shrinking contact finger width, the risk of accidental mechanical damage rises. Furthermore, the shorter the fingers are, the smaller the insulation resistance is. The connector system can easily be stacked, so that a 5-way connector (which takes about 1.6 mm in height) can be extended to a 25-way connector with a height of 5.6 mm (only one ceramic base is required). Such a 25-way connector will provide an insertion force of ~20 N. During insertion, we don't expect kinking to be a problem since all contacts of our design are inserted simultaneously in contrast to the flexible rope-like construction of in-line connectors that face an increasing insertion force with every contact inserted serially. We found that our design suffers from the insulation resistance decreasing over time. Further developments need to improve the seal between adjacent channels, preventing water to form undesired conductive pathways.

Bibliography

[1] Ball Seal: SYGNUS Implantable Contact System, *Brochure TMB10-APG-5C-09/10 by Ball Seal Engineering,* 2010.

[2] Schuettler, M., et al.: Fabrication of Implantable Microelectrode Arrays by Laser-Cutting of Silicone Rubber and Platinum Foil. *JNE*, No. 2, pp. 121-128, 2005.

The Influence of Flux on the Reliability of Solder-Sealed Hermetic Packages for Active Implantable Medical Devices

Kohler F.[1,2], Johannsen B.[1], Haas N.[1], Ordonez J.S.[1,2], Stieglitz T.[1,2,3], Schuettler M.[1,2]

[1] Laboratory for Biomedical Microtechnology,
Department of Microsystems Engineering – IMTEK, University of Freiburg, Freiburg, Germany,
[2] CorTec GmbH, Freiburg, Germany, [3] Bernstein Center Freiburg, Germany

kohlerf@imtek.de

Abstract: *This paper discusses the influence of fluxing materials on the properties of lead-free solder seals on screen-printed metal thick films. Pull tests revealed a strong impact on the layer adhesion if an aggressive flux is used. A milder flux was able to improve the pull test results slightly. Investigations on the hermeticity demonstrated the difficulty of hermetic packaging with SnAg solder. None of the fluxes under test allowed the manufacturing of hermetic packages in the desired range of 10^{-9}mbar l s^{-1} or lower. Consequently we came to the decision to use lead containing SnPb solder compounds until further investigations on the processing of lead-free materials are performed.*

Keywords: *hermetic packaging, lead-free soldering, RoHS, flux, active implantable medical devices*

Introduction

To ensure the functionality of complex electronic circuits for active implantable medical devices (AIMDs) in moist environments, the enclosure in hermetic packages is a challenging and mandatory part. For a recently introduced Brain-Computer-Interface (BCI) which is capable of cortical stimulation and recording such a hermetic housing was developed [1]. The package is sealed by means of manual soldering since former hermeticity investigations where promising for this method [2]. The packaging concept is realized in conventional thick-film technology, implementing solderable metallization layers and lead-free solder materials. However in comparison to the small packages in [2] the relatively large size of the BCI package introduced new problems when it came to the process of solder sealing. This paper deals with some practical issues for the choice of applicable soldering methods and materials to create highly reliable solder seals for hermetic implants.

Methods

The BCI packages consist of three main parts. A laser structured Al_2O_3 substrate with several functional thick film layers builds the base. A 2.5mm wide copper ribbon is utilized as frame whereas the lid again consists of a metalized alumina substrate. All three parts are arranged as shown in Figure 1 and assembled by manual soldering. For the sealing (Figure 1 - A) we used a tin silver solder alloy, Sn96Ag4, which is applied on the screen-printed PtAu solder frames on base and lid and on the copper ribbon.

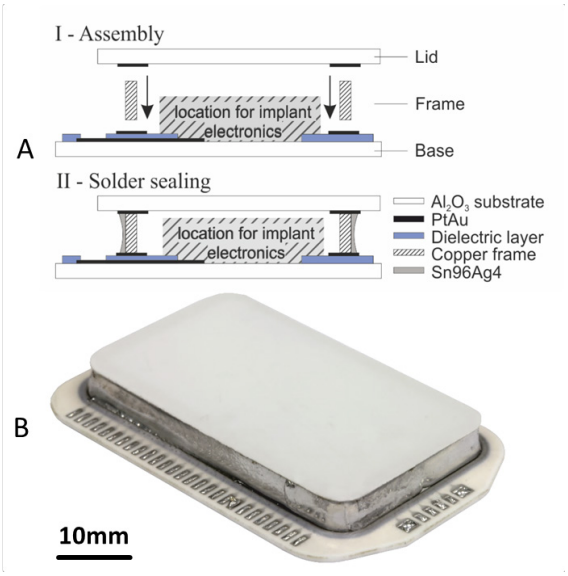

Figure 1: A) simplified sketch of the sealing procedure; B) image of sealed a hermetic BCI package.

We chose a lead-free compound to be prepared for potential future legislative changes that might prohibit the use of lead-based solder in the fabrication of AIMDs (European RoHS Directive). The RoHS Directive applies for all new electronic devices produced in the EU since 2006. However for safety critical sectors such as medical devices the Directive is not legally binding until 2014 and furthermore AIMDs are still completely left out of the scope until today [3]. In comparison to formerly popular SnPb compounds, SnAg solder possesses a higher viscosity in the liquid state and poor pad wettability. One possibility to improve wettability and flowing behavior of SnAg is the application of flux to the designated soldering areas. To quantify the influence of flux on the soldering process and on the package reliability two different investigations were performed.

Solder Adhesion / Pull Strength

The mechanical adhesion of solder on thickfilm structures was tested by pull testing, utilizing a Dage 4000 multipurpose bond tester (Nordson DAGE, Buckinghamshire, United Kingdom). On a hotplate at 120°C, pieces of tinned copper wire (ø1mm, 1cm long) were soldered to PtAu pads (2x2mm², 7.5µm layer thickness) screen printed on 96% Al_2O_3 substrates. The solder iron was kept at 350°C and a large solder tip was used for optimized heat transfer. The pads were treated with Kagerflux 330 (Ka-

ger Industrieprodukt GmbH, Dietzenbach, Germany) or Weller F-SW32 flux (Weller electronic, Auerbach, Germany) prior to soldering. Kagerflux 330 is very aggressive (DIN 8511: F-SW25 / EN 29454: 2.1.2.A) and strongly facilitates the solder wettability on thickfilms. The Weller flux on the other hand is less aggressive (DIN 8511: F-SW32 / EN 29454: 1.1.3.A) and less volatile at 120°C, which made it particularly suitable for this process. Since the printed PtAu paste tends to diffuse into liquid solder, the pull strength in force/pad area was recorded for soldering times ranging from 4s to 30s.

Hermeticity

Packages of the same size and screen printing layer sequence as utilized for the BCIs (Figure 1 – B) were fabricated with and without application of flux and sealed under helium atmosphere. Helium leakage rates as a measure for the hermeticity were recorded with a fine leak mass spectrometer (SmartTest HT570, Pfeiffer Vacuum Technologies, Asslar, Germany). Before that, all packages were placed in a water bath and visually inspected for bubbles to avoid false positive leakage test results caused by gross leaks.

Results

Pull Test

A prerequisite for high pull strengths and thus good solder adhesion to the thick film is an entire covering of the pad with solder. Figure 2 summarizes the measurements.

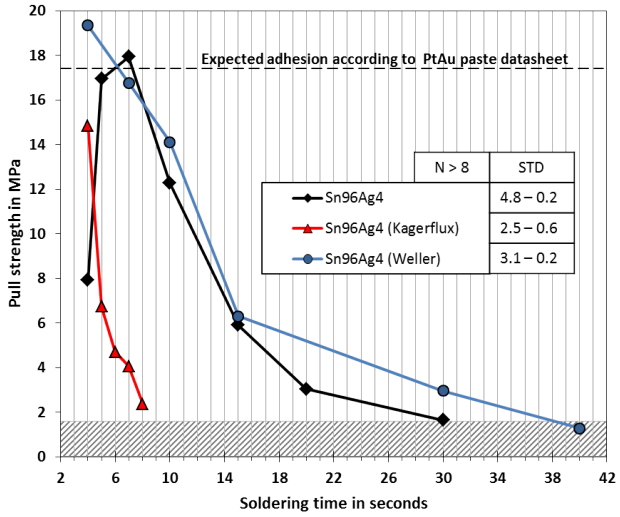

Figure 2: Pull test results for copper wires soldered to differently fluxed PtAu pads with Sn96Ag4. The shaded area marks the measuring limit of the pull tester.

Without applying flux, it took at least 7 seconds until the pad was entirely wetted and the maximum pull strength was achieved, i.e. 18 MPa. If the pad was only partly covered, the pull strength was also reduced. Longer soldering times rapidly diminished the pull strength until the detection limit was reached after 30 seconds. When flux was utilized the pads were immediately full-covered with solder. Kagerflux 330 reduced the pad adhesion directly after contact with the pad was established. Hence the full adhesion was lost in less than 8 seconds. The Weller flux enables high initial pull strengths of more than 19 MPa. Successive values develop slightly above the unfluxed measurements. Finally the detection limit was reached after 40 seconds.

Hermeticity

Without applying any flux, a hermetic sealing of the package was not possible as the value in Table 1 reveals. With Kagerflux 330 the soldering was easy due to the good wettability of the thick film structures. However the leakage rate was not satisfying for long-term applications where at least He leakage rates of three orders of magnitude higher are desired. The same holds true for the Weller flux values. Furthermore, the sealing was more difficult because of unsatisfactory solder joint formation and flowing properties.

Table 1: Leak rates of differently soldered packages.

Solder material	**He leak rate / mbar l s^{-1}**
Sn96Ag4 (no flux)	Gross leak: > 10^{-5}
Sn96Ag4 (Kagerflux)	10^{-6}
Sn96Ag4 (Weller)	5 x 10^{-6}

Discussion

This paper clearly reveals the danger of aggressive fluxes. An explanation might be the strongly reducing behavior which most likely destroys the oxide-based bond between paste and substrate. Since Kagerflux 330 severely (and continuously) impairs the thick film layer adhesion, we did not succeed in creating long-term hermetic packages when this flux was applied. On the other hand our packaging concept only worked when the PtAu frames are properly wetted with solder. Without applying any flux or even with the more gentle Weller flux this requirement cannot be fulfilled, since the lead-free Ag96Sn4 possesses poor flowing properties in the liquid state. So far, the consequence for our BCI packages to achieve hermeticity levels in the range of 10^{-9} mbar l s^{-1} and lower is one step back to SnPb solder sealing. Many SnPb solders allow omitting additional flux due to good thick film wettability. Because of the aforementioned exclusion of AIMDs from the RoHS Directive, this decision is justifiable until a lead-free solution has been found to reliably manufacture BCI packages of high hermeticity.

Bibliography

[1] M. Schuettler, F. Kohler, et al.: "Hermetic Electronic Packaging of an Implantable Brain-Machine-Interface with Transcutaneous Optical Data Communication", Proc. IEEE EMBC, pp. 3885-3889, 2012

[2] M. Schuettler, J.S. Ordonez, et al.: "Fabrication and Test of a Hermetic Miniature Implant Package with 360 Feedthroughs", Proc. IEEE EMBC, pp. 1586-1588, 2010

[3] T.S. Savage, “The Implications of RoHS on Active Implantable Medical Devices”, Proc. IEEE Reliability Physics Symposium (IRPS), pp. 3B.1.1-1.7, 2011

NEURAL ACTIVATION FOR DIFFERENT ELECTRODE DESIGNS IN SUBRETINAL IMPLANTS: A MODELING STUDY

Paul Werginz[1], Heval Benav[2], Joerg Encke[1], Eberhart Zrenner[2] and Frank Rattay[1]

[1]Institute for Analysis and Scientific Computing, Vienna University of Technology, Austria

[2]Institute for Ophthalmic Research, University Hospital Tuebingen, Germany

e0433526@student.tuwien.ac.at

Abstract: *The newest generation of retinal implants show that restoration of vision for blind patients is generally possible. However, there are still many obstacles to overcome to achieve a higher quality of artificial vision. A crucial factor in the used micro-photodiode-arrays is the shape and size of the stimulating elements. This study compares two different electrode shapes and the outcome during subretinal stimulation, respectively. Monopolar (disc) and dipolar (ring) electrodes were modeled with a finite element approach. With the calculated electric potentials we simulated the response of target cells to electric stimulation. Additionally, we concentrated on power consumption/charge limit in the modeled electrode configurations.*

Keywords: retinal implant, electric stimulation, computer simulation, compartment model, retinal bipolar cell

Introduction

Diseases like retinitis pigmentosa and age related macular degeneration affect the function of the retina. In both cases prolonged photoreceptor loss leads to partial or total blindness. If photoreceptors are damaged or not working properly the remaining network is not able to provide accurate signals to the brain. Fortunately, it seems that bipolar cells and ganglion cells are not or only little affected by these diseases. Retinal implants try to activate the remaining neurons by the means of electric stimulation using micro-electrode arrays.

Several research groups are developing retinal implants to restore vision to blind people suffering from diseases like retinitis pigmentosa and age related macular degeneration [1] [2] [3]. Two major approaches are currently in clinical trials: (i) epiretinal prostheses which are located between retina and vitreous body and (ii) subretinal implants which are positioned between retina and sclera. In this study we only examined subretinal electrode configurations which are designed to take advantage of surviving retinal circuitry.

Methods

The calculation of transmembrane voltage during extracellular stimulation requires quantitative knowledge on the extracellular voltage which is generated by the stimulating elements in a subretinal location. Therefore, we realized the computations in two separate steps. First, the examined electrode configurations (disc, ring) were positioned into a spatial volume containing the electrode carrier (2000x2000x100μm, Fig. 1A), a part of the retina (2000x2000x300μm, Fig. 1B) and a slice of the silicone tamponade (2000x2000x300μm, Fig. 1C) which replaces the vitreous body in retinal implant patients after vitrectomy [4]. The distant return electrode used in the retinal implant [5] was simulated by setting the outer boundary conditions of the retinal layer to ground potential (Fig. 1D) [6].

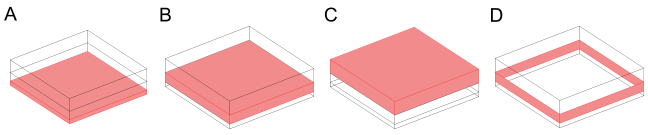

Figure 1: Volume used to calculate the extracellular potential. Edge length = 2000μm. Electrode carrier (A, height 100μm), Retinal layer (B, height 300μm), Silcone tamponade (C, height 300μm), The outer boundaries of the retinal layer are set to either a freely floating or ground potential.

Furthermore, membrane voltage over time ($\frac{dV_m}{dt}$) was calculated using a multi-compartment model with passive membrane properties [7]. Finite element calculations were performed in Comsol Multiphysics, all other calculations in MatLab.

Results

We plotted the time course of the membrane voltage for different electrode configurations and both cell types (see Fig. 2) to compare the magnitude of de- and hyperpolarization of various cell compartments. During monopolar stimulation synaptic compartments of the ON type bipolar cell were stronger depolarized at the end of the pulse than OFF center synaptic compartments. To understand why this was the case, we started to investigate morphological cell properties. Doubling and halving of the axonal compartment diameter, the synaptic end compartment diameter and variation of the soma diameter by +-20% showed almost no differences in activation. Shortening of the ON type cell to the same over-all length as the OFF type resulted in a comparable membrane depolarization of both neurons.

The surface area of the outer dipolar electrode was modeled to be equivalent to the surface area of the inner electrode ($25\mu m$ in all calculations). So a larger radius of the outer electrode corresponds to a thiner/narrower outer electrode ring. The minimum outer ring radius had to be $38\mu m$. In this configuration a stimulation with 1V over 2ms

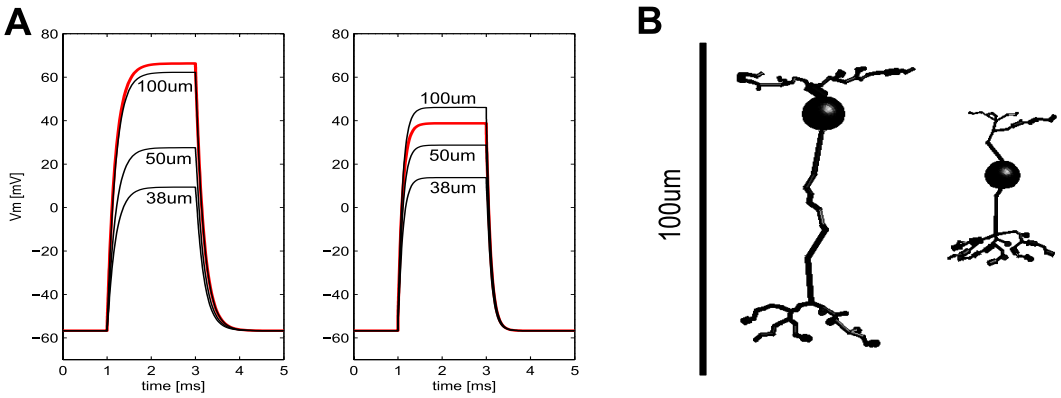

Figure 2: A: Monopolar and dipolar stimulation for ON (left) and OFF (right) bipolar cells. In both cases the bold trace (red) shows the time course of Vm for one synaptic compartment during monopolar stimulation (1V, 2ms). 38, 50 and $100\mu m$ denote the radius of the outer ring electrode in the dipolar electrode configuration. The monopolar disc electrode and the dipolar inner ring had a radius of $25\mu m$. B: Two model neurons, ON bipolar type (left) and OFF bipolar type (right).

led to a maximum depolarization of approximately 65mV (ON type) and 69mV (OFF type) above resting potential (-56.7mV). With increasing outer ring electrode diameter synaptic compartments were depolarized stronger (see Fig. 2). An outer electrode ring diameter of $100\mu m$ showed almost the same results as monopolar stimulation.

Since charge limit is a crucial parameter in functional electric stimulation we also examined the applied charge density. A stimulation with 1V results in a current density of approximately $1000A/m^2$ at the electrode surface. The corresponding charge per area is $0.2mC/cm^2$ when delivering a 2ms pulse. This is below but in the same order of magnitude as the charge limit of Platinum-Iridium electrodes ($0.4mC/cm^2$ [8]) that are commonly used in retinal implants.

Discussion

Electrode design is an important factor in retinal implants since selective stimulation of target neurons combined with reduced power consumption can improve the quality of vision and prosthetic devices. The advantage of a ring electrode configuration is that every ring on the micro-electrode array has its own ground and so can work as a small isolated electric unit. However, the dipolar configuration is consuming more power than disc electrodes to achieve the same magnitude of activation. The reason for this is that a lot of current flows directly from the inner to the outer electrode and therefore does not reach the stimulated neurons. Furthermore, this study shows no advantages in selective stimulation of ON and OFF type bipolar cells in contrast to monopolar stimulation.

New electrode configurations like pillar electrodes that 'penetrate' the stimulated tissue may be a good option for coming implant generations because the smaller distance between stimulating elements and neural tissue will lower activation thresholds and furthermore power consumption.

Bibliography

[1] J. Rizzo, J. Wyatt, J. Loewenstein, S. Kelly, and D. Shire, "Perceptual efficacy of electrical stimulation of human retina with a microelectrode array during short-term surgical trials," *Invest Ophthalmol Vis Sci*, vol. 44, pp. 5362–5369, 2003b.

[2] E. Zrenner, "Will retinal implants restore vision?," *Science*, vol. 295(5557), pp. 1022–1025, 2002.

[3] M. Abramiam, N. Lovell, J. Morley, G. Suaning, and S. Dokos, "Activation of retinal ganglion cells following epiretinal electrical stimulation with hexagonally arranged bipolar electrodes," *J Neural Eng.*, vol. 8(3), 2011.

[4] H. Sachs, T. Schanze, U. Brunner, H. Sailer, and C. Wiesenack, "Transscleral implantation and neurophysiological testing of subretinal polyimide film electrodes transscleral implantation and neurophysiological testing of subretinal polyimide film eletrodes in the domestic pig in visual prosthesis development," *J Neural Eng.*, vol. 2, pp. 57–64, 2005.

[5] E. Zrenner, K. Bartz-Schmidt, H. Benav, D. Besch, and A. Bruckmann, "Subretinal electronic chips allow blind patients to read letters and combine them to words," *Proc. Biol. Sci.*, vol. 1711, pp. 1489–1497, 2010.

[6] H. Benav, *Modelling effects of extracellular stimulation on retinal bipolar cells*. PhD thesis, Eberhard-Karls-Universitaet Tuebingen, 2012.

[7] F. Rattay, "The basic mechanism for the electric stimulation of the nervous system," *Neuroscience*, vol. 89(2), pp. 335–346, 1999.

[8] L. Hesse, T. Schanze, M. Wilms, and M. Eger, "Implantation of retina stimulation electrodes and recording of electrical stimulation responses in the visual cortex of the cat," *Graefes Archive for Clinical and Experimental Ophthalmology*, vol. 238(10), pp. 840–845, 2000.

Compliance monitoring of home based electrical stimulation training of elderly subjects

Hendling M[1], Krenn M[1], Haller MA[1], Loefler S[2], Kern H[2,3], Mayr W[1]

[1]Center for Biomedical Engineering and Physics, Medical University of Vienna, Vienna, Austria
[2] Ludwig Boltzmann Institute of Electrical Stimulation and Physical Rehabilitation, Vienna, Austria
[3] Department of Physical Medicine and Rehabilitation, Wilhelminenspital, Vienna, Austria

michaelahendling@hotmail.com

Abstract: *Home based training by using neuromuscular electrical stimulation requires sufficient monitoring to guarantee optimal training results. In a clinical study elderly subjects should follow a specific training of both anterior thighs. The schedule consists of 24 training days within 9 weeks where each training session consists of 3 series of 6 or 10 minutes. The compliance of five subjects (4 females) were evaluated based on an evaluation software programmed in Visual Studio C#. The training device is a custom-built voltage-controlled stimulator where the stimulation parameters are monitored. The average stimulation voltage of all subjects was 18,81 V with an average current of 57,33 mA. The monitoring of the training demonstrates the importance for evaluation for the study success.*
Trial Registration: ClinicalTrials.gov NCT01679977

Keywords: *evaluation software, stimulator design, pulse shape recordings*

Introduction

Aging is associated with a significant decline in neuromuscular function. Reduction of muscle mass and strength is often related to dysfunction of mobility and is a predictor of future disabilities [1]. Cross sectional studies report a decrease in muscle strength of around 40% between 25 and 80 years old subjects [1] under isometric test conditions of the knee extensors. Muscle training can dramatically improve the muscle strength, power and functional abilities of elder individuals [2][3]. There is a strong evidence that neuromuscular electrical stimulation increases muscle strength especially in periods with reduced mobilization [4].
The aim of this study was to record the intensity of home based training using electrical stimulation by monitoring compliance data.

Methods

The home based electrical stimulation training targets the anterior thigh muscles using a custom-built programmable voltage-controlled stimulator [5]. The system has an easily operable control unit and two stimulation channels. Using a universal serial bus link the stimulation parameters and the training protocol were programmed with a custom-made software. A specific stimulation training for both channels was stored on a secured digital (SD) card of the control unit. During the stimulation the subject could influence the amplitude and emergency shut-off.

The compliance monitoring was composed of the set amplitude value and the pulse voltage shape and current shape. Especially the current information, e.g. charge, is an important parameter for monitoring muscle activation [6] using voltage-controlled stimulators. Also basic information like date and number of successfully completed training series are recorded. The evaluation software is programmed in Visual Studio C# (Microsoft, Redmond, USA). It allows the analysis of a specific training series up to the whole training. The main measures of the compliance were the average stimulation voltage amplitude and current amplitude.

The compliance data of five subjects (4 females) were evaluated from a current study. Stimulation training was performed for 9 weeks, with 2 sessions per week in the first two weeks and then increased to 3 sessions per week. A training session consisted of 3 series of training separated by 5 minutes breaks. A series took 6 minutes in the first two weeks and then 10 minutes which consisted of 75 contractions of one thigh (stimulation time: 3.5 s; off time: 4 s). The stimulation pulses were rectangular, biphasic and voltage controlled with pulse width of 2x300µs and a rate of 60 pulses per second.

Results

The output voltage amplitude of the stimulation training was set over all subjects to 18,81 V with a corresponding current amplitude of 57,33 mA (Table 1). The variability over the whole training of subject A227 (Fig. 2) was +/- 12% and +/- 15% of the voltage and current, respectively. For each burst one stimulation pulse (Fig. 1-B,C) is recorded. Figure 1-A shows the manually set amplitude of each burst during one training series (6 min. training, 45 bursts).

Table 1: Average (avg.) voltage and current (standard deviation) of all training sessions for each subject.

subject	avg. voltage (V)	avg. current (mA)
A227	22,22 (3,37)	48,59 (5,96)
FTVS028	19,05 (2,97)	61,61 (6,63)
FTVS026	16,62 (3,76)	58,89 (5,02)
FTVS029	20,22 (2,47)	62,80 (5,14)
FTVS024	15,93 (2,83)	54,75 (4,74)
mean value	**18,81 (2,58)**	**57,33 (5,78)**

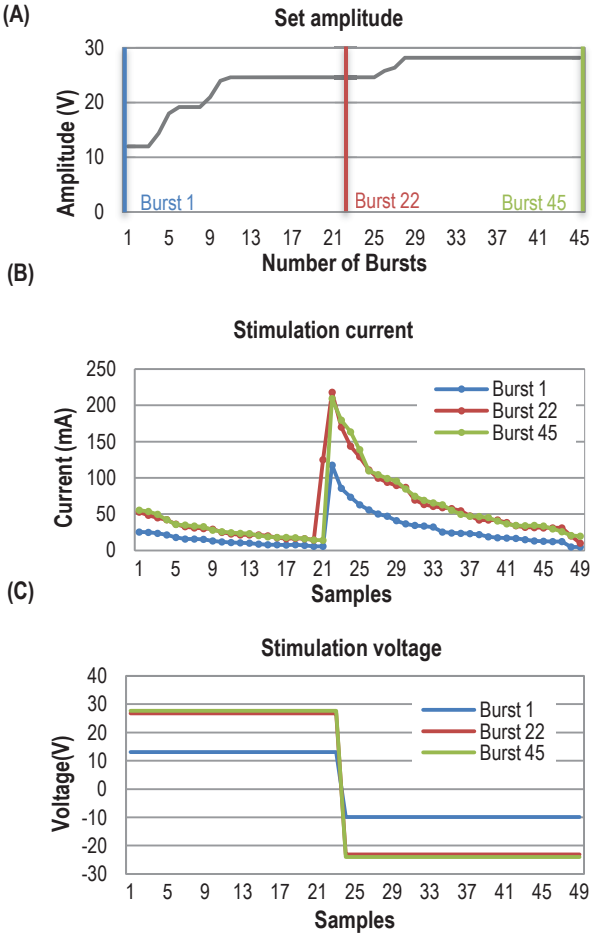

Figure 1: Stimulation current (A) and voltage (B), with a sampling rate of 83,3 kS/s. Set amplitude value (C) of one training series. Three impulses (Burst 1, Burst 22, Burst 45 of a training series) are visualized. The data refers to training series number 48 of subject A227.

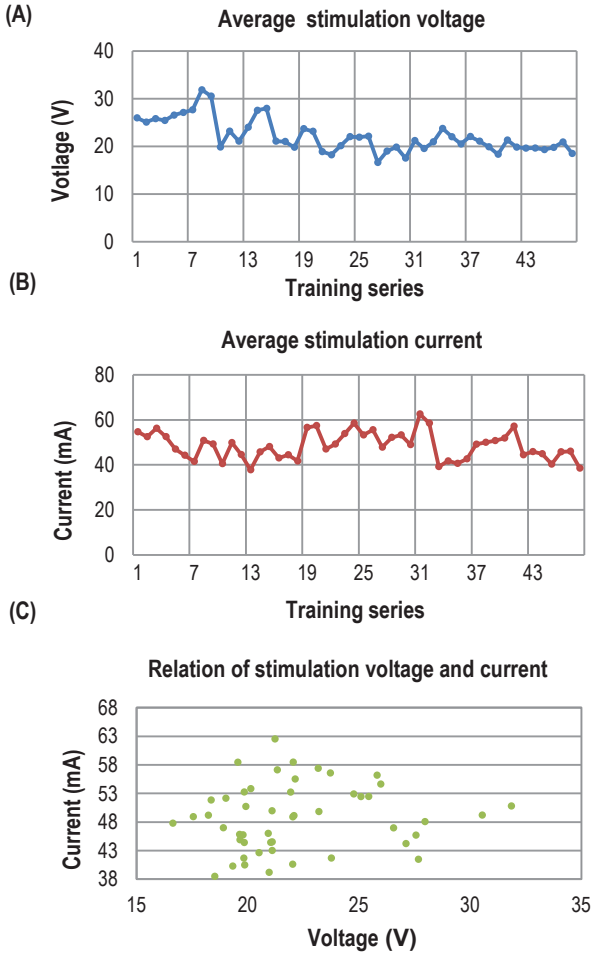

Figure 2: Average stimulation voltage amplitude (A) and current amplitude (B). The correlation between both measurements (C). The data refers to the first 48 training series (16 days) of subject A227.

Discussion

Monitoring of the training is important for evaluation of the study success, especially concerning home based training. It gives knowledge about the usage of the stimulator at home. Therefore, electrode interface failure, wrong or insufficient usage of stimulator can be detected. This information makes it easier to interpret training results.

Acknowledgment

This work was supported by the ERDF Cross Border Cooperation Programme Slovakia – Austria 2007–2013 (Interreg-IVa) for funding the project Mobilität im Alter, MOBIL, N_00033.

Bibliography

[1] Lauretani F, Russo CR, Bandinelli S et al., "Age-associated changes in skeletal muscles and their effect on mobility: an operational diagnosis of sarcopenia," *J Appl Physiol*, vol. 95, no. 5, pp. 1851-1860, 2003.

[2] Ferri A, Narici M, Grassi B et al., "Neuromuscular recovery after a strength training session in elderly people," *Eur J Appl Physiol,* vol. 97, no. 3, pp. 272-279, 2006.

[3] Melov S., Tarnopolsky MA, Beckman K et al., "Resistance Exercise Reverses Aging in Human Skeletal Muscle," *PLoS One*, vol. 2, no. 5, 2007.

[4] Bax L, Staes F, Verhagen A, Does neuromuscular electrical stimulation strengthen the quadriceps femoris? A systematic review of randomised controlled trials. *Sports medicine,* vol. 35, no. 3, pp. 191–212, 2005.

[5] Krenn M, Haller M, Bijak M, Unger E, Hofer C, Kern H, Mayr W. Safe Neuromuscular Electrical Stimulator Designed for the Elderly. *Artificial Organs* vol. 35, no. 3, pp. 253–6, 2011.

[6] Chen CF, Chen WS, Chou LW, Chang YJ, Chen SC, Kuo TS, Lai JS, Pulse energy as a reliable reference for twitch forces induced by transcutaneous neuromuscular electrical stimulation. *IEEE Transactions on neural systems and rehabilitation engineering*, vol. 20, no. 4, pp. 574–83, 2012.

Using acceleration sensors to quantify symptoms during deep brain stimulation surgery.

Shah A.[1], Coste J.[2], Schkommodau E.[1], Lemaire J.J.[2], Hemm-Ode S.[1]

[1]Institute for Medical and Analytical Technologies, University of Applied Sciences and Arts Northwestern Switzerland, Switzerland

[2]Centre Hospitalier Universitaire de Clermont-Ferrand, Image-Guided Clinical Neurosciences and Connectomics (EA 7292, IGCNC), Université d'Auvergne, France

ashesh.shah@fhnw.ch

Abstract: *The use of Deep Brain Stimulation (DBS) surgery is increasing as a treatment for movement related disorders. One of the important areas of improvement is the target selection procedure. To do so, we measured the acceleration of tremor by sensors in 6 patients during their DBS surgeries to evaluate the changes quantitatively. The post-operative data analysis revealed that acceleration measurements are very sensitive to the changes in tremor and that they can be used to identify clinically effective stimulation amplitudes. With the aim to increase objectivity in symptom evaluation, we intend to introduce real-time analysis so as to provide more information to the neurosurgeon to aid him in his target selection during the surgery.*

Keywords: *movement related disorders, acceleration measurements, tremor quantification, deep brain stimulation*

Introduction

The usage of Deep brain stimulation (DBS) of basal ganglia to treat neurological movement related disorders like Parkinson's disease (PD) and Essential Tremor (ET) has increased considerably in the recent years. However, due to incomplete understanding of the mechanism of action of DBS, optimal target definition is difficult. To overcome this, intraoperative stimulation tests are performed along the predetermined trajectories to semi-quantitatively evaluate the clinical effects on tremor while gradually increasing the stimulation parameters (voltage/current), determining the thresholds for clinical effects (subjective threshold) and side effects at each anatomical measurement position.

Various methods have been proposed to quantitatively evaluate tremor using accelerometer ([1], [2]) as well as other sensing techniques ([3], [4]), but not specifically during DBS surgery. Methods to quantitatively evaluate tremor intra-operatively ([5], [6]) using accelerometers have been proposed, but they were not made a part of the routine surgical protocol. Our aim is to measure the acceleration of the patient's wrist before, during and after the DBS surgery, to extract multiple parameters to quantify the changes in the tremor and use these parameters to aid the neurosurgeons in optimizing the final target for implanting the electrodes.

Methods

We have recorded acceleration data from 6 bilateral DBS implantations for PD (n=2) and ET (n=4), under an ongoing clinical study at the University Hospital Clermont-Ferrand, France. A 3-axis accelerometer is placed inside an in-house developed plastic case and tied to the patient's wrist (Fig. 1) to measure its acceleration during test stimulations. Acceleration data is recorded at all the test stimulation positions on all the planned trajectories. The acceleration recording is performed by connecting the accelerometer via a USB cable to a laptop using in-house developed application. The acceleration recording is started earlier than the test stimulation and continues while the stimulation amplitude is varied (Fig 2). No specific instructions are given to the neurosurgeon or the patient for the posture of the arm or movements. The data is recorded while the neurosurgeon performs his routine evaluation. The data recorded without any test stimulation is used as a baseline for comparison with data recorded during the test stimulation. The amplitudes of stimulation at which an effect is visually observed on the symptoms (subjective threshold) and at which side-effects occur (side-effect threshold) are noted in the software.

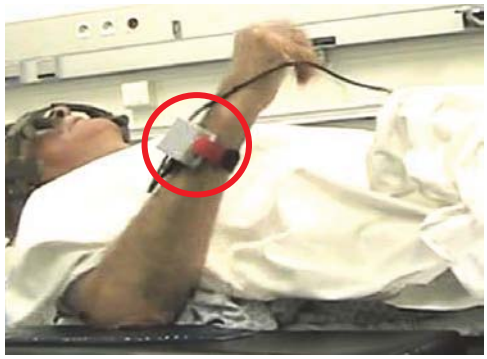

Figure 1: The plastic case containing the accelerometer tied to the patient's wrist.

The accelerometer data recorded is then post-operatively analysed to extract statistical features to quantitatively identify the changes in the symptoms. As a first step, movements other than tremor are removed (detrending) using the smoothness Priors method [7]. Then the data is low pass filtered at 10 Hz to remove the noise. From this data, statistical features (viz. standard deviation, energy, entropy, main frequency component and main frequency

amplitude) are extracted by moving a window of 2 seconds over it.
The extracted features are then normalized to the baseline value and the normalized feature set is used to find effective stimulation amplitude (acceleration threshold). Based on the normalized data, 3 different acceleration thresholds are extracted: 1) more than 75% change compared to baseline 2) more than 50% and less than 75% change compared to baseline 3) more than 25% and less than 50% change compared to baseline.
The accelerometer thresholds and the side effect thresholds are examined visually and a final implant location is decided based on them to compare with the actual final implant location.

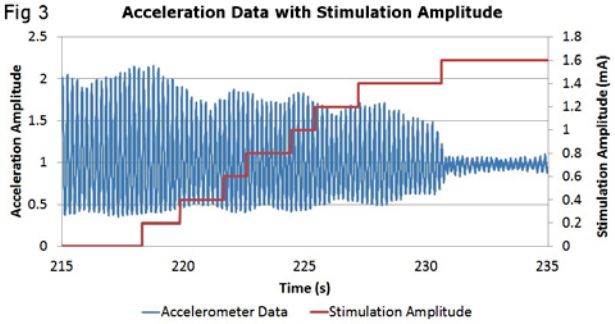

Figure 2: Graph showing acceleration data (blue) along with stimulation amplitude (red) with time.

In order to have a statistically significant comparison, we used Wilcoxon two-sided signed rank test to compare the features 1) before the subjective threshold and at the subjective threshold 2) before the acceleration threshold and at the acceleration threshold.

Results

The Wilcoxon two-sided signed rank test has identified a statistical significant change in tremor ($p<0.01$) for signal energy, standard deviation and peak frequency amplitude. The signal energy and peak frequency amplitude seem to be the most sensitive statistical features showing a higher percentage change compared to baseline. The results also say that, in most cases (>80%), the accelerometer threshold was found at a lower stimulation amplitude than the subjective threshold (Fig. 3). The final implant site decided based on the acceleration measurements were not always consistent with the ones decided subjectively during the surgery. In some cases, the choices were on different trajectories. This suggests that the use of acceleration measurements during the surgery may improve the target selection for DBS surgery.

Discussion

The present study describes a method to quantitatively evaluate tremor using statistical parameters extracted from the acceleration signal of the wrist and the significance of the results from 6 patients. Based on the results of this study we can say that the use of such quantitative methods may improve the target selection procedure for the DBS surgeries. Such quantitative methods make the surgical treatment more objective for individual patients. We also found that the addition of acceleration measurement equipment in the OR did not increase the duration of the surgery or interfere with any other procedure.

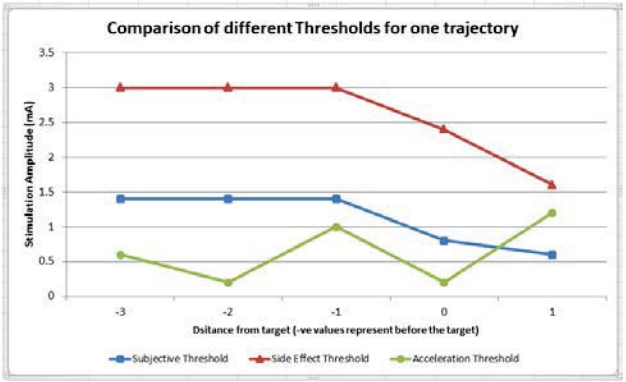

Figure 3: Comparison of different thresholds for one trajectory of a DBS patient.

The results of the study clearly suggest that acceleration measurements in the OR are feasible. One of the main factors that affect the acceleration measurements is the recording of the baseline data. It is important that during the baseline recording, the patient shows high tremor symptoms. Our next steps are to perform the data analysis in real-time during the surgery so that the quantitative information is made available to the neurosurgeon to aid in his decision. Further analysis and research is also planned with the recorded data. We intend to use the acceleration sensor to evaluate rigidity during DBS surgery as well. We intend to correlate the data with the anatomical brain structures stimulated during the surgery and other electro-physiological information. This might bring new information related to the mechanism of action of DBS.

Bibliography

[1] Keijsers, N. L. (2006). "Ambulatory motor assessment in Parkinson's disease." Mov Disord 21(1): 34-44

[2] Dunnewold, R. J. (1997). "Quantitative assessment of bradykinesia in patients with Parkinson's disease." J Neurosci Methods 74(1): 107-12

[3] Papapetropoulos, S. (2008). "Objective monitoring of tremor and bradykinesia during DBS surgery for Parkinson disease." Neurology 70(15): 1244-9

[4] Koop, M. M. (2006). "Improvement in a quantitative measure of bradykinesia after microelectrode recording in patients with Parkinson's disease during deep brain stimulation surgery." Mov Disord 21(5): 673-8

[5] Journee, H. L. (2007). "Intraoperative neurophysiological assessment of disabling symptoms in DBS surgery." Neurophysiol Clin 37(6): 467-75.

[6] Birdno, M. J. (2008). "Tremor varies as a function of the temporal regularity of deep brain stimulation." Neuroreport 19(5): 599-602

[7] Tarvainen, M.P; Ranta-aho, P.O; Karjalainen, P.A. An advanced detrending method with application to HRV analysis.

Intraoperative optical flow based tremor evaluation - a feasibility study

Hemm-Ode S[1], Wettmann P[1], Kistler B[1], Behm P[1], Schkommodau E[1], Coste J[2], Lemaire J[2], Shah A[1]

[1]Institute for Medical and Analytical Technologies, School of Life Sciences, University of Applied Sciences and Arts Northwestern Switzerland, Switzerland

[2]Centre Hospitalier Universitaire de Clermont-Ferrand, Image-Guided Clinical Neurosciences and Connectomics (EA 7292, IGCNC), Université d'Auvergne, France

Simone.hemm@fhnw.ch

Abstract: *Deep brain stimulation as treatment for movement related disorders is a common neurosurgical procedure. Nevertheless the targeting procedure can still be optimized as the clinical outcome resulting from intraoperative test stimulation is in general subjectively evaluated. The aim of the present study was to analyse the feasibility of objective tremor evaluation based on optical flow analysis in videos and to compare the results with in parallel performed acceleration measurements. The results demonstrate the feasibility but as well limitations of the applied set-up. Solutions to increase the quality in the future are proposed.*

Keywords: *optical flow, deep brain stimulation, acceleration measurements, intraoperative tremor evaluation*

Introduction

Deep brain stimulation (DBS) is a common neurosurgical procedure for relieving movement related disorders such as Parkinson's disease. DBS extends uncertainties associated with suboptimal target selection. In order to refine the target selected on the anatomical images, microelectrode recording and test stimulations are intraoperatively performed and subjectively evaluated.

The idea to objectively analyse tremor via video recording is not new. The motion between two image frames can be estimated by optical flow methods. Uhrikova has presented a tool for automatic detection and frequency measurement of tremor [1]. A comparison with accelerometer measurements showed closely related frequencies. Other authors used infrared LEDs attached to the body which are tracked by a simple CCD camera [2]. To our knowledge, no study has been published so far dealing with optical flow analysis for evaluating tremor in the operating room (OR). Consequently, the aim of the present study was to investigate the feasibility to evaluate tremor in the OR by optical flow analysis and to compare the data with in parallel recorded acceleration.

Methods

Patients: Two patients referred for bilateral DBS-implantation (1 Parkinson's Disease, 1 Essential Tremor) were included in the study after having given informed consent.

Surgical Procedure: Surgery was performed as described in [3]. After preoperative stereotactic MRI and CT acquisitions, the surgical planning was performed the day before surgery. The final implantation site was determined the day of surgery based on intraoperative microelectrode recording (MER) and test stimulation. Two trajectories were tested for each hemisphere. While the intensity of electric current used for stimulation was increased, changes in tremor amplitude were analysed by the neurosurgeon to determine the moment of and the amplitude at tremor improvement (surgeon threshold). During the evaluation, a 3-axis accelerometer (sampling rate 400Hz) synchronized with the stimulation amplitude, was fixed to the patient's wrist and the observed arm was filmed with a digital video camera (Canon LEGRIA FS200) on a tripod at a distance of approximately 2m. Resolution and recording frequency were 720x576 pixels and 25 frames/s respectively.

Data analysis: Synchronisation between video and acceleration data had to be performed manually. They were both grouped according to stimulation amplitudes. Interesting sequences were extracted from the video and software was developed to analyse the movement of the arm within a chosen region of interest (ROI) based on the Lucas-Kanade algorithm [4] implemented in Java (JavaCV using OpenCV 2.4.2): a vector field was calculated for the ROI based on the highest probability of movement of a 5x5 mask from one frame to the next (Fig. 1).

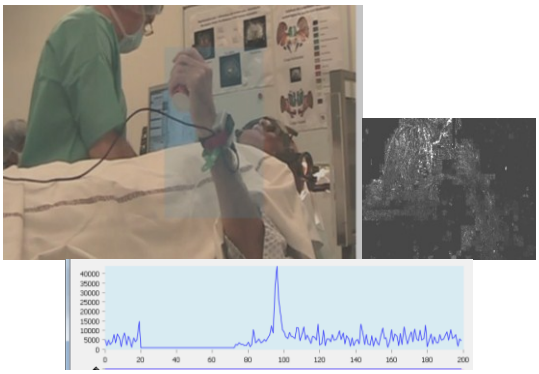

Figure 1: Top left: Scene with chosen analysis window (blue); top right: vector field between two frames; bottom: optical flow [arbitrary units] over time [s]

The absolute values of the vectors were determined. To reduce camera specific noise, data were filtered with a median filter. Statistical features (standard deviation, energy, entropy) were extracted for each test stimulation position using Matlab (MathWorks Inc., Bern, Switzer-

land) (Fig. 2). An optical flow specific threshold for significant clinical improvement was determined for each position: the percentage change of all three mathematical features compared to baseline recording without stimulation had to be of 75% or, if no such high improvement existed, of 50%. The three features were statistically compared before and after this threshold (Wilcoxon signed rank test). Their correlation with acceleration data and the neurosurgeon's observations was performed visually and statistically (Spearman rank test).

Results

Synchronisation of acceleration and optical data could be performed for both patients (+/- 0.5 - 2 seconds). Statistical parameters were calculated for all positions and stimulation amplitudes. Optical, acceleration and surgeon's thresholds were compared. In all cases, tremor decrease corresponded to a clear decrease in statistical parameters. The visual comparison of optical flow and acceleration thresholds showed nearly similar trends for all trajectories (Fig. 2).

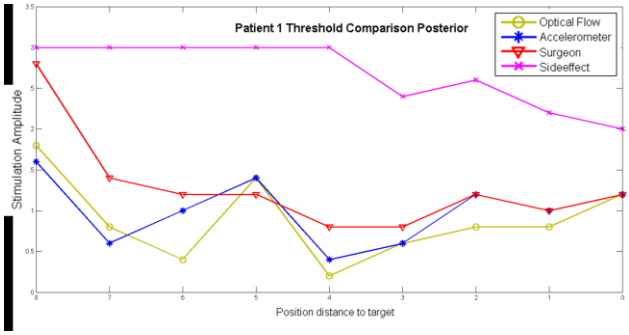

Figure 2: Threshold comparison - stimulation amplitude [mA] over the distance to the exploration endpoint [mm].

The statistical comparison between accelerometer and optical flow data for each position separately showed mostly high correlation in patient 1 and weaker correlation in patient 2. For patient 1 the optical flow thresholds were in general at or even below the surgeon's thresholds (Fig. 2). In patient 2 the optical flow threshold was in many cases higher than the surgeon's and the acceleration one.

Discussion

The aim of the present study was to analyse the feasibility to intraoperatively use video recordings for tremor analysis by comparing the results to accelerometer measurements. The accelerometer has the advantage that no line of sight problem exists but on the other hand it has to be connected by USB for use in the OR. Another weakness mentioned before [2] is that the sensors cannot satisfactorily track slow or constant speed motion where some of tremors may have significant spectral components.

The present study demonstrated the general feasibility of using video recording for tremor evaluation in the OR as a decrease in tremor is always visible as a decrease in the statistical features. Even if correlation between the two data types is not optimal, results are satisfying considering the fact that the analysis of video recording was not pre-planned and in consequence recording conditions have not been optimal. We propose different solutions for the identified limitations of the current set-up (Tab. 1).

Table 1: Solutions to identified limitations

Limitation	Possible solutions
Suboptimal camera position	Positioning closer to the patient or optimally at the ceiling
Suboptimal synchronisation	Synchronisation managed by software
Fixed window for optical flow analysis	Optical flow recording based on marker detection and tracking
Artefacts caused by the low camera resolution	HD camera

First experiments solving some of these issues have been recently performed in the lab with a high definition camera (Canon IXUS 220 HS) and based on marker tracking within the image frames. The results show promising correlation between acceleration and optical flow data (Fig. 3). The next step will be to check its intraoperative usability.

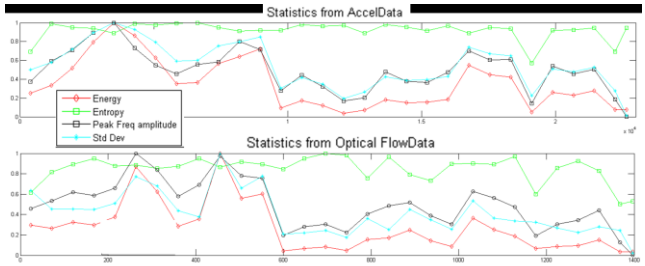

Figure 3: Comparison of optical and accelerometer raw data and extracted mathematical features over time [s]

Acknowledgement

This research has been supported by the Swiss National Science Foundation (SNSF) and the School of Life Sciences.

Bibliography

[1] Z. Uhríková, O. Sprdlík, et al.: Validation of a new tool for automatic assessment of tremor frequency from video recordings. *Journal of neuroscience methods*, vol. 198(1), pp. 110–3, 2011

[2] M. Asyali, T. Dalbasti: An image analysis based method for the quantification of tremor, vol. 2(7), pp. 631–640, 2007.

[3] J. Coste,L. Ouchchane et. al.: New electrophysiological mapping combined with MRI in parkinsonian's subthalamic region, *EJN*, vol. 29, pp. 1627–1633, 2009

[4] B. Lucas, T. Kanade: An image registration technique with an application to stereo vision. In: Proc. of the Internat. Joint Conf. on Artificial Intelligent, pp. 674–679, 1981.

EVALUATION OF SPINAL CORD RESPONSE DURING MAGNETIC STIMULATION OF THE LUMBAR AREA

Mihaela Cretu[1], Radu V. Ciupa[1], Laura Darabant[1]

[1]Technical University of Cluj-Napoca, Romania
Mihaela.Cretu@ethm.utcluj.ro

Abstract: *This paper aims in determining the necessary characteristics of a magnetic stimulator, capable to trigger stimulation of the spinal cord in a healthy subject. Our previous work showed that the magnetic stimulator used in some preliminary experiments, performed in cooperation with researchers from the Medical University of Vienna, was unable to stimulate the spinal cord, and only adjacent spinal nerves were activated during the procedure.*
Keywords: *Spinal cord, magnetic stimulation, activation function*

Introduction

Severe injuries of the spinal cord can cause total or partial loss of functions corresponding to motor tracts that are responsible for lower limbs muscle activation. The result is the loss of voluntary control of movement and the ability to stand and walk. Recent studies in this field are investigating non-invasive methods aiming to facilitate functional motor activities, including standing and stepping in paralyzed people [1], [2]. One potential technique that could directly stimulate the spinal cord is magnetic stimulation, because the electromagnetic field can pass layers of high resistivity, i.e. the vertebral bone.
Preliminary experiments [2], aimed to evaluate if transcutaneous magnetic stimulation is able to directly stimulate the spinal cord. To do so, we examined the responses elicited in the leg muscles by stimulation. The experimental results are explained by evaluating the electrical field induced in the human body during magnetic stimulation using a simplified computer model of the thorax [3].

Experimental Method

Seven subjects (aged 20-35, 5 males, 2 females) with intact nervous system participated in the study. Electromyography (EMG) signals were recorded from quadriceps (QM), hamstrings (HM), tibialis anterior (TA) and triceps surae (TS) muscles, with subjects in the prone position. Magnetic stimulation was applied to several stimulation sites, at maximum tolerable intensity. We used a Magstim Rapid² (Magstim Co) magnetic stimulator. The nervous impulses generated in this area are propagated through nervous pathways to the lower limbs, producing muscular contractions. The compound muscle action potentials (CMAP) were recorded through EMG. The established experimental protocol started by defining the coil (we used the figure of eight coil) position with respect to the vertebral column. The abbreviations we used are L for left, R for right and M for middle, followed by the angle between the spine and the handle of the stimulation coil, i.e. M90 means that the coil is placed centered above the vertebras and its handle is perpendicular to the spine [2].
The nature of muscles responses obtained experimentally was demonstrated using the double stimulus paradigm. One can notice that the CMAP response to the second stimulus has much lower amplitudes or is completely suppressed, which is usually an indication of the refractory period similar to the posterior roots muscle (PRM) reflexes (Fig. 1).

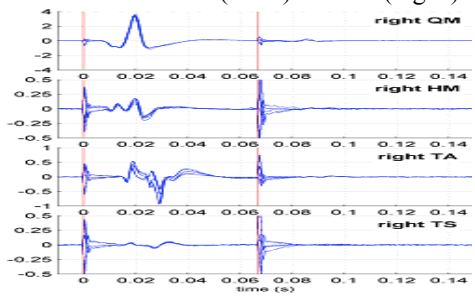

Figure 1: Leg muscles responses to a magnetic stimulus, with coil above T12 vertebra, position of the coil with respect to the spine R270

At a certain point of our investigations we concluded that these kinds of responses are not PRM reflexes and formulated the hypothesis that they could be due to direct stimulation of the cortical-spinal tract [2]. In the next section of the paper we compute the electric field induced in the spinal cord and the transmembrane potential in order to evaluate if the field is strong enough to directly stimulate the spinal cord, or only adjacent nervous structures can be activated using this technique.

Simulation Model and Results

To evaluate the response of the spinal cord to magnetic stimulation, we imagined a simplified model of the spinal cord, as a continuous cylinder, surrounded by concentric interrupted cylinders, representing the vertebras. The model is fully described in [3].
According to the electromagnetic field theory, the electric field inside the tissue can be computed by means of the vector magnetic potential and the scalar electric potential, which depends on the geometry of the tissue-air interface [4]. The electric potential, V, inside the domains (i) with different electrical properties is numerically evaluated by solving Laplace equation $\left(\Delta\phi^{(i)} = 0\right)$ inside each domain. The computations were performed using a Matlab routine, based on the Finite Difference Method. The created system of equations was solved using Gauss elimination algorithm [3]. To describe the mechanism of magnetic stimulation, we compute the response of the neuronal

structures to the applied stimulus. We model the neuronal structures in the form of a cable and the membrane response can be computed by solving the equations describing the transmembrane potential across the membrane of the cable in the presence of induced electric fields [3]. The coil used in our simultations has the same constructive parameters as the coil used in experiments: diameter equal to 70 [mm], and the total number of turns was 18 - 9 turns on each of the two leafs [2]. The inductivity of this coil is given by the manufacturer of the magnetic stimulator and is L=16.35 [μH]. To use the magnetic stimulator to 100% of its total power, the initial voltage on the stimulator's capacitor was set to U_0= 50 [V]. The maximum value of the stimulator's current derivative is $\partial I/\partial t = U_0/L$ [A/μs]. It is known that the magnetic stimulator circuit (RLC series) works in transient state (overdamped R =3 [Ω] or underdamped regime R =0.565 [Ω] and C=200 [μF]). Considering the medical application, the overdamped regime is used for single pulse magnetic stimulation, while the underdamped oscillatory regime is more suitable for repetitive stimulation.
For every coil position considered (Fig. 2a, 3a), we first computed the axial component of the **E** field induced by the magnetic stimulation inside the spinal cord (Fig. 2b).

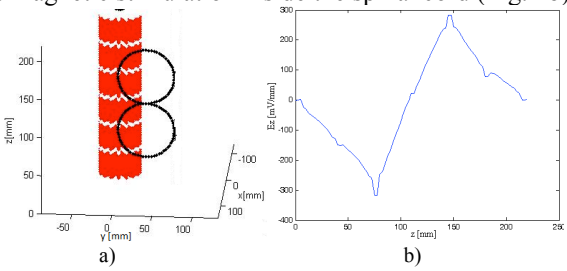

a) b)

Figure 2: a) Position of coil with respect to the spinal cord (R270); b) Axial component of the electric field induced in the spinal cord for U_0=1800 [V].

Next, we compute the axial derivative of the E_z component of the electric field, the activation function (Fig. 3b). To achieve stimulation, the nerve fiber must be located in the area where the derivative of the electric field is negative ($\frac{\partial E_z}{\partial z}$<0) [3]. Therefore, we introduce this negative minimum value in the active behavior model of the nerve fiber, and then we check if it is sufficient to produce activation of the spinal cord. With the value of 50 [V] for the initial capacitor's voltage, we could only achive stimulation of the spinal nerves, located outside the spine, and not direct stimulation of the spinal cord. Therefore, we increased the value of the initial voltage on the capacitor until we achieved stimulation of the spinal cord (an action potential is evoked). According to [5], the maximum load that can be retained by a magnetic stimulator's capacitor must be smaler than 3 [kV].
The minimum negative value for the activation function produces the activation of the spinal cord. This value is about dE_z/dz=-50 [mV/mm^2] for both positions, sufficient to achieve an action potential (Fig. 4 (a, b)).
From Fig. 4, one can see that using the appropriate values of the capacitor's initial voltage, the spinal cord is activated for both considered positions. For the overdamped state, the first magnetic stimulation of the spinal cord occurs at U_0=1750 [V] for M0, and for U_0=1800 [V] for R270. These values are lower than those needed to trigger activation for the underdamped state. If the same value of the initial voltage is considered (Fig. 4), we get a larger latency period for the underdamped regime than for the overdamped one (2.25 [ms] compared to 1.65 [ms]).

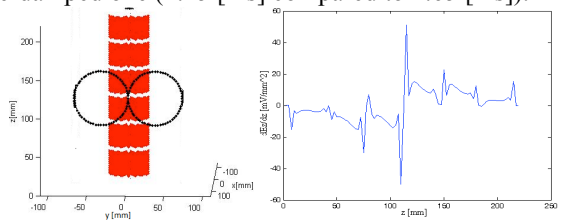

a) b)

Figure 3: a) Position of coil with respect to the spinal cord (M0); b) Activation function for U_0=1750 [V].

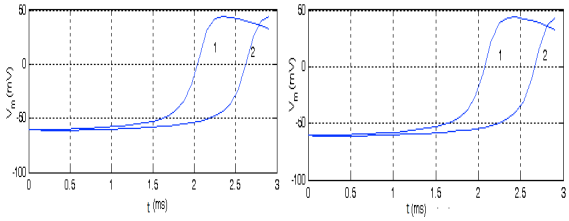

a) b)

Figure 4: Variation of the transmembrane potential in time, 1– overdamped and 2– underdamped regime. a) M0 position (U_0= 2000 [V]); b) R270 position (U_0= 2050 [V])

Conclusions

Even considering the limitations of our simplified model, the simulation results emphasize that the spinal cord could not have been directly stimulated during our experiments, but activation can be triggered by the use of larger values of the input voltage of the magnetic stimulator (this requires a more powerful magnetic stimulator). Our work suggests that to directly stimulate the spinal cord tracts, a magnetic stimulator with a maximum initial voltage of the stimulator's capacitor is required, that exceeds available ones by a manifold (1800/50). The technical feasibility and applicability of such a device will be discussed in a future paper.

Bibliography

[1] K. Minassian, I Persy et al., *Posterior root–muscle reflexes elicited by transcutaneous stimulation of the human lumbosacral cord*, Muscle & Nerve, vol. 35, pp. 327–336, 2007.

[2] L. Darabant, M. Krenn, et. al., *Double stimuli paradigms should be careful interpreted When Applying Lumbar Magnetic Stimulation*, IFMBE Proceedings, vol. 36, pp. 168–171, 2011.

[3] L. Darabant, M. Cretu, A. Darabant, *Magnetic Stimulation of the Spinal Cord: Experimental Results and Simulations*, IEEE Trans. on Magn., vol. 49, 2013.

[4] B. J. Roth and P. J. Basser, *A Model of the Stimulation of a Nerve Fiber by Electromagnetic Induction*, IEEE Trans. on Biomed. Eng, vol. 37, no. 6, pp. 650-612, 1990.

[5] J.Ruohonen, *Coil Optimization for Brain Magnetic Stimulation*, Ann. of Biomed. Eng., vol. 25, 1997.

THE EFFECT OF SPINAL CORD STIMULATION ON EPILEPTIC SEIZURES SUPPRESSION

Jianhang Jiao[1], Winnie Jensen[1], Kristian R. Harreby[1],
Line Elisabeth Lykholt[1], Sahana Ganeswarathas[1], Cristian Sevcencu[1]
[1]Health Science and Technology, Aalborg University, Denmark

jj@hst.aau.dk

Abstract: *Spinal cord stimulation (SCS) has been applied for the treatment of chronic pain for decades. Recent studies have shown that SCS may also reduce or prevent epileptic seizures, but it is not known which stimulation parameters may be effective. The objective of the present study was to investigate the effect of several SCS frequencies on seizures induced in rats by pentylenetetrazole (PTZ) infusion. The effect was evaluated by analysing electrocorticogram (ECoG) recordings. SCS using 0.3 and 0.8 mA biphasic 100/500 μs pulses delivered at five frequencies was administered in two rats in 60 s stimulation sessions. The present results indicate that 130 and 180 Hz SCS may have anti-epileptic effects and 30 Hz SCS may be pro-convulsive. Further data are needed to validate these results to establish an effective SCS pattern.*

Keywords: *spinal cord stimulation, epilepsy, seizure, pentylenetetrazole*

Introduction

Epidural spinal cord stimulation has been applied for the treatment of chronic pain for more than 40 years (1). Schlaier et al. found decreased cortical excitability during SCS in patients treated for pain (2). To the best of our knowledge, there are only two studies where SCS has been applied with the aim to investigate the effect on epileptic seizures. In one of those studies, Ozelik et al. showed that SCS (2 Hz) had an inhibitory effect on interictal spikes induced in rats (3). In the second study, Harreby et al. showed that low frequency SCS (4 Hz) was epileptogenic whereas higher frequency SCS (54 Hz) tended to reduce seizure susceptibility (4). Based on that research, Harreby et al. suggested that seizures could be inhibited by SCS if a suitable SCS pattern could be established and indicated that further experiments are necessary to establish such patterns.

The objective of the present work is to investigate the effect of SCS on seizure susceptibility when performed at five different stimulation frequencies ranging from 0 to 180 Hz.

Methods

All experimental procedures were approved by the Danish Animal Welfare Committee. Two male Sprague Dawley rats (250-350 g) were anesthetized using ketamine/xylazine (90/10 mg/kg). The rectal temperature was monitored and maintained within 37.5±1°C using an ATC1000 Animal Temperature Controller (WPI, USA).

The cervical and upper thoracic vertebrae of the animals were exposed and a custom made SCS electrode was inserted in the dorsal epidural space between C4 and C6. The rats were then placed in a stereotaxic frame and their skull was exposed through a midline incision. A hole was drilled at 2.3 mm posterior and 2.6 lateral (right) from *bregma*, and further extended using a rongeur. After removal of the dura, a stainless steel electrode was placed on the cortex to record the ECoG (pass – band filter = 1 Hz – 4 kHz).

Spike-and-wave (SW) discharges indicative of absence seizures were induced in those rats by 150 s infusion of an initial dose of 10 mg/kg/min PTZ in the femoral vein and maintained at a constant level until the end of experiments by continuous infusion of 0.21 mg/kg/min PTZ.

Before PTZ administration, the SCS current was determined by gradually increasing the pulse amplitude until muscle twitches were observed near the area of the SCS electrode location. The SCS current was set immediately below the muscle activation threshold, i.e. 0.3 mA in rat 1 and 0.8 mA in rat 2. SCS was performed using charge balanced biphasic 100/500 μs pulses delivered at 0, 30, 80, 130 and 180 Hz in consecutive 60 s stimulation sessions separated by 5 min stimulation off intervals. The mentioned stimulation frequencies were randomly set by a custom made Matlab program. Four stimulation loops comprising 5 sequences of 60 s SCS with each frequency/5 min stimulation off were performed in each rat. SCS was delivered after the rats have been brought to stable SW activity by controlled PTZ infusion as described above. To confirm stimulation of the dorsal columns, the SCS-induced antidromic activation of the sural nerve was recorded using a stainless steel hook electrode placed on this nerve. At the end of the experiments, the animals were sacrificed by an overdose of anaesthesia.

SCS was performed using a STG4008 stimulator (AD Instruments, Australia). All signals were recorded (PCI NIDAQ 6251, NI, USA) at 10 kHz using a custom made Matlab program. The ECoG energy was calculated as squared ECoG after filtering the raw signals (pass – band filter = 1 – 200 Hz). The mean ECoG energy was calculated based on a 60 s interval and used as a measure of SW activity.

Results

In both stimulated rats, 30 Hz SCS was pro-convulsive, i.e. increased the SW amplitude from 0.7 to 1.3 mV and the SW frequency from 1.2 to 1.7 Hz. In contrast, 80 Hz SCS induced mild anti-convulsive effects and 130 Hz SCS stronger anti-convulsive effects, i.e. a decrease of the SW amplitude from 0.7 to 0.3 mV and SW frequency from 1.2 to 0.5 Hz (Fig. 1). 180 Hz SCS induced mild effects in rat 1 and strong anti-convulsive effects in rat 2, i.e. almost total inhibition of SW discharges (Fig. 1).

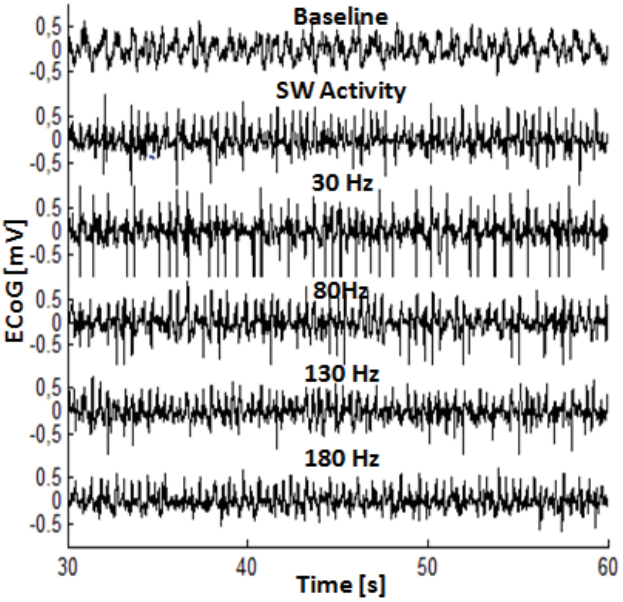

Figure 1: ECoG in response to SCS in rat 2. The baseline ECoG was recorded prior to PTZ administration.

ECoG energy analysis further supports the results mentioned above. Whereas 30 Hz SCS increased the ECoG energy, the other stimulation frequencies reduced the ECoG energy in a proportional manner and even almost to baseline in the case of 180 Hz SCS in rat 2 (Fig. 2).

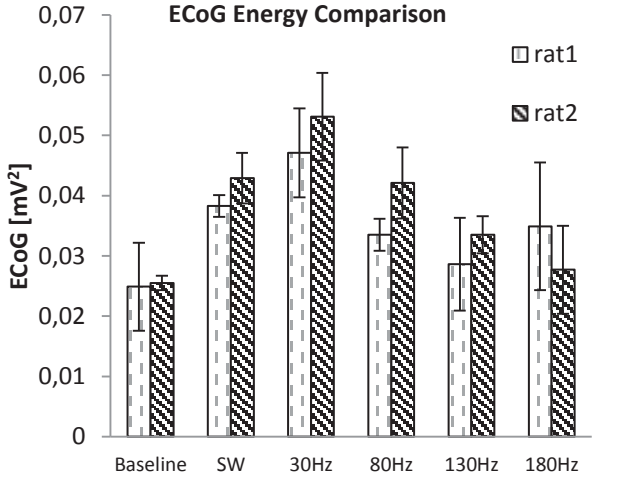

Figure 2: ECoG energy comparison in rat 1 and rat 2. Each number represents the mean ECoG energy calculated before PTZ administration (baseline), during SW activity and within each 60 s stimulation interval from the first stimulation loop.

Discussion

The present results indicate that epileptic SW discharges can be influenced by SCS and that the effects of SCS on SW seizures may depend on the stimulation parameters. In our SW rat seizure model, 130 Hz and 180 Hz SCS induced anti-convulsive effects and 30 Hz SCS worsened the SW activity. In addition, 180 Hz SCS only slightly influenced the SW activity when using 0.3 mA pulses, but inhibited the SW discharges almost totally when using 0.8 mA pulses, which may indicate a trend towards more effective seizure inhibition at higher current intensity.

These results are consistent with our previous studies, which suggested that an SCS frequency higher than 54 Hz may have anti-convulsive effects [4]. In addition, the present results are consistent with studies investigating deep brain stimulation for epilepsy which showed that high frequency (130 Hz) stimulation of the sub-thalamic nucleus suppresses absence seizures in rats [5].

Although the data available at this moment are limited and cannot support a definitive conclusion, we consider that the present results are positive and suggest that a proper combination of SCS parameters may have antiepileptic effects. Further studies are necessary to collect more data with the investigated SCS frequencies and test several combinations of stimulation parameters in order to verify this possible outcome. If successful in acute studies, the efficiency of the method and potential side effects should be explored in a chronic animal model before testing the methods in humans

Acknowledgement

We thank the staff at Aalborg Biomedical Laboratory for the generous help during our experiments.

Bibliography

[1] Shealy CN, Mortimer JT et al., *Electrical inhibition of pain by dorsal column stimulation : Preliminary clinical report*. Anest analg, 46:489,1999.

[2] Schlaier JR, Eichhammer P et al., *Effects of spinal cord stimulation on cortical excitability in patients with chronic neuropathic pain: a pilot study*. Eur J Pain; 11:863-868, 2007.

[3] Ozcelik L, Acar Fet al., *The influence of cervical spinal cord stimulation on induced epileptic discharges in rats*. Brain Res, 1135:201–205,2007.

[4] Harreby K, Sevcencu C et al, *The effect of spinal cord stimulation on seizure susceptibility in rats.* Neuromodulation, 14(2):111-6, 2010.

[5] Vercueil L, Benazzouz A et al, *High-frequency stimulation of the sub-thalamic nucleus suppresses absence seizures in the rat: comparison with neurotoxic lesions.* Epilepsy Research, 31: 39-46, 1998.

PATTERN GENERATING NETWORKS IN THE HUMAN LUMBAR SPINAL CORD: ELECTROPHYSIOLOGY AND COMPUTER MODELING

Danner SM[1,2], Rattay F[1], Hofstoetter US[2], Dimitrijevic MR[3] and Minassian K[2]

[1]Institute for Analysis and Scientific Computing, Vienna University of Technology, Vienna, Austria
[2]Center for Medical Physics and Biomedical Engineering, Medical University of Vienna, Vienna, Austria
[3]Department for Physical Medicine and Rehabilitation, Baylor College of Medicine, Houston, TX, USA

simon.danner@tuwien.ac.at

Abstract: *Epidural spinal cord stimulation can produce rhythmic motor output to the lower limbs of motor complete spinal cord injury people. The electromyographically recorded activity consists of a series of modulated stimulus time-related compound muscle action potentials (CMAPs). Here, we investigate phase dependent modification of the CMAP latencies and present a computer model that mechanistically describes putative locomotor pattern generating circuitries of the human lumbar spinal cord. Thereby we gained insight into the organization of the human spinal pattern generating networks, revealed common control characteristics with the central pattern generators for locomotion described in animal experimental work and highlighted specifities of the studied model.*

Keywords: *Locomotor pattern generators, human lumbar spinal cord, spinal cord injury, epidural spinal cord stimulation*

Introduction

The existence of locomotor pattern generating neural networks in the human lumbar spinal cord is meanwhile well accepted. Yet, little is known about their organization. Epidural stimulation over the lumbar spinal cord can produce rhythmic activities in the paralyzed lower limbs [1, 2], comprised of stimulus-triggered compound muscle action potentials (CMAPs), the posterior root-muscle (PRM) reflexes [3, 4]. Their modulation gives insight into the operation of the neural circuits in the lumbar spinal cord.
Here, we present electrophysiological analyses of CMAP modulation during rhythmical EMG activity in motor complete spinal cord injured subjects during epidural spinal cord stimulation as well as a computer model incorporating the findings of the electrophysiological study.

Methods

Electromyographic recordings of quadriceps, hamstrings, tibialis anterior and triceps surae, bilaterally in response to epidural stimulation at 2 Hz–42 Hz were analyzed in 10 individuals with motor complete posttraumatic SCI. Thrity-nine segments (duration: 10 s) of rhythmical activities found in all four-muscle groups of one lower limb were identified in 7 subjects. Phases of bursting and suppressed activities were identified. Latencies of PRM reflexes, composing the bursts, were calculated. The measurement set-up is described in figure 1.

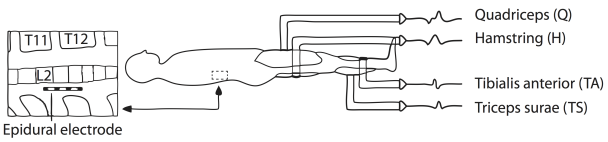

Figure 1: Measurement set-up. The electrode was located in the epidural space near the lumbar enlargement. The electrode had 4 programmable contacts that can be set as the cathode, anode or inactive. Charge balanced, pseudo-monophasic pulses of 0.21 ms width at a set frequency and intensity can be applied. Electromyographic signals were recorded from four major lower limb muscle groups.

The computer model consists of various classes of neurons with Hodgkin-Huxley-like membrane dynamics, including a pattern generating half-center model, Ia inhibitory interneurons and Renshaw cells as well as motoneurons [5, 6]. Furthermore, presynaptic inhibition of the afferents synapsing on the motoneurons and disinhibition of an additional central pathway on the flexor half-center as well as conduction delays were incorporated. All model assumptions and hypotheses followed the findings of the electrophysiological part of this study and included: i) the pattern generating networks are set into operation via large diameter afferents and with input frequencies above 20 Hz, ii) the motor output consists of stimulus-triggered responses, and iii) the flexor half-center can prolong the PRM reflex latencies. Synapses were modeled as exponential synapses. The simulation was conducted with the software Brian [7] using an exponential Euler method with a time-step of 0.1 ms.

Results

In all 10-s segments, rhythmical activities of all muscle groups had the same cycle frequency. In-between muscles, rhythmic activity occurred largely synchronous or alternating, in other words bursts were either co-active or reciprocal between any two muscle groups. PRM reflexes constituting bursts during the extension phases had monosynaptic latencies. These responses were predominantly suppressed during flexion and were replaced by delayed, oligosynaptic PRM reflexes in quadriceps, tibialis anterior and triceps surae (for an example see figure 2).

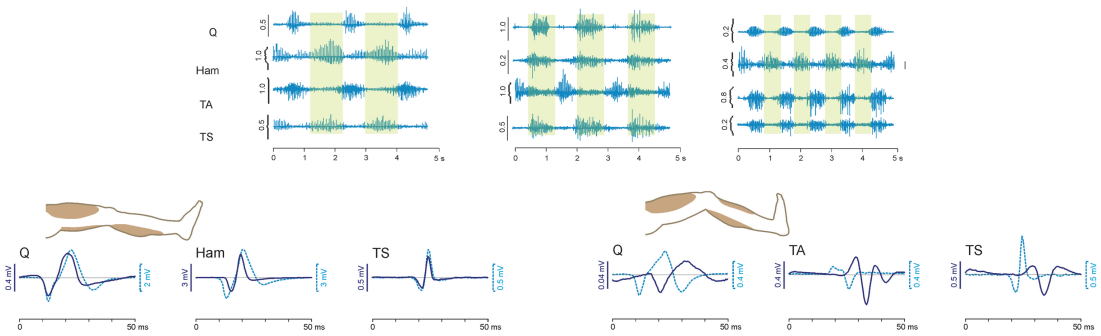

Figure 2: Three sample traces of rhythmic activity in all four muscle groups (quadriceps, Q; hamstring, Ham; tibialis anterior, TA; triceps surae, TS). Left: In the compound muscle action potentials (CMAPs; solid lines) recorded in the extension phases (TA is not active; shaded phases) have similar latencies and shapes as their unconditioned counterparts (controls, i.e. responses to a single stimulus; dotted line). Right: During flexion phase (TA is co-active; not shaded) CMAP latency is markedly increased in comparison to the unconditioned ones, whereas the CMAP shape can be similar (Q) or different (TA and TS).

The modeled pattern generating networks could be activated by pulsed stimulation. Their frequency-dependent activation was strongly related to the time constant of persistent Na channels. Rhythmic activity was produced by bursting and non-bursting neurons of the pattern generating half-centers. Stimulus-coupled responses as the only components comprising the rhythmic activity can be explained when the interneuronal network is only exerting subthreshold modifications of the motoneurons' membrane potential when activated by pulsed epidural stimulation, thus only modifying their excitability. In the extension half-center, direct afferent connections play a dominant role in exciting motorneurons as suggested by constant CMAP latencies. The existence of a mono- and a separate oligosynaptic pathway with presynaptic inhibition of the afferent fibers of the flexor half-center synapsing on the motoneurons and disinhibition of an oligosynaptic pathway explains the substitution of the short latency CMAPs by prolonged ones. Inhibition acting on the motoneurons through postsynaptic potentials would influence both pathways and would not explain their independent regulation. Again, the timed input from the afferents, here over the mono- or oligosynaptic path, are causative for the action potential generation in the motoneurons, hence producing stimulus time-related CMAPs.

Discussion

The pulsed nature of the stimulation, providing a causal relation between input and output, along with the computer simulation of the processing network revealed components of the organization of the locomotor pattern generating networks in humans. Together, the electrophysiological data and the computer model suggest a half-center organization of the human locomotor pattern generating networks in the lumbar spinal cord with asymmetric control of flexors and extensors with common rhythm generating circuits.

Acknowledgement

Vienna Science and Technology Fund (WWTF), LS11-057, and the Wings for Life Spinal Cord Research Foundation, WFL-AT-007/11.

Bibliography

[1] M. R. Dimitrijevic, Y. Gerasimenko, and M. M. Pinter, "Evidence for a spinal central pattern generator in humans," *Ann N Y Acad Sci*, vol. 860, pp. 360–376, 1998.

[2] S. Grillner, "Neuroscience. human locomotor circuits conform," *Science*, vol. 334, pp. 912–913, Nov 2011.

[3] K. Minassian, B. Jilge, F. Rattay, M. M. Pinter, H. Binder, F. Gerstenbrand, and M. R. Dimitrijevic, "Stepping-like movements in humans with complete spinal cord injury induced by epidural stimulation of the lumbar cord: electromyographic study of compound muscle action potentials," *Spinal Cord*, vol. 42, no. 7, pp. 401–416, 2004.

[4] K. Minassian, I. Persy, F. Rattay, M. R. Dimitrijevic, C. Hofer, and H. Kern, "Posterior root-muscle reflexes elicited by transcutaneous stimulation of the human lumbosacral cord," *Muscle Nerve*, vol. 35, no. 3, pp. 327–336, 2007.

[5] I. A. Rybak, N. A. Shevtsova, M. Lafreniere-Roula, and D. A. McCrea, "Modelling spinal circuitry involved in locomotor pattern generation: insights from deletions during fictive locomotion," *J Physiol*, vol. 577, no. Pt 2, pp. 617–639, 2006.

[6] V. Booth, J. Rinzel, and O. Kiehn, "Compartmental model of vertebrate motoneurons for ca2+-dependent spiking and plateau potentials under pharmacological treatment.," *J Neurophysiol*, vol. 78, pp. 3371–3385, Dec 1997.

[7] D. F. M. Goodman and R. Brette, "The brian simulator.," *Front Neurosci*, vol. 3, no. 2, pp. 192–197, 2009.

Mechanisms of rhythm generation of the human lumbar spinal cord in response to tonic stimulation without and with step-related sensory feedback

Minassian K[1], Hofstoetter US[1], Danner SM[1,2], Mayr W[1], McKay WB[3], Tansey K[3], Dimitrijevic MR[4,5]

[1]Center of Medical Physics and Biomedical Engineering, Medical University Vienna, Austria
[2]Institute of Analysis and Scientific Computing, Vienna University of Technology, Austria
[3]Hulse Spinal Cord Injury Lab, Crawford Research Institute, Shepherd Center, Atlanta, GA
[4]Deptartment of Physical Medicine and Rehabilitation, Baylor College of Medicine, USA
[5]Foundation for Movement Recovery, Norway

karen.minassian@meduniwien.ac.at

Abstract: *Independent studies have shown that the human lumbar spinal networks below a complete spinal cord injury can produce rhythmic motor outputs in response to step-related sensory feedback or sustained electrical spinal cord stimulation (SCS). Here we present our current studies applying lumbar SCS in motor-complete spinal cord injured (SCI) individuals in the supine and supported standing position, and during assisted treadmill stepping, to explore the mechanisms of spinal rhythm generation. SCS could produce rhythmic EMG activities without step-related sensory feedback; in each case, all muscles were active with a common rhythm frequency. During SCS and passive treadmill stepping, muscle activities were normally synchronized to the imposed step frequency, but activities with an independent rhythm frequency were generated as well. The results suggest rhythmic reflex actions and central spinal generation as two different causes of rhythm generation.*

Keywords: *human, sensory feedback, spinal cord injury, spinal cord stimulation, spinal rhythm generator*

Introduction

One consequence of severe injury to the long tracts of the spinal cord is the loss of voluntary control over lower limb movement, including the ability to walk. Yet, neuronal networks within the human lumbar spinal cord involved in processing of sensory feedback signals and generation of locomotion can remain largely intact caudal to such injury [1]. Independent studies have shown that these networks can be activated to generate rhythmic motor outputs to the paralyzed lower limbs by two different types of inputs: *(i)* by patterned sensory feedback from the lower limbs produced by the mechanical events during passive stepping movements on a treadmill [2], and *(ii)* by a non-patterned sustained drive provided by continuous electrical spinal cord stimulation (SCS) [3].

Little is known about the interaction of step-related sensory feedback and multi-segmental tonic neural drive at the lumbar spinal level in the generation of locomotion in humans. First studies combining manually assisted treadmill-stepping with epidural lumbar SCS in a few spinal cord injured (SCI) subjects have shown that the lumbar spinal cord can integrate the two different types of inputs to generate rhythmic activities that were not produced by either type of stimulation alone [4,5,6].

Here, we present our current studies that explore the roles of sustained inputs and step-related sensory feedback to the human lumbosacral spinal cord in the generation of rhythmic motor patterns. We applied epidural or transcutaneous lumbar SCS in motor-complete SCI individuals in the supine position (preventing hip extension and axial limb load that are otherwise critical for rhythm generation), in a supported standing positions with the lower limbs being 'mechanically immobilized' (preventing movements at hip and knee), and during assisted and body-weight supported (BWS) treadmill stepping.

Based on their characteristically different signal profiles, the hypothesis was that the non-patterned and patterned inputs to the spinal cord neural networks would reveal different mechanisms of rhythm generation.

Methods

Epidural SCS in the supine position and during assisted treadmill stepping: EMG data of 7 motor-complete SCI subjects were studied who had been previously implanted with epidural electrodes over the lumbar spinal cord for the control of lower limb spasticity [7]. 10-second segments of stable rhythmical activities generated by tonic stimulation (2–42 Hz) present in quadriceps (Q), hamstrings (Ham), tibialis anterior (TA), and triceps surae (TS) of one limb were extracted by a semiautomatic algorithm for further analysis. Two subjects were tested during passive treadmill stepping without and with 30-Hz epidural lumbar SCS. Treadmill belt speed was 0.8 km/h, 60% BWS was provided, and stepping movements were manually imposed by 2 therapists.

Transcutaneous SCS in the supported standing position and during assisted treadmill stepping: In 4 motor-complete SCI subjects, transcutaneous SCS was combined with a robotic-driven gait orthosis (DGO). Transcutaneous SCS was applied as described in [8], but here in a continuous mode at a frequency of 30-Hz and an intensity producing EMG responses in Q, Ham, TA, and TS bilaterally in a supported standing position. The DGO was used to support a standing position of the subjects, as well as to impose stepping-movements at speeds of 1.8 km/h and 2.5 km/h. BWS was set to 60%.

The studies were approved by the Ethics Committee of the City of Vienna, Austria, and the institutional human use committee at the Shepherd Center, Atlanta, GA, USA.

Results

Epidural SCS in the supine position: Four to nine examples of 10 seconds-EMG segments of stable rhythmic activity expressed in all studied muscle groups of one limb were identified in each subject. The effective stimulation frequency to generate rhythmic activities was 29.5 ± 4.85 Hz, with a range of 22.5 Hz – 42 Hz (the latter being the highest frequencies considered). Stable EMG patterns ranged from locomotor-like, with reciprocal relation between antagonists, to patterns of co-activation between all muscle groups. Regarding rhythmicity, within each given EMG segment, the activities of all studied muscles had the same, common rhythm cycle frequency (0.71 ± 0.41 Hz; min=0.27 Hz, max=1.84 Hz).

Epidural SCS during manually assisted treadmill stepping: Assisted passive stepping movements without epidural SCS generated low-amplitude, gait-phase synchronized EMG activity in some muscles. The most responsive muscle groups were Ham, activated during the hip-flexion and concomitant knee-extension segment of the swing phases, and TS activated during the late flexion phases and throughout the stance phases. Each muscle responded with a single activation per step cycle – the rhythm frequency of all EMG activities was equal to the manually imposed step frequency. Application of SCS immediately augmented the EMG activities as generated by passive stepping alone, as well as activated muscles that did not respond otherwise. Both, EMG activities with a rhythm equal to the step frequency, as well as ones with an independent rhythm frequency were observed. Different lower limb muscles could be rhythmically active with either of these two frequencies during the same recording segment. One example was the generation of rhythmic activities occurring in-phase in bilateral TA with a rhythm frequency of 0.38 Hz during epidural SCS while step frequency was 0.18 Hz.

Transcutaneous SCS during supported standing: Rhythmic EMG activities could be generated in the paralyzed lower limb muscles by continuous 30-Hz transcutaneous SCS in the absence of step-related sensory feedback. Examples were found in 6 of 32 cases (4 subjects tested x 8 muscles) in Q, Ham, and TA. One example was the generation of rhythmic activities occurring in-phase in the bilateral Hams with a rhythm frequency 0.41 Hz.

Transcutaneous SCS during manually assisted treadmill stepping: EMG activities as produced by imposed stepping motions alone could be augmented or suppressed when transcutaneous SCS was supplied, and rhythmic activity could be generated in muscles that were not active in the SCS-off condition. These various modifications could be all found concomitantly in the muscles of a single subject. In most cases, the rhythm cycle frequency of the generated activities was equal to the step-cycle frequency given by the DGO. Yet, similarly as with epidural SCS, there were examples with independent rhythm cycle frequencies, e.g. unilateral synchronous rhythmic activities of Q and TA with a rhythm frequency of 0.38 Hz were found in one subject, that did not synchronize to the step frequency of 0.56 Hz.

Discussion

There are several theories for the generation of patterned EMG activity in paralyzed lower limbs in response to step-related patterned sensory input to the human spinal cord during passive treadmill stepping [9]. Suggested mechanisms range from cyclically entrained stretch reflexes generated by the imposed movements [10] to the direct activation of human spinal cord pattern generators for locomotion by the sensory feedback input [11]. Our data suggest that the observed rhythmic muscle activities during passive stepping alone are directly related to mechanical events rhythmically occurring at specific times of the gait cycle. We propose that inhibitory and excitatory spinal reflex pathways to the motoneurons re-act in a time-dependent way to the sequential activation of afferents of multiple sensory modalities, including afferents signalling muscle-tendon stretch, velocity of muscle-tendon stretch and extensor-load during the step cycle. The rhythm frequencies are given by rhythmic reflex actions rather than by central spinal generation.

Both, epidural SCS applied in the supine position, as well as transcutaneous SCS in a supported standing position, could produce rhythmic activities in the paralyzed lower limb muscles. While the influence of some rhythmic proprioceptive feedback cannot be ruled out, the rhythmic muscle activities were generated without step-related sensory information critical for rhythm-generation. The constant phase relation of the rhythmic activities produced in one limb suggests rhythm generation by a common source. The spinal neural networks that were activated by the rather unspecific neural drive with a predominantly tonic signal profile to produce rhythmic efferent activity can be viewed as a central spinal rhythm generator [12].

Essentially, there were two temporarily stable types of rhythmic muscle activities generated by the combined application of SCS and externally guided stepping, one with a rhythm frequency equal to the imposed step frequency observed in the majority of cases and another oscillating with an independent frequency. This finding suggests two different causes of rhythm generation. In cases where both rhythms were observed in different muscles of the lower limb, neural circuits of the lumbar spinal cord must have been active rhythmically with different frequencies, one given by the central spinal rhythm generator and the other imposed by the rhythmic mechanical events related to stepping.

One could speculate that a relatively autonomous rhythm generating network that is ‘coupled’ but not ‘hard wired’ to the periphery would be essential in the neural control of locomotion to achieve a target rhythm frequency planned and set by supraspinal neural structures. Through coupling of separate mechanisms of rhythm generation, one centrally generated and causative, the second imposed by peripheral conditions and regulative, the differ-

ent rhythms would tend to synchronize and ensure effective locomotor behaviour.

Acknowledgement

We wish to acknowledge the support of the Austrian Science Fund (FWF), Proj.Nr. L512-N13, the Vienna Science and Technology Fund (WWTF), Proj.Nr. LS11-057, and the Wings for Life Spinal Cord Research Foundation (WfL), Proj.Nr. WFL-AT-007/11.

Bibliography

[1] Illis, L.S.: Central nervous system regeneration does not occur, *Spinal Cord*, vol. 50, pp. 259-263, 2012

[2] Beres-Jones, J.A., Harkema, S.J.: The human spinal cord interprets velocity-dependent afferent input during stepping, *Brain*, vol. 127, pp. 2232-2246, 2004

[3] Dimitrijevic, M.R., Gerasimenko, Y., Pinter, M.M.: Evidence for a spinal central pattern generator in humans, *Ann. N. Y. Acad. Sci.*, vol. 860, pp. 360-376, 1998

[4] Minassian, K., Persy, I. et al.: Effect of peripheral afferent and central afferent input to the human lumbar spinal cord isolated from brain control, *Biocyber. Biomed. Eng.*, vol. 25, pp. 11-29, 2005

[5] Minassian, K, Hofstoetter, U, et al.: Neuromodulation of lower limb motor control in restorative neurology, *Clin. Neurol. Neurosurg.*, vol. 114, pp. 489-497, 2012

[6] Harkema, S., Gerasimenko, Y. et al.: Effect of epidural stimulation of the lumbosacral spinal cord on voluntary movement, standing, and assisted stepping after motor complete paraplegia: a case study, *Lancet*, vol. 377, pp. 1938-1947, 2011

[7] Minassian, K., Jilge, B. et al.: Stepping-like movements in humans with complete spinal cord injury induced by epidural stimulation of the lumbar cord: electromyographic study of compound muscle action potentials, *Spinal Cord*, vol. 42, pp. 401-416, 2004

[8] Minassian, K., Persy, I. et al.: Posterior root-muscle reflexes elicited by transcutaneous stimulation of the human lumbosacral cord, *Muscle Nerve*, vol. 35, pp. 327-336, 2007

[9] Capaday, C.: The special nature of human walking and its neural control, Trends Neurosci., vol. 25, pp. 370-376, 2002

[10] Stewart, J.E., Barbeau, H., Gauthier, S.: Modulation of locomotor patterns and spasticity with clonidine in spinal cord injured patients, Can. J. Neurol. Sci., vol. 18, pp. 321-332, 1991

[11] Dietz, V.: Spinal cord pattern generators for locomotion, Clin. Neurophysiol., vol. 114, pp. 1379-1389, 2003

[12] K.G. Pearson, J. Gordon, "Locomotion", in *Principles of Neural Science*, (E.R. Kandel, J.H. Schwartz and T.M. Jessell, eds.), 4th edition, ch. 37, pp. 737-755, New York: McGraw-Hill, 2000

Effects of transcutaneous spinal cord stimulation on voluntary locomotor activity in an incomplete spinal cord injured individual

Hofstoetter US[1], Hofer C[2], Kern H[2], Danner SM[1,3], Mayr W[1], Dimitrijevic MR[4,5], Minassian K[1].

[1]Center of Medical Physics and Biomedical Engineering, Medical University Vienna, Austria
[2]Department of Physical Medicine, Wilhelminenspital, Vienna, Austria
[3]Institute of Analysis and Scientific Computing, Vienna University of Technology, Austria
[4]Deptartment of Physical Medicine and Rehabilitation, Baylor College of Medicine, USA
[5]Foundation for Movement Recovery, Norway

ursula.hofstoetter@meduniwien.ac.at

Abstract: *Non-patterned electrical spinal cord stimulation (SCS) via epidural electrodes can activate neural circuits involved in lower-limb motor control in individuals with spinal cord injury (SCI), and generate automatic, rhythmic flexion-extension movements in the paralyzed lower limbs. Here, we studied whether SCS can increase the excitability of locomotor circuits in a motor-incomplete SCI individual capable of voluntary treadmill stepping without support and whether this augmentation can be integrated into the residual voluntary motor control. SCS was applied through skin electrodes during active treadmill stepping. Sub-motor stimulation enhanced the voluntary lower limb EMG activities in a step-phase appropriate manner as well as reproducibly modified the coordination of hip and knee movements during stepping. Further study in a larger population is warranted.*

Keywords: *locomotor activity, non-invasive, spinal cord injury, spinal cord stimulation, treadmill stepping*

Introduction

Non-patterned, continuous electrical stimulation of the lumbar spinal cord via implanted electrodes can produce various motor outputs to the lower limb muscles of individuals with motor complete SCI depending on the applied stimulation parameters [1,2]. The motor effects range from the generation of bilateral extension (effective stimulation frequencies 5–15 Hz) to automatic rhythmic lower-limb movements (25–60 Hz) [1,3]. Further, epidural SCS at 20-50 Hz augmented the rhythmic EMG activities produced by passive, body-weight supported treadmill stepping in subjects with chronic, motor-complete SCI [2,4,5]. Thus, the locomotor circuits within the lumbar spinal cord below the lesion can be activated by non-patterned SCS and integrate step-related sensory feedback in the generation of rhythmic motor outputs. Here, we studied whether the non-patterned input provided by SCS along with step-related sensory feedback could be integrated into the voluntary motor task of active treadmill stepping. The rationale was to test whether the combination of these inputs would augment functional motor outputs in a motor-incomplete SCI subject capable of voluntary treadmill stepping without support.

We applied a previously described skin-electrode based method of SCS that consistently stimulates (a subset of) the same neural structures as epidural lumbar SCS, i.e. afferent fibers within the L2–S2 posterior roots in humans [6,7,8]. When applied in a continuous mode, this transcutaneous SCS (tSCS) was suggested to modify the central state of excitability of lumbar circuits in SCI individuals [7,9,10,11]. Here, the immediate effects of 30-Hz tSCS at intensities below the motor threshold of the lower limbs in a motor-incomplete SCI person actively stepping on a treadmill without manual assistance and body-weight support will be elaborated.

Methods

Subject: Data were derived from a female (age 29 y) with sensory- and motor-incomplete SCI (neurological level: T9), 11 years post-injury, classified as grade D on the American Spinal Injury Association impairment scale. The subject had spastic muscle hypertonia and clonus in the lower limbs. She could complete the 10-meter walk test with two crutches. The study was approved by the local Ethics Committee.

Transcutaneous spinal cord stimulation: tSCS was applied using a pair of self-adhesive stimulating electrodes (Ø 5 cm, Schwa-medico GmbH, Germany) placed over the T11/T12 spinous processes and a pair of rectangular reference electrodes (8 x 13 cm each) over the lower anterior abdomen. A constant-voltage stimulator delivered charge-balanced, symmetric, biphasic rectangular pulses of 2 ms width (1 ms per phase). Electrode placement over the lumbar spinal cord was confirmed by the elicitation of posterior root-muscle reflexes in the lower limb muscles [6,7,8].

Treadmill stepping: The subject actively stepped on the treadmill without braces, manual assistance, or body-weight support at 1.6 km/h and 0.8 km/h.

Data acquisition: EMG recordings from quadriceps (Q), hamstrings (Ham), tibialis anterior (TA), and triceps surae (TS) muscles bilaterally were acquired using pairs of silver-silver chloride recording electrodes (Intec Medizintechnik GmbH, Austria) [12]. EMG signals were amplified (EMS-Handels GmbH, Austria) with a gain of 502, filtered to a bandwidth of 10–500 Hz and digitized at 2048 samples per second per channel. Data recorded by electro-goniometers (Penny & Giles Biometrics, Ltd., UK), used to measure knee and ankle movements, and by four pressure-sensitive switches (strain gauges, RS Components, Germany) distributed over each foot sole, detecting stance phases, were synchronized to the EMG, bandpass-filtered between 0–100 Hz and sampled at 2048 Hz.

Stimulation and study protocol, data analysis: The sessions started with a recording of treadmill stepping without

tSCS, followed by a recording done with the same treadmill parameters and tSCS at 30 Hz and 18 V, an intensity producing paraesthesias in most of the lower-limb dermatomes, yet below motor threshold for the lower-limb muscles. This procedure was repeated for both treadmill speeds.

A fourth-order band-pass Butterworth filter was used to filter EMG data (10-700 Hz) and goniometers data of hips and knees (0-15 Hz). Foot switch recordings were used to define gait cycle durations and to distinguish between stance and swing phases. Goniometric data averaged from ten consecutive gait cycles were utilized to produce hip-knee cyclograms.

Results

Without tSCS (Fig. 1, left), the EMG activity during active treadmill stepping of bilateral Q was characterized by two bursts per gait cycle, one occurring during the early stance phase and a second one of smaller amplitude and shorter duration at the stance-to-swing transition. In LQ, stretch-like EMG activities emerged at heel strike. Both Ham featured a single EMG burst per cycle, starting at the transition from swing to stance, and lasting up to mid-stance. RTA activity occurred at the stance-to-swing transitions, while in LTA, no gait-phase appropriate EMG activity was observed. Clonus-like EMG activities in both TS occurred during the respective stance phases. The EMG patterns were immediately modified when 30-Hz tSCS was supplied (Fig. 1, right). The stretch-like activity in LQ appeared less frequently. A second burst of activity emerged in both Ham during the concentric contraction-like activity preceding the maximum hip and knee flexion during swing. A burst of activity emerged in LTA during left swing. The clonus-like EMG patterns in TS were not modified. Regarding the amount of EMG activity, Q-activity was augmented during swing and Ham-activity during stance when tSCS was applied. TA-activity was increased during swing while TS-activity was decreased. During stance, TA-activity was reduced and TS-activity augmented.

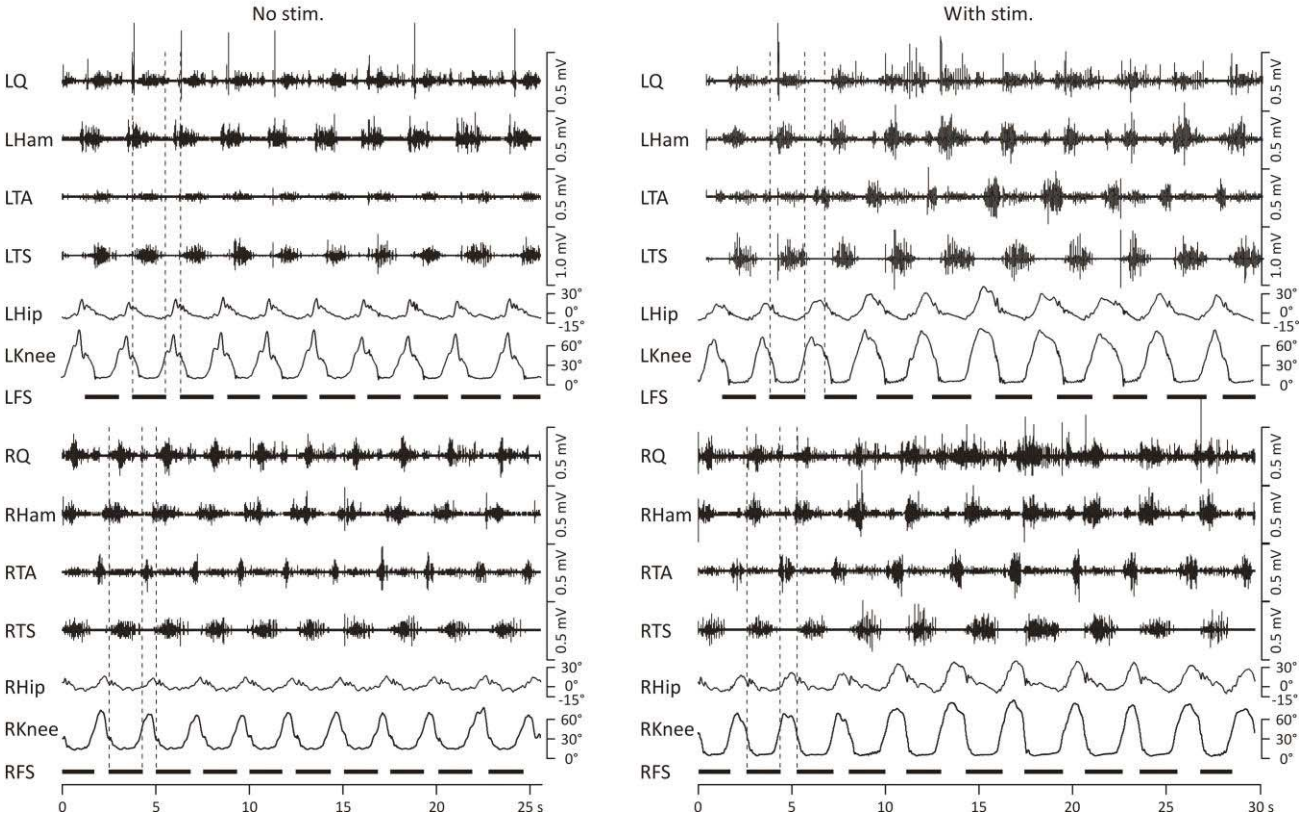

Figure 1. EMG activity of left (L) and right (R) quadriceps (Q), hamstrings (Ham), tibialis anterior (TA), and triceps surae (TS) along with hip and knee goniometric data and foot switches (FS) marking stance phases. Displayed are ten step cycles of voluntary treadmill stepping at 1.6 km/h without (left) and during (right) the application of 30-Hz sub-motor stimulation. EMG patterns and amount of activities were immediately modified by the stimulation.

During tSCS, stride length changed from 1.13 m to 1.32 m, on average, and cycle duration increased from 2.6 s to 3.0 s, while only the swing phases were prolonged ($p < 0.01$). The goniometric data in Fig. 1 also clearly show changes of the gait kinematics by tSCS. Figure 2 summarizes these stimulation-related modifications of the hip-knee movement coordination. The range of movement of hip and knee increased significantly ($p < 0.01$), and the coordination between hip- and knee-movements changed characteristically during tSCS. These modifications were reproducible at both treadmill speeds tested (cf. cyclogram labelled as *rep.* in Fig. 2). Generally, tSCS facilitated a more fluid multi-joint movement with an exaggerated flexion component and augmented foot clearance.

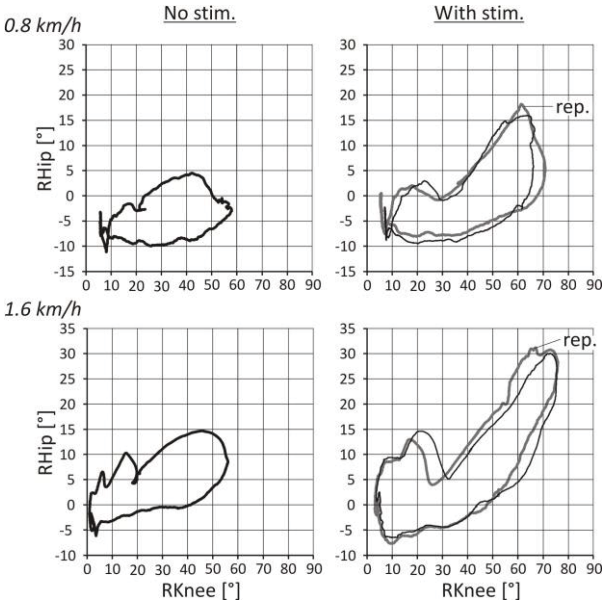

Figure 2. Hip-knee cyclograms calculated for right hip and knee during average gait cycles at 0.8 km/h (upper trace) and 1.6 km/h (lower trace) without (left) and with (right) 30-Hz stimulation (stim.). The stimulation considerably increased the range of movement of hip and knee and augmented the flexion component of the movement. These modifications were reproducibly observed at both treadmill speeds (rep.).

Discussion

Non-patterned 30-Hz tSCS applied over the lumbosacral spinal cord in a person with a chronic, motor-incomplete SCI during voluntary treadmill stepping caused immediate effects on the lower-limb EMG activities and reproducibly modified the gait kinematics. TSCS was applied at an intensity below the threshold of the lower limb muscles at a level producing paraesthesias in the lower limb dermatomes. The observed stimulation-induced effects were not due to the direct activation of spinal motor pools. Specifically, during tSCS alone, i.e. without the subject's voluntary attempt to step, no EMG activities were produced in the lower limbs. It is thus plausible that the continuous tSCS elevated the physiological state of the lumbar locomotor circuits that in turn became more responsive to the supraspinal commands via the residual descending pathways [4,5]. The gait-phase appropriate manner of the stimulation-induced EMG modifications further hints on the capability of the involved neural circuits to efficiently integrate the non-patterned input delivered by tSCS and the step-related proprioceptive feedback into the voluntary execution of coordinated multisegmental movements. The present findings suggest that tSCS can be used to facilitate residual voluntary locomotor control in motor-incomplete SCI individuals. Further study in a larger subject population is warranted.

Acknowledgement

We wish to acknowledge the support of the Austrian Science Fund (FWF), Proj.Nr. L512-N13, the Vienna Science and Technology Fund (WWTF), Proj.Nr. LS11-057, and the Wings for Life Spinal Cord Research Foundation (WfL), Proj.Nr. WFL-AT-007/11.

Bibliography

[1] Dimitrijevic, M.R., Gerasimenko, Y., et al.: Evidence for a spinal central pattern generator in humans, Ann. N Y Acad. Sci., vol. 16, pp. 360-376, 1998

[2] Minassian, K., Persy, I., et al.: Human lumbar cord circuitries can be activated by extrinsic tonic input to generate locomotor-like activity, Hum. Mov. Sci., vol. 26, pp. 275-295, 2007a

[3] Minassian, K., Jilge, B., et al.: Stepping-like movements in humans with complete spinal cord injury induced by epidural stimulation of the lumbar cord: electromyographic study of compound muscle action potentials, Spinal Cord, vol. 42, pp. 401-416, 2004

[4] Minassian, K., Persy, I., et al.: Effect of peripheral afferent and central afferent input to the human lumbar spinal cord isolated from brain control. Biocybernetics and Biomed. Eng., vol. 25, pp. 11-19, 2005

[5] Harkema, S., Gerasimenko, Y., et al.: Effect of epidural stimulation of the lumbosacral spinal cord on voluntary movement, standing, and assisted stepping after motor complete paraplegia: a case study. Lancet, vol. 377, pp. 1938-1947, 2011

[6] Minassian, K., Persy, I., et al.: Posterior root-muscle reflexes elicited by transcutaneous stimulation of the human lumbosacral cord. Muscle Nerve, vol. 35, pp. 327-336, 2007b

[7] Minassian, K., Hofstoetter, U., Rattay, F., "Transcutaneous lumbar posterior root stimulation for motor control studies and modification of motor activity after spinal cord injury", in *Restorative Neurology of Spinal Cord Injury*, (*M.R. Dimitrijevic*, *B.A. Kakulas*, *G. Vrbova* and *W.B. McKay*, eds.), ch. 10, pp. 226-255, New York: Oxford University Press, 2011

[8] Hofstoetter, U.S., Minassian, K., et al.: Modification of reflex responses to lumbar posterior root stimulation by motor tasks in healthy subjects, Artif. Organs. vol. 32, pp. 644-648, 2008

[9] Minassian, K., Hofstoetter, U., et al.: Neuromodulation of lower limb motor control in restorative neurology, Clin. Neurol. Neurosurg., vol. 114, pp. 489-497, 2012

[10] Minassian, K., Hofstoetter, U., et al.: Transcutaneous stimulation of the human lumbar spinal cord: Facilitating locomotor output in spinal cord injury. Program No. 286. 19. Neuroscience Meeting Planner. San Diego, CA: Society for Neuroscience; 2010 [Online]

[11] Hofstoetter, U., Mayr, W., et al.: Effects of transcutaneous spinal cord stimulation on spasticity electrophysiologically evaluated in spinal cord injured individuals. Program No. 808.02. Neuroscience Meeting Planner. Washington, DC: Society for Neuroscience; 2011 [Online]

[12] Sherwood, A.M., McKay, W.B., Dimitrijević, M.R., Motor control after spinal cord injury: assessment using surface EMG. Muscle Nerve, vol. 19, pp. 966-979, 1996

Towards physiological ankle movements with the ActiGait implantable drop foot stimulator in chronic stroke

Jennifer Ernst[a], Jessica Grundey[a], Manuel Hewitt[a], Friederike von Lewinski[a], Jürgen Kaus[b], Thomas Schmalz[b], Veit Rohde[c], David Liebetanz[a]

[a]Department of Clinical Neurophysiology, University Medical Center Göttingen, Germany.
[b]Department of Research, Otto Bock Healthcare, Duderstadt, Germany.
[c]Department of Neurosurgery, University Medical Center Göttingen, Germany.

Abstract— Most studies so far have not compared the effects of peroneal FES with the effects of conventional orthotic treatment. The implantable system ActiGait is a treatment for drop foot that improves walking speed, endurance and ankle joint movements during the gait cycle. This study is the first to show that even compared to AFO the implantable system was more physiological under the different conditions tested during the gait cycle at prominent points of the gait cycle. Thus the ActiGait drop foot stimulator is an alternative way of correcting drop foot in chronic stroke patients. The implantable neuroprosthesis does add an almost physiological range of ankle joint movements.

I. Introduction

Drop foot is a major disability, which often remains after a stroke. Reduced ankle excursions during the swing phase of walking due to weak anterior tibial muscles, calf spasticity or ankle stiffness is among the persistent gait abnormalities contributing to a poor or inefficient lifting of the toes during the swing phase. Drop foot leads to decreased speed, limited endurance and increases the risk of falls. These factors limit mobility, independence and reduce the quality of life [1]. 20%- 30% of patients entering neurologic rehabilitation suffer from drop foot [2]. The conventional way to improve insufficient ankle dorsiflexion during the swing phase is the prescription of an ankle foot orthosis (AFO). An AFO holds the foot in a fixed position to assist in lifting it during walking [3].

An alternative is to electrically stimulate the muscles used for ankle dorsiflexion and eversion. Since Liberson et al. in 1961 [4], several studies have tested the benefits of peroneal nerve stimulation [5-17]. Most of the stimulation systems used in these studies have been external and transcutanous. The main drawbacks of a surface drop foot stimulator are the awkwardness in handling the external parts [8].

Implantable systems as the ActiGait system solve the above-mentioned problems. Burridge et al. [9] demonstrated that the partly implantable 4-channel drop foot stimulator ActiGait safely improves walking speed and endurance. Recently, a case report [17] pointed to the positive effects of the same system on knee and hip motion angles, as well as on gait symmetry and variability.

To further evaluate the beneficial effects of the ActiGait system on functional gait parameters, the present study focused first on ankle joint movements during the gait cycle in addition to walking parameters like walking speed and endurance. We explored whether the implantable system may represent a competitive alternative treatment of drop foot to conservative orthotic treatment.

II. Methods

The ActiGait system is a partly implantable 4-channel drop foot stimulator, which selectively and directly stimulates via a cuff electrode the common peroneal nerve. The heel switch (HES) is worn externally and sensitive to pressure, thus controlling wireless the time point of the stimulation (bipolar pulse shape, 1.2 mA amplitude, pulse width 0-255 µs; 5-50 Hz, interpulse interval 20-200ms; detailled explanation of the system and the surgical procedure in [9]).

Walking speed (10 meter gait test, [m/s]) and endurance (6 minutes gait test [m/ 6 min]) of 5 patients suffering drop foot due to a cerebro-vascular accident (CVA) were tested prior to, as well as 6 and 12 weeks after the implantation of the ActiGait. During the activation visit, 3 weeks after implantation, the patients were instructed to use the system during the 1st week one hour daily, during the 2nd week 2-3 hours daily, building up to 4-6 hours by the 3rd week. Reaching week 4 there was no more recommended restriction in using the system. This instruction was given to avoid excessive use of dorsiflexion muscles leading to muscle soreness.

In addition to walking tests, ankle joint gait kinematics were assessed at baseline and 12 weeks after implantation (Vicon, optoelectronic six camera system). Three different scenarios were compared: walking without walking aid, with AFO and walking with the implantable drop foot stimulator ActiGait. Passive reflective markers fixed to anatomical reference points were used. Seven markers were attached to each side of the body (acromioclavicular joint, lateral epicondyle of elbow, wrist, greater trochanter, lateral femoral condyle, lateral malleolus, and fifth metatarsal head).

The following selected parameters refer to gait analysis by Perry (1992) [18] and were calculated from each trial: walking speed [m/s], initiation angle of the ankle joint [°] (IA), initial plantar flexion of the ankle joint [°] (IPF), maximum dorsiflexion [°] during mid-stance phase (DF), as well as final plantar flexion of the ankle joint [°] at the end of the stance phase (FPF).

The initiation angle (IA) results by a line through the lateral femoral condyle marker and the lateral malleolus marker and a second line through the lateral malleolus marker and fifth metatarsal head marker. The IA represents an absolute angle measured at the time point of initial heel contact of the foot to the ground. This is identical to the term "Initial Contact" of Perry [18]. We refer to an absolute physiological IA of 115°, in the ankle joint measured in a healthy control group [19]. The angles of IPF, DF and FPF are given relative to the physiological IA.

III. Results

After 6 weeks, gait speed increased (ActiGait ON vs. OFF: 0.55 vs. 0.77 m/s) as had walking endurance (211 vs. 260 m). After 12 weeks, improvements in gait speed (ActiGait ON vs. OFF: 0.55 vs. 0.77 m/s) and endurance (ActiGait ON vs. OFF: 214 vs. 248 m) while walking assisted by the the ActiGait system were still present. In addition, gait analysis after 12 weeks revealed a towards physiological range restored initiation angle (IA) (ActiGait ON vs. walking without a walking aid: 113° vs. 122°, FIG. 1, 2A) and an

increase in the initial plantar flexion in the early stance phase (ActiGait ON vs. walking without a walking aid: 7° vs. 0°, FIG.2B).

FIGURE 1.

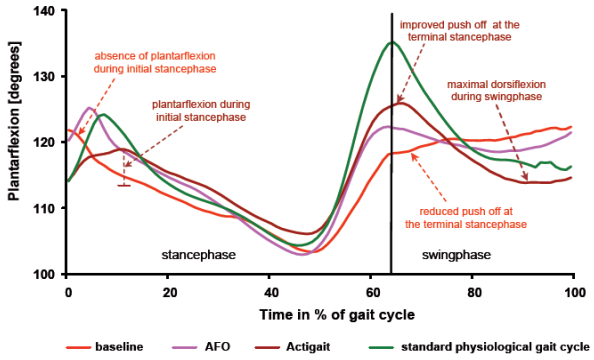

Fig.1 Improvements of specific gait parameters when walking with ankle foot orthosis (AFO) or drop foot stimulator. Data are degrees of flexion-extension movements in the ankle joint of the affected side during the gait cycle. The flexion-extension curve without walking aid (n=5) is compared to the condition with AFO (n=5) and with the ActiGait drop foot stimulator (n=5). The green curve shows the standard physiological gait cycle measured in a healthy control group (n=15) in a gait laboratory. Please note the initiation angle (IA) as a marker for the level of DF during the swing phase, which is specifically improved by the drop foot stimulator as compared to the rigid AFO or to no walking aid. DF= dorsiflexion; FPF= final plantar flexion; GC= gait cycle; IPF= initial plantar flexion.

FIGURE 2A.

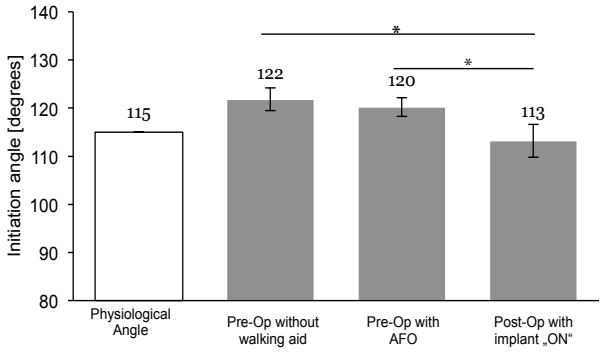

FIGURE 2B.

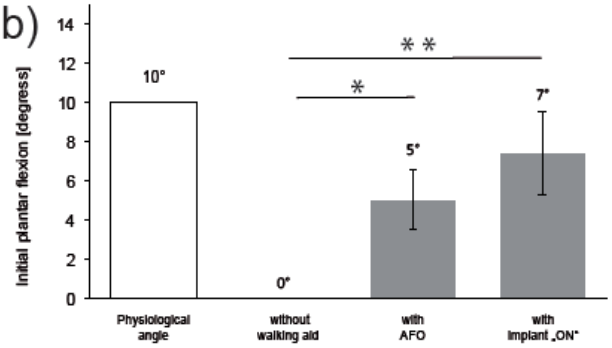

Fig. 2 Evaluation of the effects of the different walking aids on characteristic gait parameters. Based on an assessment of the flexion-extension movement in the ankle joint at several points of the gait cycle, different walking aid conditions were compared to a healthy control group (Waldmann, 2006, n=15) for IA, and as physiological set values measured by Perry, J. (1992) for comparison of IPF, DF and FPF. Fig. 2A shows, that the initiation angle (IA) in the ankle joint of the affected leg is significantly improved by the drop foot stimulator as compared to no walking aid (* p=0.047). (B) The drop foot stimulator produces a much more normal physiological initial plantar flexion as compared to no walking aid or AFO (* p= 0.005, ** p= 0.019).

IV. Discussion

The parallel curve progression for walking with the implantable system (n=5) to that of a healthy control group (green, n=15) revealed the physiology of gait produced by the implantable system compared to the different conditions tested during the gait cycle (Fig.1). However this effect was not accompanied by significantly different ankle joint movements at all defined time points during the gait cycles. Particularly the active correction of the IA in contrast to the rigid AFO demonstrated that this system is as an alternative treatment of drop foot due to a cerebrovascular accident. Different factors contributed these results. Further investigations will now explore additional effects on gait parameters, such as stability, balance and improved ground clearance as well as possible limitations of the system.

V. Conclusion

ActiGait system is a more natural way to actively lift the foot clear of the ground. In contrast to the conventional treatment of a drop foot this system based on FES activates muscles during the swing phase. Especially the resulting restoration of the IA at the beginning of stance phase as it represents a well-suited parameter for adequate pre-positioning of the foot at the beginning of the stance phase this being necessary to prevent stumbling and falling, revealed that the implantable system is an alternative treatment of drop foot due to CVA with a strong tendency to physiological ankle movements during the gait cycle.

Annotation

J. Kaus and T. Schmalz are employed by the Otto Bock Company, which provided the stimulator unit.

References

[1] Perry, J (1992). Gait analysis: normal and pathological function.Thorofare, N. J. , Slack.
[2] Karsinia, A., Dillner, S., Eberfors, I., Lundmark, P (1990). Why patients use or reject a peroneal muscle stimulator. Advances in External Control of Human Extremities, 251-260
[3] Lehmann, J.F., Condon, S.M., de Lateur, B.J., Price, R (1986). Gait abnormalities in peroneal nerve paralysis and their corrections by orthoses: a biomechanical study. Arch Phys Med Rehabil. 67(6), 380-386
[4] Liberson, W.T., Holmquest, H.J., Scott, D., Dow, M. (1961). Functional electrotherapy, stimulation of the peroneal nerve synchronized with the swing phase of the gait of hemiplegic subjects. Arch. Phys. Med. 42,101-105.
[5] Bogataj, U., Gros, N., Kljajić, M., Aćimović, R., Malezic, M. (1995). The rehabilitation of gait in patients with hemiplegia: a comparison between conventional therapy and multichannel functional electrical stimulation therapy. Phys Ther. 75(6), 490-502.
[6] Bogataj, U., Gros, N., Malezic, M., Kelih, B., Kljajić, M., Acimović, R. (1989). Restoration of gait during two to three weeks of therapy with multichannel electrical stimulation. Phys Ther 69(5), 319-27.
[7] Burridge, J.H., Taylor, P.N., Hagan , S.A., Wood, D.E., Swain, I.D. (1997). The effects of common peroneal stimulation on the effort and speed of walking: a randomized controlled trial with chronic hemiplegic patients. Clin Rehabil. 11(3), 201-10.
[8] Burridge J., Taylor, P., Hagan, S., Swain, I. (1997). Experience of clinical use of the Odstock dropped foot stimulator. Artif Organs. 21(3), 254-60.
[9] Burridge, J.H, Haugland, M., Larsen, B., Pickering, R.M., Svaneborg, N., Iversen, H.K., Christensen, P.B., Haase, J., Brennum ,J., Sinkjaer, T. (2007). Phase II trial to evaluate the ActiGait implanted drop-foot stimulator in established hemiplegia. J Rehabil Med. 39(3), 212-8.
[10] Granat, M.H., Maxwell, D.J., Ferguson, A.C., Lees, K.R., Barbenel, J.C. (1996). Peroneal stimulator; evaluation for the correction of spastic drop foot in hemiplegia. Arch Phys Med Rehabil. 77(1), 19-24.
[11] Kottink, A.I.R., Buschmann, R., Kenny, L., Veltink, P.H., Slycke, P. (2004). The sensivity and selectivity of an implantable two channel peroneal nerve stimulator system for restoration of dropped foot. Neuromodulation, 7, 277-283.
[12] Kottink, A.I., Hermens, H.J., Nene, A.V., Tenniglo, M.J., van der Aa, H.E., Buschman, H.P., Ijzerman, M.J. (2007). A randomized controlled trial of an implantable 2-channel peroneal nerve stimulator on walking speed and activity in poststroke hemiplegia. Arch Phys Med Rehabil. 88(8), 971-8.
[13] Kottink , A.I., Hermens, H.J., Nene, A.V., Tenniglo, M.J., Groothuis-Oudshoorn, C.G., Ijzerman , M.J.(2008). Therapeutic effect of an implantable peroneal nerve stimulator in subjects with chronic stroke and footdrop: a randomized controlled trial. Phys Ther. 88(4), 437-48.
[14] Merletti, R., Zelaschi, F., Latella, D., Galli, M., Angeli, S., Sessa, M.B. (1978).A control study of muscle force recovery in hemiparetic patients during treatment with functional electrical stimulation. Scand J Rehabil Med. 10(3), 147-54.
[15] Merletti , R., Andina, A., Galante , M., Furlan, I.(1979). Clinical experience of electronic peroneal stimulators in 50 hemiparetic patients. Scand J Rehabil Med., 11(3), 111-21.
[16] Taylor, P.N., Burrdige, J.H., Dunkerley. A.N.,Lamb A., Wood , D.E., Norton , J.A., et al. (1999). Patients ´perceptions of the Odstock Dropped Foot Stimulator (ODFS). Clin Rehabil 13, 439-446.
[17] van Swigchem R, Weerdesteyn V, van Duijnhoven HJ, den Boer J, Beems T, Geurts AC. (2011) Near-normal gait pattern with peroneal electrical stimulation as a neuroprosthesis in the chronic phase of stroke: a case report. Arch Phys Med Rehabil. 2011 Feb;92(2):320-4.
[18] Perry, J. (1992). Gait analysis: normal and pathological function. Thorafare, N.J., Slack.
[19] Waldmann, D (2006). Biomechanik des Gehens auf verschiedenen Neigungen- eine kinetische, kinematische und elektromyelographische Untersuchung. Magisterarbeit *(master´s thesis),* Georg-August-Universität, Göttingen.

RECOVERY OF TETANIC CONTRACTILITY OF DENERVATED MUSCLE: A STEP TOWARD A WALKING AID FOR FOOT DROP

Marcante A[1], Zanato R[2], Ferrero M[3], Zampieri S[3,4], Kern H[4,5], Stramare R[2], Gargiulo P[6,7], Carraro U[3], Masiero S[1]

[1] Rehabilitation Unit of the Department of Neurosciences; [2] Radiology Unit of the Department of Medicine, Padua General Hospital; [3] Translational Myology Lab, Department of Biomedical Science, University of Padova, Italy; [4] Ludwig Boltzmann Institute of Electrical Stimulation and Physical Rehabilitation; [5] Dept. Physical Medicine and Rehabilitation, Wilhelminenspital Wien, Austria; [6] Dept. Biomedical Engineering, University of Reykjavik; [7] Dept. Science, Education and Innovation, Landspitali University Hospital, Reykjavik, Iceland

"Andrea Marcante" endriu83@gmail.com

Abstract: *This is a single case report about the possibility to recover tetanic contractility in a peripherally denervated and atrophic tibialis anterior muscle (TA). We performed a first electrostimulation test (ET1) to assess the muscular reactivity to electrical stimulation and measured TA thickness by US. Based on the parameters obtained during ET1, we suggested home-based surface electrostimulation training for 2 months and then we performed a second electrostimulation test (ET2). In ET2 there was an evident reduction of the impulse length necessary to evoke a twitch response, reflecting the fact that there was a recovered excitability of the muscle.*
Lowering duration of the impulse it could possible to use a higher frequency of stimulation to obtain tetanic contractility, that could represent the best muscular training to avoid atrophy and to use electrical stimulation as walking aid in peripheral denervation.

Keywords: *electrostimulation, peripheral denervation, denervated muscle, echomyography, walking-aid*

Introduction

Electrostimulation of denervated muscle is still a controversial issue with lack of clinical studies based on patients with peripheral nerve lesions.
We report on a case of a 26 years old man with a complete sciatic nerve injury related to a subtrochanteric fracture of the right femur caused by car accident in 2010. Femur fracture was correctly fixed with a long gamma nail but clinically, patient has still presented a complete anesthesia under his right knee and some pain on the gluteal region. The strength of the hamstrings was almost spared, but flexion and extension of the ankle were impossible, with a severe impaired deambulation. In 2011 the patient underwent a surgery of neurolysis of sciatic nerve with removal of a voluminous neuroma and positioning of an 8 cm contralateral sural nerve graft. One year after the surgery the patient refers disappearance of gluteal pain, strengthening of the hamstrings but no improvement in the muscles of the shank.

Methods

We performed a first electrostimulation test (ET1) to verify the response of tibialis anterior (TA) and tricep surae muscles. Using a Neuroton (Philips) stimulator, we applied a current of 10 to 30 mA with triangular monophasic waves, impulse length from 5 to 150 msec with a pause of 1 or 2 sec. The best muscular response was evaluated by clinical examination and by echomyographic scans during the electrostimulation [1,2]. We also measured the TA thicknesses in three points of the muscle (proximal, middle and distal 1/3rd of muscular belly). At home, the patient applied similar electrostimulation parameters using the electro stimulator SM1 (Demitalia, Medical Technology S.r.L., Torino, Italy) with the schedule: 2 sessions (lasting 30 minutes each) per day for the first month, then 5 sessions per week. This schedule was applied for 2 months, then the patient underwent a second electrostimulation test (ET2) and the muscular responses were evaluated again by clinical examination and echomyographic scans. Moreover, to assess the reliability of echomyographic measurements, the patient underwent an MRI scan of the lower legs and the TA thicknesses were compared to those obtained by echomyographic scans.

Results

During the ET1 we found that the best muscular response was a single twitch and was evident using an impulse length of 150 msec and pause for 2 seconds.
After 2 months, in the ET2 we still used a 20-25 mA current with pause of 2 seconds, but we found that there was the same twitch response using only 50 msec impulse length. At the ET2 we also compared the echomyographic measurements with those obtained at the ET1 (Tab.1) and with those obtained with the MRI scan (Tab. 2).
As seen in Table 1, there is a reduction in diameters of the left TA, reflecting the fact that 2 months of "twitch training" were not able to stop atrophy process [3-5]. There is also a misleading discordance in measurements of the proximal third of the not affected right leg, probably due to a technical difficulty to measure in this specific site of

the muscle [2]. In Fig. 1 the effects of atrophy process on TA muscle are well visualized on a 3D reconstruction of the MRI scan [6].
The comparison of TA thickness measurements using MRI or echomyographic scans reveals that there is a good reproducibility between the two methods.

Table 1: TA thickness compared in ET1 and ET2

	ET1		ET2	
Muscle level	**Left leg** (mm)	**Right leg** (mm)	**Left leg** (mm)	**Right leg** (mm)
Proximal third	13.1	21.3	10.3	17.1
Middle third	19.6	26.8	16.5	24.8
Distal third	22	26.9	13.5	27

Table 2: comparison of TA thickness measurements using MRI or Echo scans

	MRI		Echo	
Muscle level	**Left leg** (mm)	**Right leg** (mm)	**Left leg** (mm)	**Right leg** (mm)
Proximal third	10	20	10.3	17.1
Middle third	17	31	16.5	24.8
Distal third	17	29	13.5	27

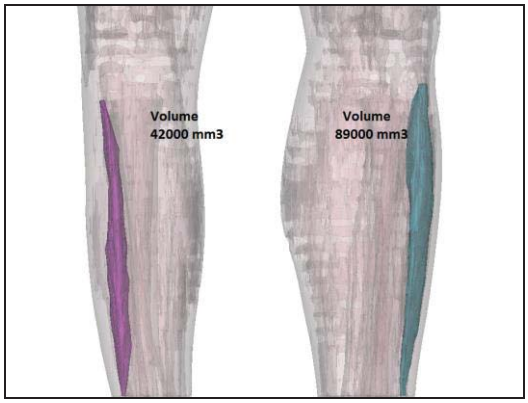

Figure 1: 3D reconstruction of TA muscles at MRI scans, revealing severe atrophy of right TA

Discussion

This case report shows how a correct home-based electrostimulation protocol is the right training to recover contractility in a peripherally denervated muscle. Lowering the duration of the impulse it could possible to use a higher frequency of stimulation to obtain tetanic contractility. "Tetanising" protocol may be attained, despite the fact that the twitch-training did not hampered the process of atrophy or improved kinetics of contraction/relaxation of the twitch, induced by home-based surface Functional Electrical Stimulation (h-b FES) [4,5].

The next step in the process of functional recovery will be to recover mass and force of TA with "tetanic" training (series of impulse trains of 2-3 seconds duration at intervals of 3 sec) against increasing resistance to dorsiflexion of the foot (by acting a "spring device" opposing foot dorsiflexion). In conclusion the patient improved in two months of twitch-stimulation so much the excitability of the persistently denervated TA that a tetanising protocol, with its therapeutic potential to be used in a “walking aid for denervated muscle”, would be the next “step” in the rehabilitation program.

Bibliography

[1] Zanato R, Martino L, et al., Functional Echomyography: thickness, echogenicity, contraction and perfusion of the LMN denervated human muscle before and during h-b FES. *European Journal of Translational Myology/Basic Applied Myology.;* vol. 20, pp.33-40, 2010

[2] Zanato, R., Martino, L., Stramare, R., Functional Echomyography of the human denervated muscle: first results, *European Journal Translational Myology - Basic Applied Myology*, vol. 21, pp. 3-29, 2011

[3] Boncompagni S, Kern H, et al., Structural differentiation of skeletal muscle fibers in the absence of innervation in humans. *Proc. Natl. Acad. Sci. USA,* vol. 104, pp 19339-19344, 2007

[4] Kern, H., Boncompagni, S., et al., Long-term denervation in humans causes degeneration of both contractile and excitation-contraction coupling apparatus that can be reversed by functional electrical stimulation (FES). A role for myofiber regeneration? *J Neuropath Exp Neurol,* vol. 63, pp. 919-931, 2004

[5] Kern H, Carraro U, et al., Home-based Functional Electrical Stimulation (h-b FES) recovers permanently denervated muscles in paraplegic patients with complete lower motor neuron lesion. *Neurorehab. Neur. Rep.*, vol. 24, pp. 709-721, 2010

[6] Gargiulo, P., Pétursson, T., et al., Assessment of Total Hip Arthroplasty by Means of Computed Tomography 3D Models and Fracture Risk Evaluation. *Artif. Organs*, vol. 37: pp. 567-673. June, 2013

Ant Colony Optimization Tuning PID Algorithm for Precision Control of Functional Electrical Stimulation

Shuang Qiu[1], Rui Xu[1], Tianchen Zhai[1], Anshuang Fu[1], Qiang Xu[1], Hongzhi Qi[1], Peng Zhou[1], Lixin Zhang[1], Baikun Wan[1], Weijie Wang[2], Rami Abboud[2], Dong Ming[1,*]

[1] Lab of Neural Engineering & Rehabilitation, Department of Biomedical Engineering, College of Precision Instruments and Optoelectronics Engineering, Tianjin University, Tianjin 300072, China
[2]Department of Orthopaedic and Trauma Surgery, Ninewells Hospital and Medical School, University of Dundee, Dundee, UK

* Corresponding author, richardming@tju.edu.cn

Abstract: Functional electrical stimulation (FES) can restore motor function in individuals with spinal cord injury (SCI). Neuroprostheses based on FES apply electric stimuli to induce muscle contractions and the corresponding joint movements. The goal of this study was to design a novel FES controller, and the attention is focused on the feedback control of the knee-joint movements induced by electrical stimulation of the quadriceps muscle group. Ant colony optimization algorithm is employed to modulate the proportional, integral and derivative values of PID controller. The promising results showed the ACO-PID controller functioned as expected and performed better than the GA-PID controller. This method for a knee-joint movement resulted in decrease of the tracking error and shortened delay in the response, which may be applied in walking-assisted FES.

Keywords: *feedback control, FES, PID, ACO, GA*

Introduction

The spinal cord acts as the main pathway for information connecting the brain and peripheral nervous system, but it cannot currently be repaired even by modern medical technology as it lacks of capability of self-regeneration. The restoration of walking function following severe paralysis due to spinal cord injury (SCI) is of importance to both clinicians and patients [1]. Functional Electrical Stimulation (FES) can provide the missing electrical stimuli in order to induce muscle contraction and the corresponding joint movement, which is an advancing technology for restoring paralyzed motor functions caused by a SCI [2]. One important research subject on FES is the development of adequate controllers for generating appropriate electrical stimulation patterns, which is necessary to induce functional movements. In the last decade, neural networks have been incorporated into the control schemes as they are able to learn complex nonlinear mapping. Moreover, fuzzy logic method and the feedback error learning scheme have been modified and applied for FES controllers. Several groups have recently developed and tested some modern control approaches to control lower extremity movement in paraplegia. Their application yielded better tracking performance than the open-loop controlled FES devices, but still did not achieve very good performance for both tracking accuracy and response time and unable to guarantee stability.

The goal of this study was to address the closed-loop FES control design for the realization of effective neuroprostheses for the lower extremities. In particular, the attention is focused on the feedback control of the knee-joint movements induced by electrical stimulation of the quadriceps muscle group. Ant colony optimization algorithm (ACO) was employed to modulate the proportional, integral and derivative values of PID controller separately and its performances was evaluated.

Methods

A. Experimental protocol

Twelve healthy subjects, six males and six females, participated in this experiment. All experiments were carried out subjected to the regulations and approval of the appropriate Institutional Review Board, and after obtaining informed consent. In this study, the subjects sat on the platform with relaxed calf and the knee extensors (quadriceps muscle group) were stimulated by a pair of surface electrodes (Sigmedics, US). The cathode was placed on the motor point of rectus femora's and the anode was placed distally at the quadriceps tendon. The knee joint angle was controlled by changing the amplitude of the stimulation pulse. The NAXMAX muscle model was applied in this study.

B. ACO tuning PID

PID controller attempts to minimize the error between a measured variable and a desired setpoint through close loop feedback using the proportional, integral and derivative mechanism. The discrete-form of the PID algorithm, with input $e(k)$ and output $u(k)$ is given as

$$u(k) = K_p\{e(k) + \frac{T}{T_i}\sum_{i=1}^{k} e(i) + \frac{T_d}{T}[e(k) - e(k-1)]\} \qquad (1)$$

where, K_p is the proportional value; $K_i = K_p T / T_i$ is the integral value; $K_d = K_p T_d / T$ is the derivative value; $e(k)$ is the difference between desired and measured output.

ACO includes two basic stages: adaptive stage and cooperation stage. At the adaptive stage, every candidate solution will adjust structures themselves based on accumulated pheromone. The more ants pass through the way, the more pheromone, then this path will be chosen easily;

whereas the pheromone will be smaller if the time last too long. At the cooperation stage, all the can date solutions expect a better solution through the information communication [4]. There are three parameters about PID controller need to be determined, and the issues about the parameter tuning is to determine the best combination of K_p, T_i and T_d, which can make some performance index best in control system.

Results

The step response from GA-PID controller and ACO-PID controller was compared with the sampling period of 1-ms. With a particular joint angle preset as input signal, the rising interval of signal changing from a specified low value (i.e., 10% of the height value) to a specified high (i.e., 90% of the height value) value was 0.521 and 0.777 for GA-PID controller and GA-PID, respectively. Note that the ACO-PID controller has the better performance on robustness, time efficiency, and overshoot restriction.

The tracing results of the knee joint position by GA-PID controller and ACO-PID from twelve subjects were also compared. It showed clearly that the presented algorithm significantly reduced the error rate and improved the performance of PID to control the knee joint position dramatically with strong robustness Relevant parameters of PID controller were controlled by ant colony optimization (ACO) algorithm to accurately control the current modes of FES system. According to the simulation results, the error between the preinstalled angle and the feedback signal was less than 5.6° with root-mean-square error (RMS error) at 3.7° and correlation coefficient at 0.97. As displayed in Fig. 1, with two experimental controllers and

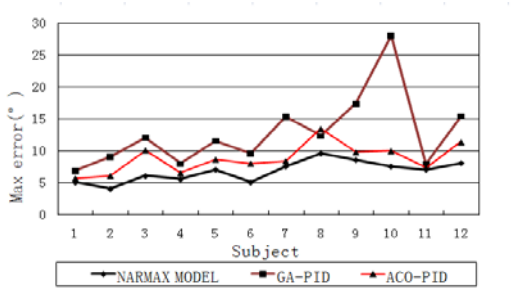

Figure 1. The comparison chart of the twelve subjects' max errors

the muscle model, the max absolute errors are less than 10°, verifying that the stimulation current mode control of FES is more reliable with the PID parameters optimized by ACO.

Discussion

The presented study proposed a FES-PID system modulated by ACO control knee joint position during quadriceps stimulation to solve the problem of control for FES in paraplegic patients. Our results showed that FES-PID system modulated by ACO was superior to GA to make the knee joint angle track the preset-trajectory. Theoretical analysis and simulation examples also demonstrated that parameters optimization strategy design of PID controller based on ant colony algorithms is effective and feasible. It does not rely on the accurate mathematical models, but could effectively overcome the complex optimization problems. Therefore, a PID controller based on ACO is an effective approach to improve the performance of the FES system.

With the effective controller, ant algorithm converges on the optimization path through information pheromone accumulation and renewal. It has the ability of parallel processing and global searching. With low speed for ant colony optimization algorithm, there is little information pheromone on the path early. Recently, a new hybrid algorithm combining ant colony system (ACS) with genetic algorithm (GA) was proposed. The proposed algorithm adds GA to ACS' every generation. Making use of GA's advantage of whole efficient convergence, ACS' convergence speed would be improved. It would be of great application to modulate FES-PID system modulated ACO and GA algorithm to control knee joint position during quadriceps stimulation. Meanwhile, further work to assess such control system on other trajectories or other joints should be done to get more accurate evaluation. Extension of the controller and the experimental setup for controlling multiple and multiple joint movements would be the main concerns in the following study. Considering the real application, evaluation of the controller with actual patients is necessary as well.

Acknowledgement

This research was supported by National Natural Science Foundation of China (Grant No. 81222021, 31271062, 61172008, 81171423, 51007063), National Key Technology R&D Program of the Ministry of Science and Technology of China (Grant No. 2012BAI34B02) and Program for New Century Excellent Talents in University of the Ministry of Education of China (Grant No. NCET-10-0618).

Bibliography

[1] D. Ming, Y. R. Bai et. Al. A gait stability investigation into FES-assisted paraplegic walking based on the walker tipping index. Journal of Neural Engineering, pp. 1-10, 2009.

[2] L. Griffin, M. J. Decker, and J. Y. Hwang et al. "Functional electrical stimulation cycling improves body composition, metabolic and neural factors in persons with spinal cord injury," in Journal of Electromyography and Kinesiology, vol. 19, no. 4, pp. 614-622, 2009.

[3] L. L. Cheng, G. J. Zhang, and B. K. Wan et al. "Radial Basis Function Neural Network-based PID model for functional electrical stimulation system control," in Conference proceedings: Annual International Conference of the IEEE Engineering in Medicine and Biology Society. CA: Tianjin, China, 2009.

[4] R. J. Mullen et al. "A review of ant algorithms," in Expert Systems with Applications, pp. 9608-9617, 2009.

STIMULUS ARTIFACT REMOVAL OF SEMG SIGNALS DETECTED DURING FUNCTIONAL ELECTRICAL STIMULATION

Xi Zhang, Shuang Qiu, Yufeng Ke, Penghai Li, Xin Zhao, Hongzhi Qi, Peng Zhou, Lixin Zhang, Baikun Wan, Dong Ming*

Lab of Neural Engineering & Rehabilitation, Department of Biomedical Engineering, College of Precision Instruments and Optoelectronics Engineering, Tianjin University, Tianjin 300072, China
* Corresponding author, richardming@tju.edu.cn

Abstract: *The recording and interpretation of surface electromyography (SEMG) under functional electrical stimulation (FES) is a useful technique for diagnostic, prognostic and therapeutic purposes. However, the stimulus artifact(SA) is a particularly troublesome form of interference. The paper developed a software-based two-level peak detection technique for SA removal. The results showed by repeatedly changing the values of the peak threshold, the entire SA was removed as expectation leaving the uncontaminated SEMG remaining.*

Keywords: *SEMG, FES, artifact, high threshold, low threshold*

Introduction

The recording and interpretation of surface electromyography (SEMG) under functional electrical stimulation (FES) is a useful technique for understanding muscle activity for diagnostic, prognostic and therapeutic purposes. While FES evokes the contractions in paralyzed muscles for spinal cord injury (SCI), it also results in an interfering potential referred to as the stimulus artifact (SA) [1].Due to some factors, the SA is a particularly troublesome form of interference. First, the amplitude of the SA is typically orders of magnitude larger than the SEMG [2]. Second, the SA is synchronous or coherent with the SEMG and thus cannot be reduced by ensemble averaging--the common method for reducing other forms of interference. Third, in most cases the SA overlaps the SEMG in both the time and frequency domains, such that conventional time windowing and frequency filtering are not capable of removing the SA without distortion of the SEMG [3]. Fourth, due to the non-linearities of the stimulation procedure, most techniques suffer from an inability to adapt to the dynamic nature of SA, and hence suffer residual artifact.

This paper proposed a new approach for the dynamic SA removal based on a fundamental characteristic of the recorded signal. When recording an SEMG, the recorded artifact signal was usually several orders of magnitude greater than the pure SEMG. Using a two-level peak detection algorithm, the data matrix was scanned until a peak was detected and using two levels of amplitude threshold, the entire SA was removed leaving the uncontaminated SEMG remaining.

Methods

1 Algorithm

The artifact removal program was written in MATLAB. The program set high threshold (HT) and low threshold (LT) values to identify the SA and removed the total artifact including both positive and negative spikes.

The program control flow was as follows:

(1) The recorded composite (stimulus artifact and SEMG) data was inputted to the program. The low-frequency drift (20Hz) and the influence of 50Hz as well as other harmonic wave disturbances were removed firstly.

(2) The program then scanned through the absolute data matrix of the composite signal and calculated the maximum value in the array. This value was exactly the peak artifact amplitude. Then the program initially set two threshold values: a high threshold (HT) that was the same as the half of the peak artifact amplitude and a low threshold (LT) corresponded to 1/20 times the peak value. By using the absolute matrix both positive and negative polarities were processed with the same HT/LT values.

(3) The program then scanned the matrix until it reached an amplitude value that passed the LT level in an ascending trend. This maybe indicated a stimulation artifact peak, so the initial LT index point was marked. If the amplitude continued to go up and passed the HT value, the program marked this sequence which started at the passing of the initial LT value as a valid stimulation artifact. The program continued to monitor the progress of the data when it passed the HT and then the LT in decline. The program then marked and recorded the length of the artifact array (from the matrix index of the initial LT point to the matrix index of the final LT point as a detected valid peak). The program then replaced this stimulation artifact with baseline of SEMG data.

(4)On the other hand, if after passing the initial LT value upward, the data dropped back to the LT value again, then it was not an artifact and was either an SEMG or sporadic noise, therefore, the program would ignore it and went on scanning the matrix for artifacts .

2. Data Collection

Six healthy students (4 men and 2 women, age 22–25 years) in lab volunteered for the study. The subjects were seated comfortably in the adjustable chair with leg naturally falling. A portable stimulator (University of Illinois at Chicago & Sigmedics Company，USA) was used to deliver biphasic symmetric pulses to quadricep femoris with the following characteristics: Pulse frequency:25Hz;Maximum output current:300mA ； Maximum open-loop output voltage: 225V.

Surface ME signals were obtained from rectus femoris. The signals were detected by two surface electrodes (Ag-AgCl) 10 mm in diameter, with 20 mm centre-to-centre distance. The electrodes were attached parallel to the muscle fibers on the longitudinal midline of the muscle belly. A reference electrode was attached to the knee.
The SEMG signals were recorded by a bipolar isolated amplifier with a gain of 5000 and CMMR> 120db. A computer with Labview software for raw data acquisition, associated with an A/D converter, permitted to sample the whole SEMG signals (sampling frequency 1000 Hz).

Results

The collected experimental data was analyzed at the base of the method mentioned in this paper. The SA amplitude differed with different stimulus levels, so the HT/LT could be adjusted to detect the entire artifact. The raw data were equally divided into a number of pieces of data of 1 s and proceeded batch processing. The table 1 displayed the processing procedure of a piece of data. After setting up the HT and LT with initial conditions, the first iteration found 16 SA. Over the next few iterations, the program continued to lower its threshold values until, iteration four, when it found all of the 25 SA waveforms.
After batch processing, it was apparent that the SEMG signal of 60s was almost overwhelmed by the huge SA wave in the figure 1(a). After the two-level peak detection program, the entire SA was removed leaving the uncontaminated SEMG remaining showed in the figure 1(b).

Table 1: The processing procedure of a piece of data

iteration	detect/expectation	LT	HT
1	16/25 (64%)	0.173	1.73
2	20/25 (80%)	0.173	1.60
3	22/25 (88%)	0.172	1.51
4	25/25 (100%)	0.171	1.48

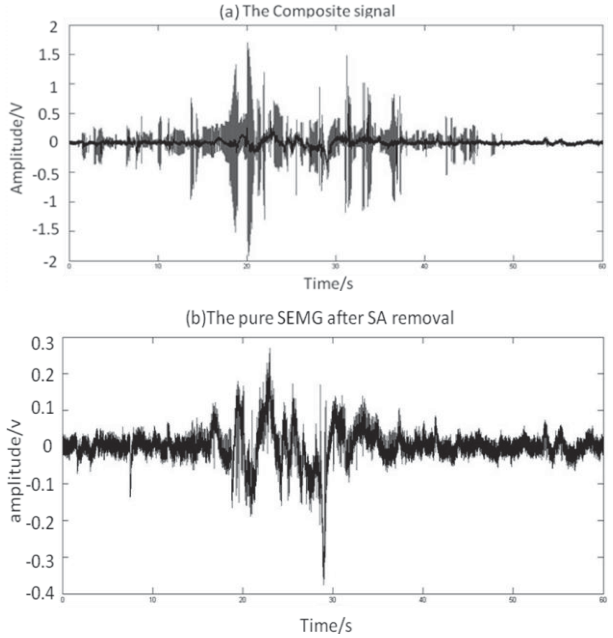

Figure 1. The composite signal and the pure SEMG

Discussion

The method also assumed that the SEMG and artifact were non-overlapping. The stimulation electrode location strongly influenced the effect of artifact on the SEMG signal features. The artifact amplitude was almost linearly decreasing with increasing distance between the stimulation electrode and recording electrode [4]. In this paper the recording electrode locations far from the stimulation point (60mm) insured that the artifact was almost completely separated from the SEMG.
The main advantage of the technique was that the technique could dynamically adapt to different stimulation artifact wave-forms with diverse amplitude and length. It was important to note that if only the stimulation artifact spike would be removed with SEMG unaffected. The effectiveness of artifact removal was checked. If the pulse frequency was A, the time length of composite signal was B, the expected peak artifact number is A*B. If the number of artifacts detected was within 5% tolerance of that expected number, then the artifact detection process was considered successful. If the number of stimulation artifacts detected is outside of this 5% tolerance, then the program automatically changed the values of the HT and LT appropriately and performed iterations.

Acknowledgement

This research was supported by National Natural Science Foundation of China (Grant No. 81222021, 31271062, 61172008, 81171423, 51007063), National Key Technology R&D Program of the Ministry of Science and Technology of China (Grant No. 2012BAI34B02) and Program for New Century Excellent Talents in University of the Ministry of Education of China (Grant No. NCET-10-0618).

Bibliography

[1] Winchman T. A digital averaging method for the removal of stimulus artifacts in neurophysiologic experiments. J Neurosci Meth, vol.98,pp:57–62, 2000.
[2] M. Malboubi, F. Razzazi, M. Aliyari Sh, "Elimination of Power Line Noise from SEMG Signals Using an Efficient Adaptive Laguerre Filter", 7th IEEE International Conference on Signals and Electronic system (ICSES2010), accept to publish, 2010
[3] R. Grieve, P. A. Parker, B. Hudgins, and K. Englehart, “Nonlinear adaptive filtering of stimulus artifact,” IEEE Trans. Biomed. Eng., vol. 47, pp. 389–395, Mar. 2000.
[4] Mandrile, Francesco, Stimulation artifact in surface SEMG signal: effect of the stimulation waveform, detection system, and current amplitude using hybrid stimulation technique, Neural Systems and Rehabilitation Engineering, vol. 11, pp:407-415, Dec. 2003.

CORTICO-MUSCULAR COHERENCE ANALYSIS UNDER VOLUNTARY, STIMULATED AND IMAGINARY NEUROMUSCULAR ACTIVITIES

Tianchen Zhai, Anshuang Fu, Rui Xu, Shuang Qiu, Hongzhi Qi, Peng Zhou, Lixin Zhang, Baikun Wan, Dong Ming*

Lab of Neural Engineering & Rehabilitation, Department of Biomedical Engineering, College of Precision Instruments and Optoelectronics Engineering, Tianjin University, Tianjin 300072, China

* Corresponding author, richardming@tju.edu.cn

Abstract: *A cortico-muscular analysis using EEG and sEMG could elicit a new research idea in the field of sports medicine and rehabilitation engineering. The correlation between motion and brain would be further understood by the comparative analysis of inner relevance of EEG and EMG in diverse motion modes. To this end, we designed 3 motion modes at long and short intervals under the neuromuscular activity of finger flexion to investigate the independent variation mechanisms between EEG and EMG. Our results demonstrate that there is high causality in the short time interval and stimulation mode. The research may provide a reference for clinical and rehabilitative treatment protocol in the future.*

Keywords: *Cortico-muscular coherence, neuromuscular activity, median nerve, Partial Directed Coherence*

Introduction

Cortico-muscular coherence (CMC) analysis is greatly concerned in recent years as it can provide some advantage in neuromuscular research. Since the early 1990s, extensive studies of cortico-muscular interpreted that EEG-EMG coherence is diverse among alpha-, beta-, and gamma-range [1]. Over the last decade, the CMC research mainly concentrated on specific tasks. As revealed by Hashimoto (2010), the task-related EEG power increasing during motor execution and motor imagery grow with the EEG–EMG coherence peaks [2]. In respect of clinic, it was found that a wide range of cortical regions may influence EMG activity in the affected muscles after stroke [3]. Here, the authors analyze the EEG from C3/C4 channels and the sEMG from flexor digitorum superficialis in different motion modes (voluntary, median nerve stimulated and imaginary motion) and intervals to demonstrate internal relation and mechanism of coupling fluctuation between central and muscular systems.

Methods

Experimental Design: Ten right handed healthy volunteers were recruited to participate in this research aging between 23 -27 years. All subjects were fully rested. Each subject was seated in a chair with a straight back. The experiment collected EEG from C3/C4 channels using A1/A2 as reference. Attached to the subject's arm, two FES electrodes outputted pulses in the median nerve stimulation mode. During the experiment, subjects were asked to perform four modes of tasks under each interval (2s and 10s): (1) remain in a resting state (2) be stimulated median nerve with a pulse of 100μS width and 0.5Hz at an increasing current which begins with 5mA (3) twist the middle finger of right hand briskly (4) imagine twisting the middle finger of right hand. In each task, EEG and sEMG were sampled for 60s.

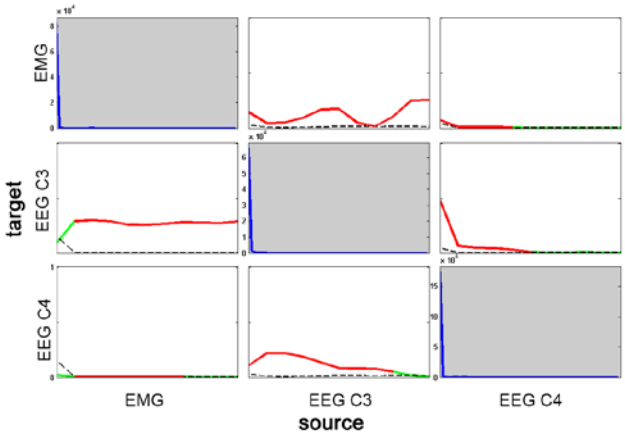

Figure 1: An example of the PDC analysis of subject S1 under short-interval stimulated motion mode. The horizontal axis represents the source of PDC, while the vertical represents the target which has a rage from 0 to 1. Diagrams on diagonal were auto power spectrums of EEG or sEMG.

Signal Processing: To get pure EEG and sEMG signals, band-pass filters are adopted (EEG: 0.5Hz-40Hz, sEMG: 5Hz-200Hz). In the stimulation mode sEMG signal should be treated with a different process since the FES electrodes are quite close to the recording electrodes. To this end, a two-point peak threshold detection algorithm is used in pre-processing in order to eliminate the stimulus artifact of FES. Partial Directed Coherence (PDC) is an approach to describe the concept of Grange causality in the frequency-domain. PDC is applied in data analysis as a means of estimating the relevancy between multivariate neural systems [4]. A PDC diagram (see Fig. 1) can give a visually description of the causal analysis result. An improved cross-correlation coefficient which overcomes the limitation of 40Hz is also applied to evaluate the correlation using the following formulae:

$$S_{c1,c2}(f_1 f_2) = \frac{1}{n}\sum_{i=1}^{n} C1_i(f_1)C2^*_i(f_2) \quad (1)$$

$$Coh_{c1,c2}(f_1 f_2) = \frac{|S_{c1,c2}(f_1 f_2)|^2}{|SP_{c1}(f_1)| \times |SP_{c2}(f_2)|} \quad (2)$$

here Sc1,c2(f1f2) is the cross-spectrum for c1 at a frequency f1 and c2 at a frequency f2. With improved cross-correlation algorithm, we can calculate the coefficient of the 0-40Hz EEG and the 0-200Hz EMG. The top 5% cross-correlation coefficients were chosen to be the extreme points of coherence that were divided to alpha-, beta-, and gamma-range. The extreme points of each band range were summed as an evaluating index. Following comparative experiments were discussed under each interval (2s and 10s): (1) voluntary motion (2) stimulated motion (3) imaginary motion.

Results

The EEG-EMG correlation can be measured by the PDC coefficient which is shown in Figure 2. In order to be more reliable, a statistical average of subjects was used as final comprehensive assessment indicator.

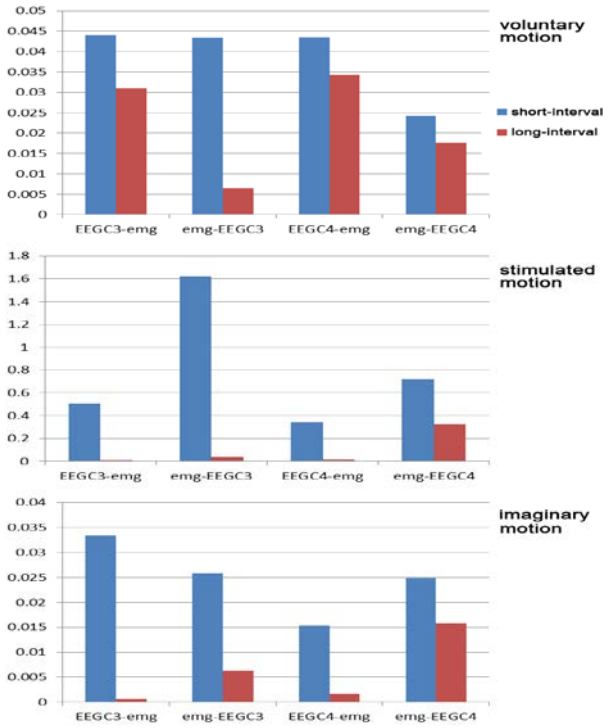

Figure 2: A comparison of the PDC coefficient under different motion modes and intervals.

In voluntary motion, an opposite brain activity was the cause of sEMG, and sEMG was the cause in stimulated motion which had a higher EEG-sEMG PDC coefficient. There were no significant relationships between EEG and sEMG signals in imaginary motion mode, which could possibly be explained that sEMG signal was weak without a motion. In all three modes, we found that there was a communication between left and right brain, while ipsilateral EEG was not associated with sEMG. When the time interval was considered as a variable, short-interval PDC coefficient performed more dramatically than the long-interval one. One possible reason is that the neurons in the brain are activated all the time in the short-interval mode; however, neurons had enough time to be calm and adequate rest in the long-interval mode.

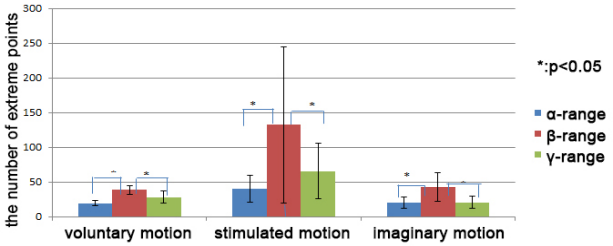

Figure 3: The number of coherence extreme points under long-interval mode.

For the comparison of extreme points of coherence, beta-range gained the most points (see Fig. 3). The analysis result under the stimulated demonstrated the same tendency with the PDC analysis.

Discussion

The purpose of this research is to explore the correlation between EEG and sEMG in different time intervals and different movement modes. Through the combination analysis, it was found that there was high causality under the short time and stimulation mode, which may be relevant to the EEG information overlapping under short time interval movement and more excited brain neutrons and higher domination for limbs movement. The research conclusion may contribute to a better understanding of motor and coordination abilities of human neuromuscular system and may provide a reference for the clinical rehabilitation treatment protocol in the future.

Acknowledgement

This research was supported by National Natural Science Foundation of China (No. 81222021, 31271062, 61172008, 81171423, and 51007063), National Key Technology R&D Program of the Ministry of Science and Technology of China (No. 2012BAI34B02) and Program for New Century Excellent Talents in University of the Ministry of Education of China (No. NCET-10-0618).

Bibliography

[1] Mima, Tatsuya, and Mark Hallett: "Corticomuscular coherence: a review. " *Journal of Clinical Neurophysiology,* vol. 16(6), pp. 501, 1999

[2] Yasunari H, et. al.: Correlation between EEG-EMG coherence during isometric contraction and its imaginary execution, *Acta Neurobiol Experimentalis,* vol. 70, pp. 76-85, 2010.

[3] Holly E. Rossiter, et. al.: Changes in the location of cortico-muscular coherence following stroke, *NeuroImage: Clinical,* vol. 2, pp. 50-55, 2013.

[4] Baccala L A, et. al.: Partial directed coherence: a new concept in neural structure determination, *Biological cybernetics,* vol. 84(6), pp. 463-474, 2001.

Comparison of electric field distribution between simulation and measurement results in vitro.

Klaus Peter Koch[1], Pascal Martini[1], Peter Gänz[1], Christian Diekow[1,2]

[1]Department of Engineering, Trier University of Applied Sciences, Germany
[2]MED-EL Elektromedizinische Geräte Gesellschaft m.b.H., Innsbruck, Austria

Koch@hochschule-trier.de

Abstract: *For electrical stimulation of biological tissue the field distribution around the electrode could be used to understand the effects of different electrode geometries and stimulation parameters on the biological system. This paper presents the comparison two methods for determination of the electrical field. The comparison were performed on a simple in vitro configuration with homogenous field distribution. Further the influence of the measurement probe on the field distribution was investigated. It could be shown that measurement and simulation has similar results that fit to the theoretically expected values.*

Keywords: *electrical field measurement, electrical stimulation, FEM simulation*

Introduction

Electrical stimulation is used in different applications including active implants. The efficiency and selectivity of the stimulations depends on the electric field at the target structure e.g. nerves. For the estimation of the electrical field around the stimulation electrode finite element method (FEM) was used. Nevertheless the quality of the simulation depends on the available model of the tissue and the electrode. For evaluation of the field simulation we have designed a measurement setup to measure 3 dimensional field distribution [1]. This paper focus on the comparison of electric field distribution between FEM-simulation results and measurements on simple electrode setups.

Methods

The configuration of the stimulation electrodes was a simple cubic chamber. Microscope glass slides were used as bottom as well as two of the walls of the chamber. Stainless steel was used for the two front walls as stimulation electrodes. The top of the chamber was open to allow the measurement with a field probe. The length and the width of the chamber was 76 mm and 26 mm respectively. The chamber was filled up to a height of 21 mm with 0.9 % sodium chloride solution at 23 °C. The electrical current source with an amplitude of 100 µA and a frequency of 1 kHz was connected to the stainless steel walls.

Measurement: For the measurement a field probe was moved by a 3D positioning system (Physik Instrumente, M-404.4PD) in length, width and height of 16.55 mm, 20.7 mm and 9 mm with step size of 3.31 mm, 2.3 mm and 2.25 mm respectively. As measurement probe the recording area of an EMG needle electrode (Schuler, 320050) was used. The needle was used in standard configuration (orthogonal to electrical field). For the measurement with differential amplifier the cannula of two additional needle electrodes (Schuler, 320050) were placed in the solution near to one of the front walls as ground and reference electrode. The output signal of the custom made differential amplifier with a selected amplification of 100 was recorded by an analog to digital converter card (National Instruments, NI PCI 6259). The complete setup was controlled by software programmed under Labview (National Instruments, Labview 2011). As post processing the numerical gradient of the electrical potential was calculated as electrical field strength (Matlab R2012b).

Simulation: The FEM simulation in COMSOL4.3a was performed in stationary conditions with a conductivity of the NaCl solution of 1,408 S/m (25°C) [2] and a conductivity of the cannula of 4.03 MS/m. For comparison of the results the evaluated position in the simulation was in the middle of the opening of the cannula similar to the position of the recording area of the EMG needle (Figure 1).

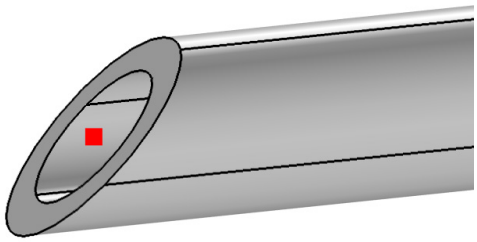

Figure 1: tip of EMG needle: red square evaluated point

The needle position was simulated at y = 13 mm and z = 10.5 mm and different positions in x direction from 20 mm to 50 mm in 2 mm steps. The needle was simulated in standard configuration (orthogonal to electrical field) and with 10 mm of the tip bended in 90 ° (parallel to electrical field). The electrical field was defined as difference between the voltages divided by the step size.

Results

Measurement: The electrical field of the measured area was in a range from 0.125 V/m to 0.135 V/m (Figure 2).

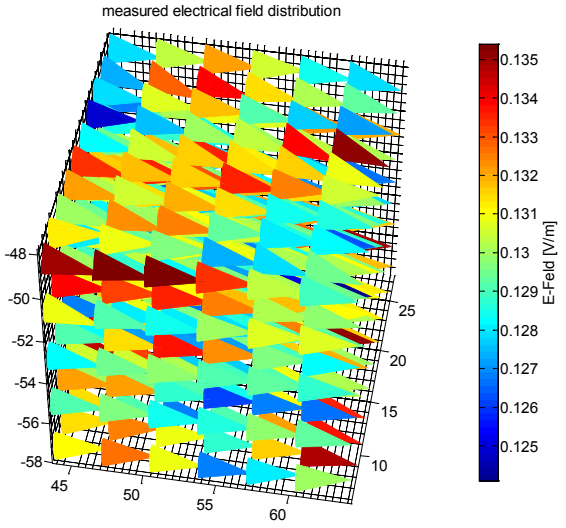

Figure 2: Measured electrical field with orthogonal needle positions

Simulation: The electrical potential as well as the electrical field strength of simulations with measurement probe in different directions and without measurement probe were compared. The electrical potential was increased by the measurement probe (Figure 2).

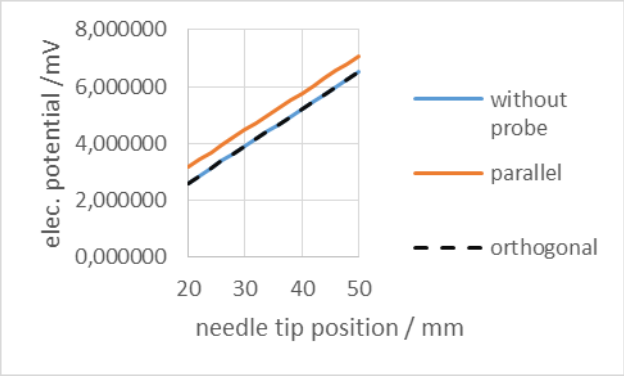

Figure 3: Simulated electrical potential at different needle positions and configurations

Also the electrical field was not influenced by the measurement probe (Figure 3).

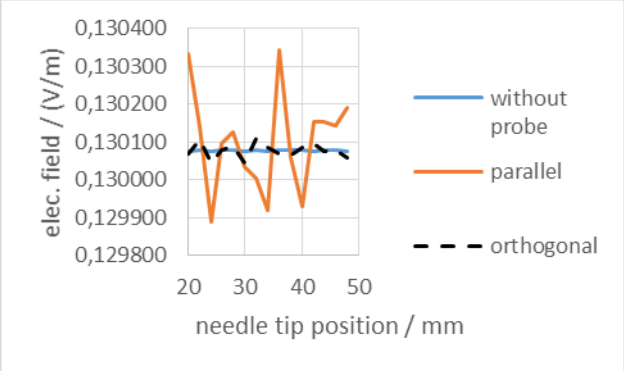

Figure 4: Simulated electrical field at different needle positions and configurations

The influence on the electrical potential is mainly for the probe that is placed parallel to the main field direction in comparison to the probe. The probe that is placed orthogonal to the main field show no significant influence on the electrical field. No significant influence on the evaluated electrical field could be observed for both probe configurations.

Discussion

The needle in parallel to the main electrical field influences the electrical potential by the short circuiting of to a higher potential region. As the needle tip (recording point) was at the lower potential side, the potential at that point was influenced by the complete surface of the cannula. As the electrical field is a relative measurement the influence on the electrical potential not influence the electrical field. The movement of the needle crease regular steps in the value of the electrical potential. In this configuration the electrical potential is mainly defined by the current density and the conductivity of the solution. Therefore no influence on the simulated electrical field can be observed with different needle configurations. For other configurations with inhomogeneous field distribution this could be critical. Even the model does not consider the phase boundary, the influence of the needle needs to be evaluated in more detail. Therefor measurement probes with insulated cannula is recommended for future measurements.
The results of the field measurement had a range of 5% around the expected value by the calculation. This is related to noise in the non-shielded measurement setup. For future versions of the measurement setup this needs to be improved. Nevertheless the results show that the measurements and simulation have the same outcome.

Acknowledgement

The project was funded by the Stiftung Rhienland-Pfalz für Innovation (Grant number 1016) and the company MED-EL Elektromedizinische Geräte Gesellschaft m.b.H..

Bibliography

[1] Martini P, Cercone M, Cheetham J, Koch KP.: "Experimental electrical field distribution measurements in a perfused *ex vivo* model.", Biomedizinische Technik in Jena, 2012, *Biomedizinische Technik Supplement 1*, 57, bmt-2012-4147 (2012).

[2] Yoshida K, Struijk J:"The Theory of Peripheral Nerve Recording" in Horch KW, Dhillon GS:"Neuroprothetics Theory and Practice" World Scientific Publishing 342-427 (2004).

Comparison of Current and Voltage Control Techniques for Neuromuscular Electrical Stimulation in the Anterior Thigh

José L. Vargas Luna[1,2], Matthias Krenn[1], Jorge A. Cortés[2], Winfried Mayr[1]

[1] Center for Medical Physics and Biomedical Engineering, Medical University of Vienna, Austria
[2] Centro de Innovación en Diseño y Tecnología, Tecnológico de Monterrey, Campus Monterrey, Mexico

jl.vargas.phd.mty@itesm.mx

Abstract: *A comparison between current control (CC) and voltage control (VC) techniques for functional electrical stimulation (FES) with different electrodes was done. A dependency on current of the ohmic resistance of the skin-electrode interface was found. A controllability study shows that the CC offers more controllability since both amplitude and pulse width (PW) of stimulation are suitable parameters for control, unlike VC, where only the amplitude is able to control the output for PWs bigger than 200µs. An efficiency study shows that large PWs are electrically inefficient since not all the applied energy is use for neuromuscular or muscular excitation and up to 50% of the energy is absorbed by the tissue. Based on these, basic suggestions for parameter selection are given to minimize the risk of tissue damage and improve electric efficiency at least for our specific set-up.*

Keywords: *Current-control, voltage-control, skin-electrode interface impedance, efficiency*

Introduction

Neuromuscular electrical stimulation is well established for rehabilitation and diagnostics. The stimulator design is in most cases based on voltage controlled (VC) or current controlled (CC) output stages. VC devices are considered to be safer than CC for transcutaneous applications, because loss electrode contact surface does not lead to dangerous high current density. On the other hand, motor unit recruitment under CC stimulation is more reliable, most likely due to the fact that the delivered current is more or less independent from electrode impedance.

However, many studies demonstrate that the skin-electrode interface impedance plays an important role in the stimulation dynamics, and several models have been proposed as equivalent circuits [1], [2]. It is aimed that this impedance variations indirectly affect both kinds of stimulation in effectiveness and controllability.

An important aim of this work was to identify the differences in the control dynamics of both stimulation control techniques and the effects of electrode selection.

Methods

Multivariable measurements were done in order to investigate the dynamics of the stimulation. CC and VC stimulation were applied to 6 subjects using two different surface electrode types of 8x13cm (self-adhesive STIMEX, Schwa-Medico GmbH and custom-made conductive rubber electrode). For the CC stimulation a Stimulette DEN2X (Schuhfried Medizintechnik GmbH, Austria) and for VC stimulation a custom-made device were used. The neuromuscular stimulation was applied transcutaneously on the anterior thigh. The output force was measured with a custom-build dynamometer chair detecting isometric force in three dimensions. Each stimulus was monitored in both voltage and current. Finally, evoked myoelectric signals (M-wave) were recorded from rectus femoris and hamstrings. The EMG electrodes were placed in a transversal disposition instead longitudinally to reduce excessive stimulus artefacts and amplifier overdrive in the EMG recordings.

The whole protocol was divided in four stages: (1) CC with self-adhesive hydrogel electrodes (ETD), (2) VC with ETD, (3) CC with conductive rubber electrodes (ETR) and, (4) VC with ETR.

Stimulation sweeps with pulse widths (PW) modulation from 2x50µs to 2x1000µs were done. The stimulations amplitudes were varied from the sensory threshold until ±120mA (in steps of 5mA) and ±60V (in steps of 5V) for CC and VC respectively. All stimulation impulses were rectangular charge-balanced biphasic pulses.

In order to compare both stimulation techniques the electrical energy applied and the current injection during the whole pulse were considered as parameters. The detected forces were transformed to a 3D vector and only the magnitude was considered for analysis. The selected equivalent electric circuit for the skin-electrode interface is shown in Fig. 1. The impedance was estimated fitting the curves to the equations that govern this circuit. For the estimation, R_s, R_p and C were considered constant within each pulse, but not between pulses.

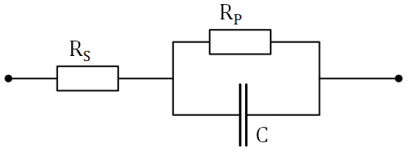

Figure 1: Equivalent model proposed for the skin-electrode interface.

Results

The impedance approximation was only valid for CC stimulation, since VC didn't follow the exponential behaviour of the circuit. The impedance results are shown in Fig. 2, only for CC. The recruitment curve is shown in Fig. 3, for both electrodes and techniques. A comparison between charge and energy is shown in Fig. 4, for isotonic curves (10N and 20N).

Discussion

The high dependence (up to 5 times the saturation value) of R_p to the stimulation intensity was congruent with other studies [2–4]. R_s and C variation due the stimulation amplitude were neglectable. Such dependency was addressed to the current amplitude since only CC stimulation was well-described by the proposed circuit, and system response at a given amplitude and different PWs shows no significant difference.

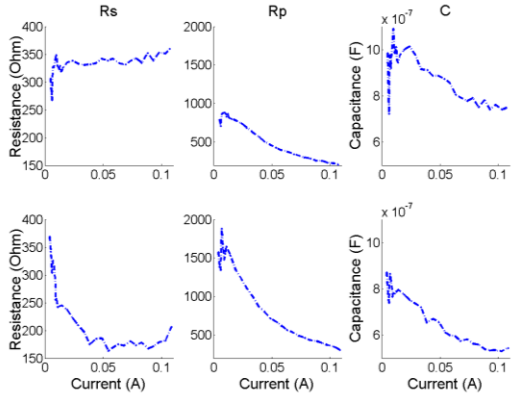

Figure 2: Impedance parameter estimation for CC stimulation with the ETR (upper part) and ETD (lower part) electrodes

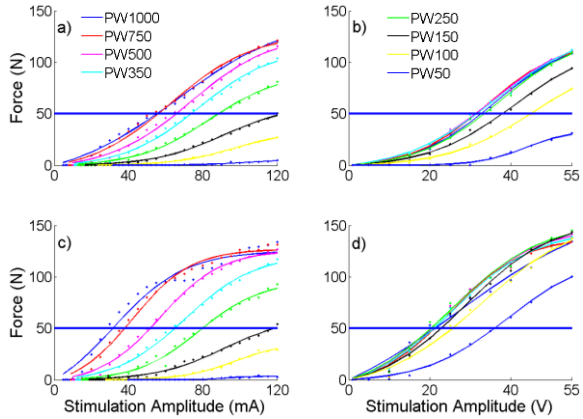

Figure 3: Recruitment curves for a) CC with ETR, b) VC with ETR, c) CC with ETD, and d) VC with ETD

Important differences on CC and VC techniques were found by means of its controllability. Both techniques were able to reach similar output force ranges. However, CC showed better characteristics since both stimulation amplitude and PW are suitable control parameters, unlike VC, were only the amplitude affect the output force significantly on PWs bigger than 200µs. This is visible in Fig. 3 for an induced contraction force of 50N, where it is evident that CC provides more freedom in control by either PW or amplitude variation than VC, where PW related traces bigger than 200µs for ETR and 100µs for ETD overlap, and only the variation of the amplitude can lead to the desired output force.

The electric efficiency in both techniques had the same behaviour as seen in Fig. 4. Beyond differences in the magnitude between techniques, it can be observed that, in general, huge PWs require more energy and inject more charge during the stimulus than smaller PWs. This means that energy was absorbed by mechanisms different to neuromuscular stimulation. This absorption leads to a difference of up to 50% for CC and 35% for VC on energy required for obtain the same output force. On the other hand, smaller PWs showed a tendency to require more electric energy to be delivered. For our set-up PW of 200µs showed a better performance by means of charge and electric energy delivered, it means a reduction of risk of tissue damage and an improvement in the power efficiency of the device.

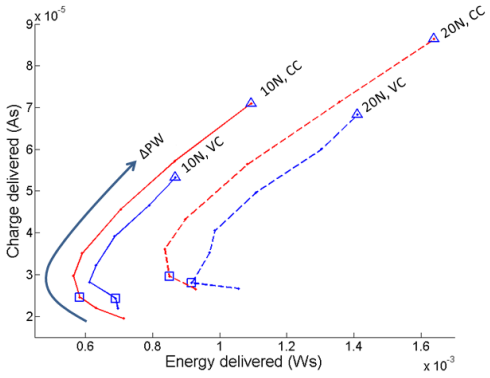

Figure 4: Comparison between necessary charge and energy to generate the stimulation impulse able to induce contraction force of 10N (continuous line) and 20N (dashed line) with CC (red) and VC (blue). Triangle indicate a duration impulse of 1000µs, and the square a duration impulse of 200µs. ΔPW arrow indicates direction of PW increasing

Regardless the current dependency of the impedance, it was observed different variation ranges of it for the two different electrodes. These differences due the material and construction of the electrodes were also reflected in the recruitment curve, showing that both CC and VC are dependent on electrode configuration.

Although these results are also valid for our set-up and further research is necessary to generalize these results, the methodology may be useful to optimizing stimulation parameters in various application scenarios.

Bibliography

[1] G. Kantor, G. Alon, and H. S. Ho, "Simulated tissue loads for testing of transcutaneous electrical stimulators," in *Proceedings of 16th Annual International Conference of the IEEE EMBS*, pp. 784–785, 1994.

[2] S. J. Dorgan and R. B. Reilly, "A model for human skin impedance during surface functional neuromuscular stimulation.," *IEEE transactions on rehabilitation engineering*, vol. 7, no. 3, pp. 341–8, Sep. 1999.

[3] D. R. Davis and D. W. Kennard, "Influence of Electric Current on the Skin," *Nature*, vol. 193, no. 4821, pp. 1186–1187, Mar. 1962.

[4] S. Grimnes, "Skin impedance and electro-osmosis in the human epidermis," *Medical & Biological Engineering & Computing*, vol. 21, no. 6, pp. 739–749, Nov. 1983.

A WIRELESS FUNCTIONAL ELECTRICAL STIMULATION SYSTEM

Adrian Derungs[1], Christian Dietrich[1] and Kenneth J. Hunt[1]

[1]Institute for Rehabilitation and Performance Technology
Division of Mechanical Engineering, Department of Engineering and Information Technology
Bern University of Applied Sciences, Switzerland

adrian.derungs@bfh.ch

Abstract: *A system for wireless electrical stimulation was designed and the feasibility evaluated. The Bluetooth communication standard and two different microcontroller systems provided the basis of the system design. The prototype allows four channels of stimulation whereby each stimulator unit contained two channels. The design permitted the possibility of generating voltage controlled biphasic stimulation patterns for muscle activation. The accuracy of stimulation parameters including pulse width, inter-pulse time, baud rate, latency, range, stimulator power consumption and also muscle stimulation were evaluated and feasiblity thereby established. Further research should solve the problem of latency in wireless communication and extend the system with sensors to design closed-loop control strategies.*

Keywords: *wireless, Bluetooth, Real-Time Operating System, four-channel FES, applications*

Introduction

Functional Electrical Stimulation (FES) provides various approaches for rehabilitation of patients who suffer paraplegia or stroke. FES allows restoring and maintaining motion, and activities of daily living (ADL) can be performed. This gives disabled people the opportunity for independence. These facts served as the motivation to implement a novel wireless device for FES. The aim of this research project was the development of a complete system to demonstrate the feasibility of wireless stimulation with four channels. A key design requirement was that each remote stimulation unit had two channels, purposely allowing activation locally of a pair of agonist-antagonist muscle groups at a given joint. The scope was defined by the requirement to evaluate feasibility. The literature shows one provisional paper regarding a wireless FES solution [1]. Most commercially available products for FES in sport and rehabilitation are not currently wireless (an exception is the *COMPEX Wireless* system from Compex) but the technology is promising for a range of products and applications.

Methods

The wireless FES system consists of two stimulators each with two channels to stimulate an antagonistic pair of muscles (Fig. 1) and one coordinator controlling the stimulators. The basis for the coordinator was a microcontroller evaluation board (MCBSTM32EXL, Keil). The coordinator ran with a real-time operating system (Keil RTX) which allowed adjustment of stimulation patterns and Bluetooth configuration via a joystick. For data transmission, Bluetooth modules were connected to the microcontrollers. For mobility, the stimulator was supplied by a 7.4 V *Li-Po* battery and enclosed in a $70 \times 52 \times 35$ mm portable case fitted with a belt to mount the stimulator to the limbs. The stimulator was voltage regulated and generated biphasic pulses of 30 V or 50 V using a boost converter. An 8-Bit microcontroller (Atmega328 Mini R5, Arduino) was used to control the stimulation patterns. The code was written with Arduino's integrated development environment (IDE). To display communication and stimulation status, LEDs were mounted on the board. For muscle stimulation, surface electrodes were used, connected to the board via USB connectors. The stimulator algorithm interpreted received data and generated desired pulses. Several modes were programmed to select the number of activated channels and pulse patterns. The pattern (Fig. 2), was defined by parameters *Mode*, *PulseTime*, *InterPulseTime*, *RestOfPeriod*, *Repetitions*, *Drift* and *OverallRepetitions*, thus determining a desired stimulation frequency.

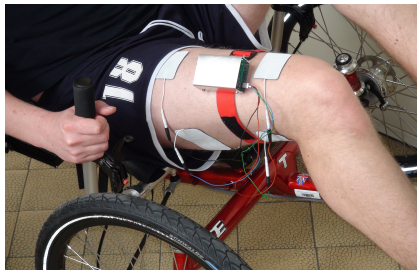

Figure 1: One stimulator with two channels.

Results

A prototype for wireless stimulation with four channels was developed. The use of Bluetooth modules enabled a communication range of 45 m indoors. Boost converter output voltage was reliable and stable and had a deviation to the calculated output voltage of 2.2 % for the stimulator with 30 V and 1.2 % for the stimulator with 50 V. Modulation time of signals with respect to baud rate was calculated to be maximally 9.8 % with respect to measured modulation time. Therefore measurements with different amounts of data were made.
Additionally, it was demonstrated that latency for data

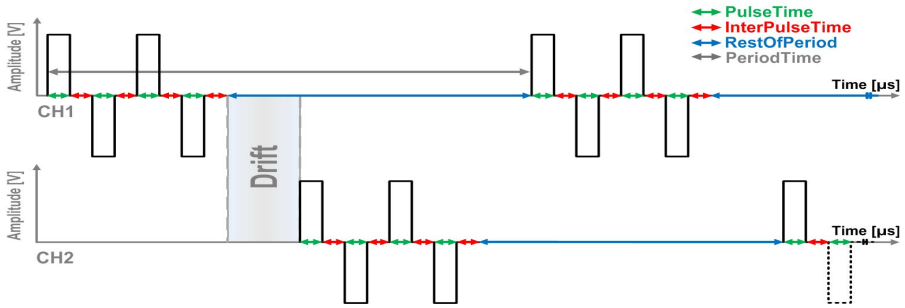

Figure 2: Two channel stimulation patterns with drift-time, the delay between antagonistic muscles.

transmission was 16.82 ms, 20.57 ms and 41.76 ms for baud rates of 115200 Baud, 57600 Baud, and 9600 Baud, respectively. Within this measurement series (n = 20) the amount of data remained constant (190 Bits). A second measurement concerning latency used the same baud rate (115200 bits per second) but varied the amount of data (10 Bits to 54000 Bits averaged over a series of 10 measurements). This showed a trend towards increased latency with increasing amounts of data.

Stimulation was as expected for different loads. For a pure resistive load the current followed the specified biphasic rectangular shape. For loads with capacitive elements (tissue and muscle) the current had an exponentially decreasing shape. Considering adjusted pattern parameters, 20 % of the parameters tested deviated more than the specified 10 %. Fig. 3 shows an acceptable pulse width deviation. Performance of the new voltage-driven muscle stimulator was further evaluated by comparing its waveform with that of a commercial current-controlled stimulator (RehaStim, Hasomed GmbH, Germany). Typical behavioural characteristics are shown in Fig. 4.

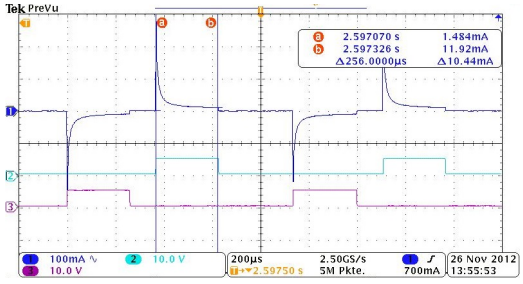

Figure 3: Measured (256 μs) vs. specified (250 μs) pulse width.

Discussion

The objective of a mobile stimulation unit with four channels, i.e. two pairs of two channels, was fulfilled. The measured output voltage of the booster corresponded with specifications given in the datasheet. The required time for data modulation was determined analytically and coincided with the measurements. Handling Bluetooth latency is a challenge for further development as a consequence of its inconsistency. It was observed that latency correlated with baud rate and with the amount of data. Further research in the details of the Bluetooth standard may allow optimisation of latency problems.

We conclude that the successful implementation and evaluation of a wireless FES system with four channels was technically feasible. The decision to implement a system based on a microcontroller was justified by the demand for mobility. Despite the limitations of Bluetooth, the presented work has potential for further technical development towards effective wireless stimulation solutions.

Future research should address the challenges of wireless communication including latency, where low-power radio technology (e.g. ANT+) could be an alternative approach. Furthermore the number of channels must be increased for an application like FES-cycling [2]. Additional topics for further development include pulse pattern waveforms, variable frequency trains and advanced wireless-based and local closed-loop control of induced muscle contractions [3], thus aiming towards more physiological stimulation to overcome rapid muscle fatigue.

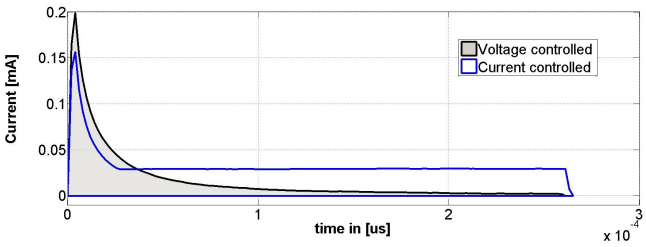

Figure 4: Voltage- vs. current-controlled muscle stimulation.

Bibliography

[1] N. Jovicic, L. Saranovac, and D. Popovic, "Wireless distributed functional electrical stimulation system," *Journal of NeuroEngineering and Rehabilitation*, vol. 9, no. 1, p. 54, 2012.

[2] K. J. Hunt, J. Fang, J. Saengsuwan, M. Grob, and M. Laubacher, "On the efficiency of FES cycling: A framework and systematic review," *Technology and Health Care*, vol. 20, no. 5, pp. 395–422, 2012.

[3] C. Lynch and M. Popovic, "Functional electrical stimulation," *IEEE Control Systems Magazine*, vol. 28, pp. 40 –50, April 2008.

STEP SIDE RECOGNITION BASED ON HANDLE REACTION FORCES DURING FUNCTIONAL ELECTRICAL STIMULATION

Rui Xu, Shuang Qiu, Tianchen Zhai, Qiang Xu, Hongzhi Qi, Peng Zhou, Lixin Zhang, Baikun Wan, Dong Ming*

Lab of Neural Engineering & Rehabilitation, Department of Biomedical Engineering, College of Precision Instruments and Optoelectronics Engineering, Tianjin University, Tianjin 300072, China

*Corresponding author: richardming@tju.edu.cn

Abstract: *In this paper, we developed and tested a novel sensing and processing method for the potential to recognize the active step side direction using handle reaction forces (HRF) during walker-assisted FES-activated walking. The HRF were collected from a dynamometer system based on 12-strain gauge bridges instrumented on the walker frame. The features of active step side direction were extracted from the HRF through k-means clustering analytical method, recognized by support vector machine and finally evaluated by k-fold cross-validation. The results showed that the mean recognition rate was 79.3% for a group of 10 subjects while the highest recognition rate reached 96.8% for the individual. Additionally, the recognition rate cross subjects reached nearly 80.0%. This favourable performance indicated an attractive possibility of HRF as a natural command source to improve the intelligence control of FES system.*

Keywords: *Functional Electrical Stimulation, Handle Reaction Forces, Clustering, Support Vector Machine*

Introduction

Functional electrical stimulation (FES) provides an opportunity for wheelchair-dependent individuals with spinal cord injuries (SCI) to achieve brace-free ambulation. In FES systems, sensing technologies can reliably distinguish the active step side direction of stimulated movement. In previous studies, Kevin L. Kilgore et al established a second-generation FES neuroprosthesis that users controlled their stimulated function through EMG signals [1]. Another study explored the pathological applications of EMG in FES control, indicating that the surface EMG (sEMG) from partially paralyzed muscles in an individual with motor incomplete injuries could be used by a linear classifier to detect the intent to initiate a step during walking and trigger electrical stimulation [2] . Actually, the application of these EMG signals for paralyzed patients was limited. Therefore, we suggested step side direction information of individual's moving coming from handle reaction forces (HRF) which were extracted from walker dynamometer system.

The goal of our study was to introduce a novel operation based on HRF for step side recognition, and to validate that HRF was potential to predict side step information for the FES automatic control during assisted walking. This could provide a stable solution to prediction of FES side control and give help to the advanced motor neuroprostheses system design for lower limbs.

Methods

Experiment: The experiment was recruited, which consisted of 10 healthy subjects (5 male and 5 female, mean age of 24.1 ± 1.4 years, range 22-26), without known neurological disorders and serious cardiopulmonary ailments. They were required to step only under FES with the walker.

Walker Dynamometer System: The instability of patients' walking was transferred from patient to walker by the force of upper extremities, in other words handle reaction forces (HRF) [3], can be defined as

$$HRF = \left[HRF_l, HRF_r\right]^T = \left[F_{lx}, F_{ly}, F_{lz}, F_{rx}, F_{ry}, F_{rz}\right]^T \quad (1)$$

where F_{lx}, F_{ly}, and F_{lz} are the forces applied on the left handle of the walker in *x*-, *y*- and *z*-direction respectively, and F_{rx}, F_{ry}, and F_{rz} are the forces exerted on the right handle.

K-means Clustering Algorithm: The *k*-means clustering algorithm was used here to extract feature values from HRF. There were three user-specified parameters in the *k*-means algorithm, including number of clusters *k*, cluster centre initialization, and distance metric. The number of clusters *k* was the number of groups which the data finally would be divided into. So *k* was set to 2 in order to get two eigenvalues during one gait cycle. The cluster initialization was very important for the method was sensitive to initial positions of cluster centres. Here we randomly select two samples of the force instance as the centre initializations. Distance metric was shown in Eq. 2.

$$d_{ij} = \left| f_j - c_i \right| \quad (2)$$

Support Vector Machine: Our problem could be regarded as a 2-class problem, which was the fundamental problem in classification methodologies. And the two classes were Class L (meaning stepping left via FES) and Class R (meaning stepping right via FES) respectively.

In the training session, the inputs were 12-dimentional feature vectors (shown in Eq. 3) belonging to Class L or Class R with the associated label $y_i = 1$ for Class L and $y_i = -1$ for Class R.

$$x_i = \left[c_{i1} \quad c_{i2} \quad \cdots \quad c_{i12}\right]^T, i = 1, \cdots, M \quad (3)$$

where M was the number of vectors in training set X and c_{i1} to c_{i12} were the 12 cluster centers of 6 forces in the ith gait cycle obtained by k-means clustering.

SVM was a kind of learning method based on kernel functions. Four kernel functions which had been commonly used in SVM included Polynomial (homogeneous), Polynomial (inhomogeneous), Radial Basis Function, Hyperbolic tangent. Different kernel functions led to different results of SVM classification. So it was necessary to choose proper kernel function when solving different problems. In our study, we investigated these four kernel functions for classification, and chose the best for subsequent research.

Results

To demonstrate the efficiency of features extracted by clustering algorithms, the support vector machine with 5-fold cross-validation was adopted to classification. The method of cross-validation means that part of data is used in training sessions, and the remaining data is used for evaluating the performance of the algorithm [4]. To reduce variability, multiple rounds of cross-validation are performed using different partitions, and the validation results are averaged over the rounds.

The recognition rates of SVM with different kernel functions were similar, so we took the result with Radial Basis Function as an example (shown in figure 1). The highest rate is 96.8% of Subject 8, the lowest is 55.8% of Subject 6, and the average of 10 subjects is 79.6%.

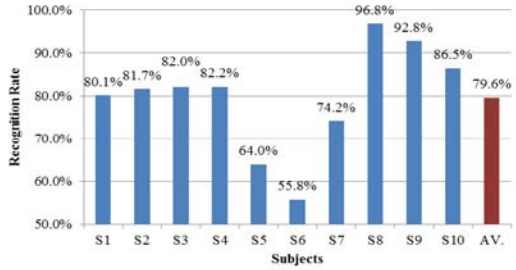

Figure 1: Recognition result of SVM with Radial Basis Function for individual.

In our study, the eigenvalues were extracted from HRF of the mixed 50 samples of 10 subjects using clustering arithmetic and recognized by support vector machines with the different kernel functions. The recognition rate of k-fold cross-validation (k=2, 3, 4, 5), is shown in figure 2, in which the recognition rate is between 63% and 80% with the highest 79.3%.

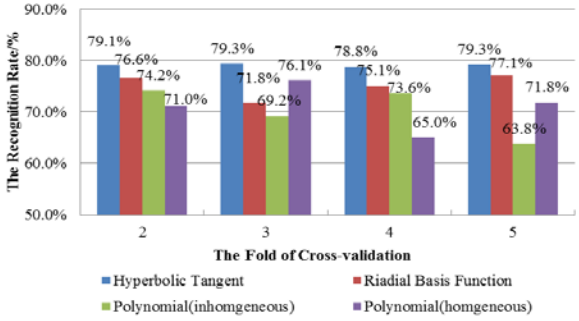

Figure 2: Recognition rate of the eigenvalues that were extracted from HRF by k-means clustering arithmetic used SVM with different kernel functions and k-fold cross-validation.

We can tell from the figure that SVM with Hyperbolic Tangent Function, which is robust to different folds of cross validation, is the best fit method.

Discussion

The feasibility of this HRF based features was tested through SVM. For single subject, the recognition rate of SVM was high enough to make two legs differentiable. But there were still some subjects with low recognition rates, which may have a relationship with the prophase of training they were subjected to and the instability of their walking. As to group recognition, the results were no doubt worse than the best individual result because of the differences in weights, strengths, and *et al* between different subjects. However, a proper classification method with nearly 80% recognition rate across individuals showed great potential for the step side direction control method proposed in this study. And necessarily, excess efforts should be taken in order to eliminate inter-individual differences and enhance the universality of FES system.

Our work on step side recognition laid the foundation of side prediction, which was the previous work for practical application of FES. The recognition rate in our study can reach above 85%. Hence, the method to extract features used in this paper is feasible. In future work, more subjects including patients will be recruited and the difference between healthy subjects and patients need to be analyzed.

Acknowledgement

This research was supported by National Natural Science Foundation of China (No. 81222021, 31271062, 61172008, 81171423, 51007063), National Key Technology R&D Program of the Ministry of Science and Technology of China (No. 2012BAI34B02) and Program for New Century Excellent Talents in University of the Ministry of Education of China (No. NCET-10-0618).

Bibliography

[1] Kevin L. Kilgore, Harry A. Hoyen et. al.: An implanted upper-extremity neuroprosthesis using myoelectric control , *J. Hand Surgery*,vol. 33, pp. 539-550, 2008.

[2] Anirban Dutta, Rudi Kobetic et. al.: Ambulation after incomplete spinal cord injury with EMG-triggered functional electrical stimulation, *IEEE Trans. Biomed. Eng.*, vol. 55, pp. 791-794, 2008.

[3] Zhaojun Xue, Dahai Wang et. al.: New gait recognition technique used in functional electrical stimulation system control, *Proc. 6th World Cong. Intelligent Control and Automation*, pp. 9421-9425, 2006.

[4] Arlot S and Celisse A: A survey of cross-validation procedures for model selection, *Stat. Surv.*, vol. 4, pp. 40-79, 2010.

A CASE STUDY FOR A NEW APPROACH OF A CONSTANT PRESSURE PERFUSED EX-VIVO MODEL OF THE EQUINE LARYNX

S. Otto, V. Tast, J. K. Michler, Ch. K. W. Mülling

Institute of Veterinary Anatomy, University of Leipzig, Germany

sven.otto@vetmed.uni-leipzig.de

Abstract: *This paper describes an improved setup for the perfusion of an isolated equine larynx under constant pressure conditions. Aim is to provide a reliable and standardized model for measurements of the three-dimensional electrical field distribution of implanted electrodes into the laryngeal muscles for the future treatment of hemiplegia laryngis in horses.*
The basic findings which are reported here provide an overview on the technical devices and show data of an exemplary case study.
Measurements were first performed to determine perfusion flow. Through increasing and decreasing the perfusion pressure and application of adrenalin it could be shown that the tissue reacted in its anticipated physiological function by adjusting the perfusion flow.

Keywords: *Horse, hemiplegia laryngis, functional electric stimulation (FES), ex-vivo model, perfusion*

Introduction

Hemiplegia laryngis, in horses also referred to as whistling or roaring, is caused by a dysfunction of the recurrent laryngeal nerve. The reported prevalence has an extremely wide range from 1.2-42% in different horse breeds [1].
Different surgical methods for the treatment of this disorder have been described. Laryngeal hemiplegia causes a relative upper airway obstruction because the recurrent laryngeal nerve shows a loss in its function to innervate the dorsal cricoarytenoid muscle (CAD). An electrical stimulation of the CAD leads to an opening of the upper airways [1].
One therapy option is called functional electric stimulation (FES). FES for this application was first described in 1977 [2]. In order to improve the outcome of this method, one approach is the measurement of the 3D distribution of the electric field around implanted stimulation electrodes [3].
The objective of this case study was to improve the ex-vivo model for the equine larynx used by Martini et al. [3] and to create a model which is intended to closely mimic the physiological in-vivo situation. Specific aims of our improved model were:
-reduction of swelling due to tissue edema
-examination of the myogenic autoregulation
-monitoring of the vessels´ physiological response through the application of adrenalin

The methodology for the perfusion in our ex-vivo model of the equine isolated larynx is outlined in this report.

Methods

One horse was euthanized in consent with the national council´s guidelines of animal care (protocol number: T66/13).
Reportedly, the horse had no hemiplegia laryngis and there were no signs of hemiplegia laryngis during our clinical examination. Via intravenous (i.v.) application of Xylazine (1 mg/kg) the horse was sedated and general anaesthesia was induced by i.v. application of Diazepam (0.08 mg/kg) and Ketamine (2.2 mg/kg). Finally the horse was euthanized with Pentobarbital (80 mg/kg).
The larynx was separated and both cranial thyroid arteries were catheterised for flushing the organ with a modified Tyrode's solution at 4°C. Subsequently, the larynx was immersed in the aforementioned solution. It was then transferred to the laboratory within half an hour.
Fig. 1 gives an overview of the experimental setup. The larynx was placed in an acrylic glass tub filled with pre-warmed perfusion solution (33°C) and was fixed at the bottom and the sides with elastomeric impression material (Eurosil Max 2, HENRY SCHEIN®, Langen). The above mentioned arterial vessels were connected to a closed constant pressure perfusion system. The perfusion solution was gassed with Carbogen (95% O_2, 5% CO_2, LINDE GAS, Unterschleißheim). The larynx was perfused with warmed perfusion solution (37°C) and constant perfusion pressure of 9.81 kPa for 2 hours.
Subsequently, perfusion flow was determined based on the difference between the influx and overflow (ΔQ) of the medium tank (Tab. 1). In order to achieve a constant influx rate a pump was used (Masterflex© Model 170100A, RADNOTI LLC, CA, USA). The overflow was measured by using a standardized glass cylinder. The perfusion pressure was increased to 10.89 kPa and the perfusion flow was measured again (Tab. 2). Afterwards, perfusion pressure was reset to the onset and measurement of perfusion flow was repeated (Tab. 3). Finally, 0.5 mg Adrenaline was injected into each cranial thyroid artery and perfusion flow was measured (Tab. 4).

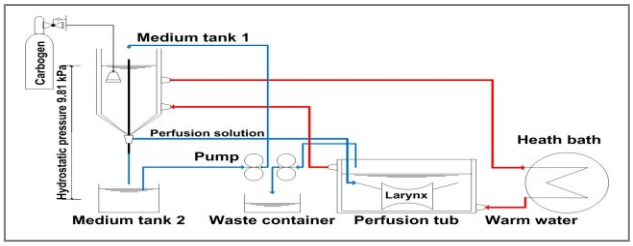

Figure 1: Diagram of the experimental setup

Results

The baseline flow after 2 hours of perfusion is shown in Tab. 1.

Table 1: Baseline perfusion flow at 9.81 kPa perfusion pressure

time (min)	1	2	3	4	5
ΔQ (ml/min)	30	28	30	30	26
calculated flow (ml/min)	70	72	70	70	74

Perfusion flow increased 2 minutes after the perfusion pressure was increased by 1.08 kPa and then decreased to the baseline perfusion flow after 5 minutes as shown in Tab. 2.

Table 2: Perfusion flow at 10.89 kPa perfusion pressure

time (min)	1	2	3	4	5
ΔQ (ml/min)	28	22	22	24	26
calculated flow (ml/min)	72	78	78	76	74

Perfusion flow decreased in relation to the initial perfusion flow 2 minutes after the perfusion pressure was reset to 9.81 kPa and then increased to the baseline perfusion flow (Tab. 3).

Table 3: Perfusion flow after perfusion pressure was reset to 9.81 kPa

time (min)	1	2	3	4	5
ΔQ (ml/min)	36	34	28	32	30
calculated flow (ml/min)	64	66	72	68	70

Finally the perfusion flow decreased markedly compared to all other measured perfusion flows after 0.5 mg Adrenaline had been administered via each cranial thyroid artery (Tab. 4).

Table 4: Perfusion flow after injection of 0.5 mg Adrenaline into each cranial thyroid artery

time (min)	1	2	3
ΔQ (ml/min)	54	62	60
calculated flow (ml/min)	46	38	40

The larynx visually showed no significant signs of tissue swelling.

Discussion

In this experiment, we developed a new approach of a pressure constant perfused ex-vivo model of the equine larynx and provide preliminary data on flow and myogenic response. To our knowledge, no data regarding the physiological perfusion flow of the equine larynx have been published.

Ex-vivo organs can be perfused in a flow constant or pressure constant model [4], [5]. When using a constant flow model, the knowledge of the physiological perfusion flow of the used organ is important in order to avoid an excessive perfusion of the organ.

The myogenic response (Bayliss effect) is a special effect in smooth vascular cells that helps to sustain a constant capillary flow independent of changes in arterial blood pressure [6]. Adrenaline is a typical α1-adrenoceptor agonist that causes vasoconstriction which in term leads to an increase of resistance and decrease of flow in vessels (Hagen-Poiseuille's law). We could show that after 2 hours of perfusion in our model the tissue of the larynx was still able to react properly in its anticipated physiological function by adjusting the perfusion flow showing maintained myogenic autoregulation. We were also able to minimize the swelling effects described by Martini et al. [3].

Using a larger number of animals would lead to more stable results. Also the use of histological methods and to weigh the used organ before and after perfusion could show the degree of tissue swelling more accurately.

Our model very closely mimics the in-vivo situation. It provides a reliable platform for further studies on the three-dimensional distribution of the electrical field of multipolar intra-muscular FES stimulation electrodes.

Acknowledgement

This work was supported by a grant from Medical-el Elektromedizinische Geräte GmbH, A-6020 Innsbruck, Austria. We thank Professor Dhein from the Heart Center Leipzig for his helpful and valuable comments on our study design and the Surgical Large Animal Clinic (University of Leipzig) for their kind support.

Bibliography

[1] Ducharme, N. G., Cheetham, Jon, et. al.: Considerations for pacing of the cricoarytenoid dorsalis muscle by neuroprosthesis in horses, *Equine Vet. J.,* vol. 42, pp. 534-540, Sept. 2010

[2] Zealear , D. L., Dedo, H.H.: Control of paralysed axial muscles by electrical stimulation, *Acta Otolaryngol.,* vol. 83(5-6). pp. 514-27, 1977

[3] Martini P., Cercone, M. et al.: Experimental electrical field distribution measurements in a perfused ex vivo model, *Biomed Tech*., vol.57, pp. 870-3, 2012

[4] Dhein, S.: „The Langendorff Heart" in *Practical Methods in Cardiovascular Research (S. Dhein, F. W: Mohr, M. Delmar, eds.)*, ch. 2.1, pp. 155-172, Berlin, Heidelberg, New York: Springer, 2005

[5] Langendorff, O.: Untersuchungen am überlebenden Säugethierherzen, *Pflügers Arch Ges Physiol*, vol. 61, pp. 291-331, 1895

[6] Bayliss, W. M.: On the local reactions of the arterial wall to changes of internal pressure, *J Physiol*., vol. 28, pp.220-231, 1902

BIOIMPEDANCE- AND EMG-TRIGGERED FES FOR IMPROVED PROTECTION OF THE AIRWAY DURING SWALLOWING

Nahrstaedt H[1], Schultheiss C[2], Schauer T[1], Seidl RO[2]

[1]Control Systems Group, Technische Universität Berlin, Berlin, Germany

[2]Department of Otolaryngology, Head and Neck Surgery, Unfallkrankenhaus Berlin, Berlin, Germany

nahrstaedt@control.tu-berlin.de

Abstract: *Dysphagia has a huge impact on the quality of life. Especially, the ability to elevate larynx and hyoid in order to guarantee airway protection is decreased in dysphagia during swallowing. In this contribution, EMG and Bioimpedance (BI) measurements at the neck are used for triggering functional electrical stimulation (FES) of the submental muscles at the transition from the oral phase to the pharyngeal phase of swallowing. It was demonstrated on a first patient that airway closure and elevating speed are improved using swallowing-triggered FES.*

Keywords: *FES, Bioimpedance, EMG, Dysphagia*

Introduction

An important part of therapeutic measures aims at improving airway protection in patients who are prone to aspirating during swallowing. Methods applied are conservative measures (e.g. dietary adaptation of food consistencies, muscle strengthening), compensatory measures (e.g. posture changes during swallowing) and sensory measures in which stimulation (cold stimuli, electrical stimulation, etc.) is used to improve sensitivity of the swallowing reflex. An additional method, by which a sensory feedback and a strengthening of the muscles could be obtained, is surface stimulation of swallowing related muscles. If the stimulation is applied in phase with the voluntary swallowing, improved airway protection may be achieved due to improved hyoid and larynx elevation.

Surface stimulation was firstly introduced in the study by Freed et al. [1] in which a fixed swallowing-independent electrical stimulation pattern was applied to patients 60 min per day. In the following years, a lot of studies, which used such swallowing-independent stimulation pattern, have been carried out with contradicting results. Leelaminit et al. [2] were stimulating the thyrohyoid muscle with surface electrodes synchronized to EMG from the posterior tongue in patients with reduced laryngeal elevation. The study showed promising results, however, the patients had to be treated for 4 h per day and submental EMG, which is only an unspecific indicator for the pharyngeal phase, was used to trigger the stimulation.

In our previous work [3], we have shown that swallows can automatically be detected using EMG and Bioimpedance (BI) measurements at the neck. This offline approach is converted in this work to an online detection method which is able to detect swallowing at the very beginning and is able to trigger FES for supporting swallowing.

Methods

The stimulation is triggered by the combination of a detected EMG activity at the submental and subrahyodial musculature and a swallowing related drop in the BI signal. The electrodes of the current source were placed on both sides of the onset of the sternocleidomastoid. The voltage measurement electrodes were placed laterally between the hyoid bone and the thyroid cartilage [4]. The measuring system PHYSIOSENSE has been used for measuring BI and EMG [3]. For electrical stimulation of the submental muscles, the RehaStim device (HASOMED GmbH, Germany) is used with one channel, by which the electrodes are placed on the left and right side of the digastric muscle above the hyoid bone [5].

Periods of muscle activation are detected by using a modified double-threshold detector which is able to detect EMG activity online with a fixed delay defined by the window length and the size of the onset-offset smoother.

The modified double-threshold detector consists of a sliding window noise variance estimator that continuously calculates the variance σ^2 in the signal. The window length is $0.25\,\mathrm{s}$ (i.e. 1000 samples at 4 kHz sampling rate), which was chosen assuming that the rest period between muscle contractions is longer than the window length. In such rest periods without EMG activity, the sliding window will contain only noise. Thus, the noise variance σ_n^2 is estimated by taking the all-time smallest value of σ^2.

The second sliding window of length $m = 60$ samples is updated every second sample. The muscle is considered active if $r_0 = 8$ values within the sliding window are above the threshold ζ. The threshold ζ is recalculated whenever the noise variance changes, according to [6] dependent on the estimated noise variance σ_n^2. Onset-offset-onset and Offset-onset-offset transitions which are shorter than $15\,\mathrm{ms}$ (120 samples) are rejected. This results in a delay of $15\,\mathrm{ms}$ for the online EMG activity detection.

In order to detect changes in the BI signal which are caused by swallowing, a piecewise linear approximation method (PLA) [7] is applied to the BI signal. For approximation, a modified sliding window algorithm is used. According to [7], the starting point of an approximating line is set to the first data point in the window. The line is then extended until the error between the line and the signal reaches the threshold $maxE$ or the difference between the last and first value exceeds $maxD$.

The stimulation of the submental muscle is activated when

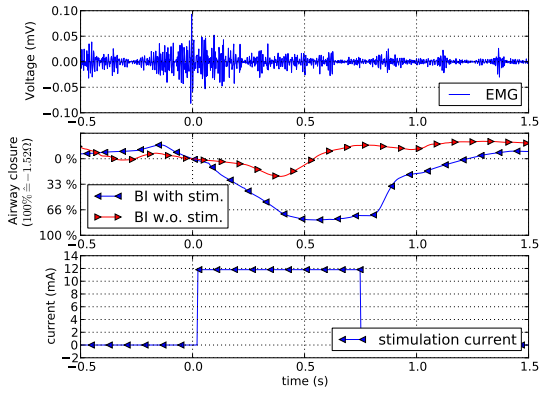

Figure 1: Assessment of a swallow with and without (w.o.) stimulation support. BI values for one patient are reported in comparison to mean values observed in healthy subjects.

slope and difference between start and end point of last and second to last approximated line of the BI signal are within a certain range. The stimulation is stopped when the slope of the approximated BI signal changes its sign. The thresholds (including $maxE$ and $maxD$) are extracted from a reference swallow without stimulation.

Results

In a first case study on a single patient, 13 swallows were recorded and the measured BI signal was compared to the normative values of healthy people in Tab. 1. Using the same measurement system, it was shown in [4] that BI correlates to the movement of hyoid and larynx and therefore correlates with airway closure. The patient was fed with thickened liquid while the stimulation triggering was switched off. After the patient had prepared the bolus and was ready to swallow, the stimulation triggering was activated. The stimulation support was then automatically activated as soon as EMG activity was present and the BI began to decrease until the BI was rising again. In Fig. 1, a swallow with stimulation support is compared to swallow without stimulation. The bipolar stimulation pattern with doublets (inter-pulse-interval of 5 ms) was set to a pulse width of 200μs and a stimulation frequency of 20 Hz. Round hydro-gel stimulation electrodes (⌀ 32 mm, KRAUTH+TIMMERMANN GmbH, Germany) were used.

Table 1: Effect of electrical stimulation on swallowing performance assessed by airway closure and corresponding speed (time to maximal airway closure after start of a swallow). Mean values for one patient are reported in comparison to mean values observed in healthy people. A - without stimulation; B - with stimulation support (I = 9.45 mA); C - with stimulation support (I = 11.81 mA).

	A	**B**	**C**
Number of swallows	5	9	4
Airway closure	37%	51%	74%
Elevation Speed	29%	44%	47%

Discussion

In a case study with one patient it has been shown, that the presented system is able to detect the beginning of a voluntary swallow early enough in order to stimulate the submental musculature for achieving a positive effect regarding elevation and acceleration of hyoid and larynx. The patient easily adapted to the stimulation system. The BI signals indicated that airway closure and closure speed were increased using FES.
These preliminary results have to be confirmed on a larger patient population in comparison to videofluoroscopy. A possible carryover effect, by which swallowing in patients may also be improved without stimulation should be examined in a long-term study.

Acknowledgement

This work was funded by the German Federal Ministry of Education and Research (BMBF) within the project BigDysPro (FKZ 01EZ1007)

Bibliography

[1] M. L. Freed, L. Freed, R. L. Chatburn, and M. Christian, "Electrical stimulation for swallowing disorders caused by stroke," *Respiratory Care*, vol. 46, pp. 466–474, May 2001.

[2] V. Leelamanit, C. Limsakul, and A. Geater, "Synchronized electrical stimulation in treating pharyngeal dysphagia," *The Laryngoscope*, vol. 112, no. 12, pp. 2204–2210, 2002.

[3] H. Nahrstaedt, C. Schultheiss, R. Seidl, and T. Schauer, "Swallow detection algorithm based on bioimpedance and EMG measurement," in *Proc. of 8th IFAC Symposium on Biological and Medical Systems*, (Budapest), 2012.

[4] C. Schultheiss, T. Schauer, H. Nahrstaedt, and R. O. Seidl, "Evaluation of an EMG bioimpedance measurement system for recording and analysing the pharyngeal phase of swallowing," *European Archives of Oto-Rhino-Laryngology*, pp. 1–8, 2013.

[5] C. L. Ludlow, I. Humbert, K. Saxon, C. Poletto, B. Sonies, and L. Crujido, "Effects of surface electrical stimulation both at rest and during swallowing in chronic pharyngeal dysphagia," *Dysphagia*, vol. 22, pp. 1–10, Jan. 2007. PMID: 16718620.

[6] L. Xu and A. Adler, "An improved method for muscle activation detection during gait," in *Canadian Conference on Electrical and Computer Engineering.*, vol. 1, pp. 357 – 360 Vol.1, May 2004.

[7] E. Keogh, S. Chu, D. Hart, and M. Pazzani, "An online algorithm for segmenting time series," in *Proc. IEEE International Conference on Data Mining*, pp. 289 – 296, 2001.

THE IMPACT OF INTRAMUSCULAR-INSERTED HOOKED WIRE ELECTRODES AND SPECIFIC STIMULATION PARAMETERS

Arnold D[1], Guntinas-Lichius O[2]

[1] Institute of Systematic Zoology and Evolutionary Biology with Phyletic Museum, FSU Jena, Germany

[2] University Hospital, Friedrich-Schiller-University Jena, Germany

d.arnold@uni-jena.de

Abstract: *The importance of FES (functional electrical stimulation) with hooked wire electrodes increases in the diagnostic and therapy methods in the last years. These new potential approaches make it necessary to impale the target muscle and stimulate them. In our pilot experiments we determine how intense the target muscle was injured by repeated impalement with hooked wire electrodes and subsequent electrical stimulation. The triceps brachii muscles of 10 female rats were investigated. Typical signs of mechanical muscle injury and subsequent regeneration can be observed. We can assume that the stimulation protocol had no undesired side effects on muscle structure and function.*

Keywords: *muscle, injuries, stimulation, hooked wire, rat*

Introduction:

FES with needle EMG (electromyogram) electrodes becomes more and more important (Cheetham et al. 2011). The information outcome of the EMG technique by itself is limited (Kim et al. 2012). Just the activity of a small area of the muscle can be registered. Because of the many necessary changes of the needle position by the investigator the muscle is injured with each trial to analyze its operational capability. The FES is an additional diagnostic tool and increases the possibilities to describe the paretic dysfunction. It supports the differentiation between intact and paretic parts. This is important if muscle compartments are able to fulfill different functions, like the PCA muscle (*M. cricoarytenoideus posterior*) of the larynx (2 or 3 different compartments Sander et al. 1993, 1994). Therapies to reduce aberrant patterns of muscle recruitment and, thus, improve muscle function (Colton et al. 2006) are another wide field for FES with needle electrodes. It can help to relax spasm, restore the natural muscle function (facial nerve paresis) or reduce symptoms of phantom pain. The target muscle will be impaled and stimulated often by all these techniques. In our pilot experiments we determine how intense the target muscle was injured by the insertion of hooked wire electrodes and subsequent electrical stimulation with prevalent parameters.

Material & Methods:

The left and right triceps brachii muscles of 10 female rats (Han Wistar) were impaled with monopolar hooked wire electrodes (CareFusion Injection Needle Ø 0.51 mm) and a third electrode was placed subcutaneously into the back. The left triceps muscle was stimulated with a Neurosign 100 for 1, 3 or 5 hours with 30 Hz and 1 mA (rectangular, monophasic pulses with 200 µs duration) under isoflurane anesthesia (Table 1). Slightly contractions of the muscle were visible at the beginning. The right muscle was not stimulated and served as a control. The animals were euthanized one or four days after the last stimulation. The muscles were dissected and frozen in isopentane pre-cooled in liquid nitrogen. Serial cross sections (20 µm thick) of the muscles were prepared using a cryostat (CM1850, Leica Microsystems) and stained with toluidine blue or haematoxylin-eosin.

Table 1: Stimulation protocol.

Animal No.	Total duration of Stimulation (days)	Stimulation duration (h/day)	Survival after last stimulation (days)
1	1	5	1
2	1	5	4
3	5	3	4
4	5	3	4
5	5	1	4
6	5	1	4
7	5	3	1
8	5	3	1
9	5	1	1
10	5	1	1

Results:

In all investigated triceps muscles we observed circumscribed areas containing small basophilic (regenerating) muscle fiber profiles (Fig. 1 A, B, C) and, less commonly, necrotic fibers surrounded by moderate cellular infiltration. These are typical signs of mechanical muscle injury and subsequent regeneration (Irintchev & Wernig 1987). The damaged areas could be traced in serial sections over distances of many millimeters (5- 10 mm) and apparently represented penetrating wounds caused by the wire electrodes. Single injury tracks were seen in muscles impaled only once (animals 1 and 2 in Table 1) and multiple (3-5) tracks were found in the rest of the muscles. The extent of muscle damage was small. Injury tracks in single sections were restricted to 10 – 20 fibers and the overall volume of tissue injury was certainly well below 1% of the muscle volume. Outside damaged areas, the muscle fibers had normal appearance and no cellular infiltrates were visible. No differences were detected between stimulated (left) and non-stimulated (right) muscles.

A)

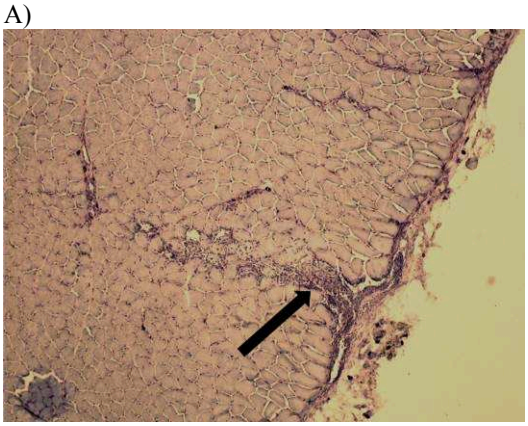

B)

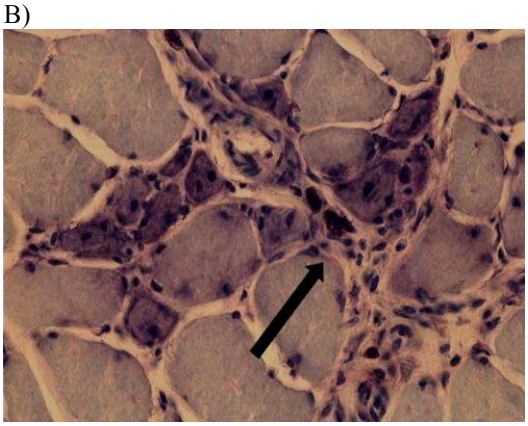

Fig.1: Lesion tracks stained in toluidine blue (black arrow), 5 days of stimulation, 3 h per day, magnification A) 5x, B) 40x

Discussion:

The results of this pilot study indicate that repeated impalement of muscles with wire electrodes causes minimal mechanical damage and the extent of this damage is similar independent of whether electrical current has been applied via the electrodes or not. We can assume that our stimulation protocol did not have undesired side effects on muscle structure and function. This notion is supported by previous observations on muscle injuries after voluntary running in wheels (Irintchev & Wernig 1987). Daily running episodes cause necrosis and regeneration of muscle fibers within the first two weeks of wheel exercise. Although the extent of damage may reach 25% of all muscles fibers, tissue repair is very successful and no functional deficits are observed even after numerous cycles of muscle damage and repair (Irintchev & Wernig 1987; Wernig et al., 1990).

Acknowledgements:
Special thanks to Heike Thieme and Med El

Bibliography:

[1] Cheetham J., Regner A., Jarvis J.C., Priest D., Sanders I., Soderholm L.V., Mitchell L.M., Ducharme N.G., Functional electrical stimulation of intrinsic laryngeal muscles under varying loads in exercising horses. PloS One. 2011, 6(8)

[2] Kim H.J., Park Y.S., Ryu J.S., Huh R., Han I., Shin D.A., Kim T.G., Cho K.G., Chung S.-S.: Intraoperative Facial Electromyography and Brainstem Auditory Evoked Potential Findings in Microvascular Decompression for Hemifacial Spasm: Correlation with Postoperative Delayed Facial Palsy. Stereotact Funct Neurosurg. 2012, 90(4):260-5

[3] Sanders I., Jacobs I., Wu B.L., Biller H.F. The three bellies of the canine posterior cricoarytenoid muscle: implications for understanding laryngeal function. Laryngoscope. 1993 Feb;103(2):171-7.

[4] Sanders I., Wu B.L., Mu L., Biller H.F. The innervation of the human posterior cricoarytenoid muscle: evidence for at least two neuromuscular compartments. Laryngoscope 1994 Jul;104(7):880-4.

[5] Colton R.H., Casper J.K. and Leonard, R. "Understanding voice problems: A physiological perspective for diagnosis and treatment (3rd ed.)", 2006, Baltimore, MD: Lippincott Williams and Wilkins

[6] Irintchev & Werning (1987): Muscle damage and repair in voluntarily running mice: strain and muscle differences. Cell Tissue Res 1987, 249:509-521.

[7] Wernig A, Irintchev A, Weisshaupt P: Muscle injury, cross-sectional area and fibre type distribution in mouse soleus after intermittent wheel-running. J Physiol (Lond) 1990, 428: 639-652

Cardiorespiratory and Metabolic Responses During FES Leg Exercise: Health and Fitness Benefits Update

Davis GM

Clinical Exercise and Rehabilitation Unit, University of Sydney, Sydney, Australia

Glen.Davis@sydney.edu.au

Abstract: *This is a review of key studies that have investigated whether FES-evoked leg exercise possesses sufficient intensity to meet the Exercise is Medicine™ guidelines for cardiovascular health. The American College of Sports Medicine and similar professional organisations have aligned their recommendations about what is sufficient physical activity or exercise to maintain good health. These key recommendations are: (i) moderate-intensity cardiorespiratory exercise 150 min/week, (ii) vigorous-intensity cardiorespiratory exercise for 75 min/week, or (iii) a combination of moderate-intensity and vigorous intensity-exercise to achieve a total energy expenditure of at least 500-1000 Met-minutes/week. However, for FES-evoked exercise there is uncertainty whether "moderate" or "vigorous" intensity can be achieved. Evidence is presented supporting or refuting the notion that FES-exercise achieves the Exercise is Medicine™ guidelines for aerobic fitness promotion and cardiovascular risk reduction*

Keywords: *FES-evoked leg exercise, cardiovascular health, aerobic fitness*

Introduction

Exercise is beneficial not only for the able-bodied population, but also for people affected by spinal cord injury (SCI). The negative sequelae after SCI can include moderate-severe muscle paralysis, loss of lower limb functionality and usually results in reduced levels of aerobic fitness. Since the 1960's, functional electrical stimulation (FES) – induced leg exercise has been widely used in post-traumatic rehabilitation or as exercise regimen for the paralysed lower-limbs of people with SCI.

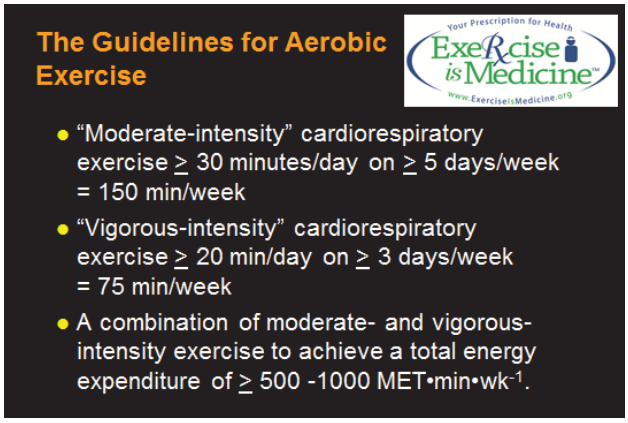

Fig 1. The ACSM Guidelines [1]

Recently, The American College of Sports Medicine and similar professional organisations have aligned their recommendations about what is sufficient physical activity or exercise to improve aerobic fitness and maintain good health [1]. Those guidelines (Fig. 1), have come to form the bases for the Exercise is Medicine™ Global Initiative. However, these is some mounting evidence that terms for exercise intensity such as "moderate" and "vigorous" may not apply well to an exercise modality that is artificially induced, such as FES.

The purpose of this study was review key studies that either support or refute the concept FES exercise can improve aerobic fitness and reduce cardiovascular risk.

Methods

A systematic search of published sources was performed in common electronic databases within the date range 1900-February 2012. In addition, relevant English language journal and conference proceedings were hand searched. The collective conclusions of the obtained RCTs and quasi-RCTs were not sufficient to position the status of the topic under question. The author included other non-randomised or controlled studies, mainly clinical trials, to encompass all available scientific evidence pertaining to FES-induced exercise.

Results – Evidence Supporting FES exercise

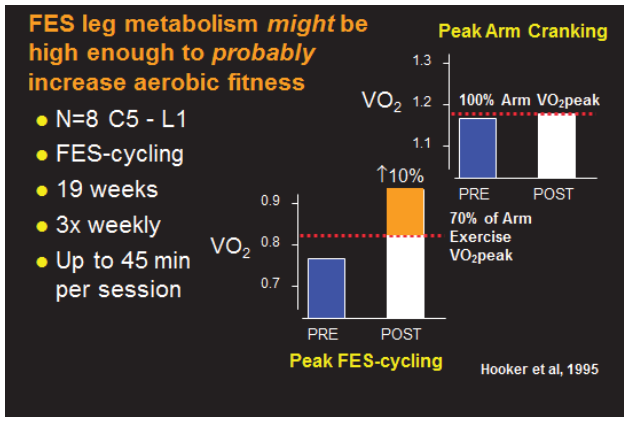

Fig 2. FES-cycling increased aerobic fitness [2]

Hooker and co-workers [2] originally observed that sedentary paraplegics and tetraplegics increased their peak oxygen uptake after only twice-weekly FES-cycling over 19 weeks (Fig.2). An important fact pertinent to the current review is that the 10% increase of leg VO_2peak, was above 70% of the arm cranking peak aerobic fitness. Thus, leg cycling was of sufficient intensity to achieve moderate-vigorous exercise intensity meeting the ACSM guidelines. Other studies reported in Hamzaid and Davis [3] supported these early findings.

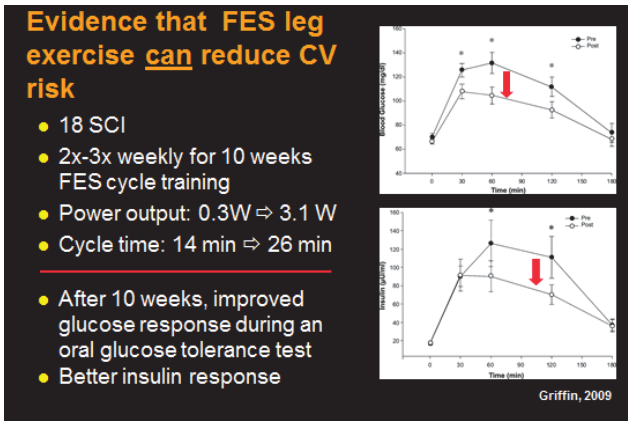

Fig 3. FES-cycling improves oral glucose tolerance and insulin responsiveness, both important factors to lower cardiovascular risk [4].

Griffin and colleagues [4] observed that 30 minutes of FES cycling per day, thrice weekly for 10 weeks significantly improved lean muscle mass, cycling power output, glucose tolerance, insulin levels, and inflammatory biomarkers (Fig. 3). This finding supported by a similar outcome by Chillibeck and colleagues (1998) strongly suggests that FES-cycling protects against certain "lifestyle diseases" associated with cardiovascular disease

Results – Evidence Refuting FES exercise

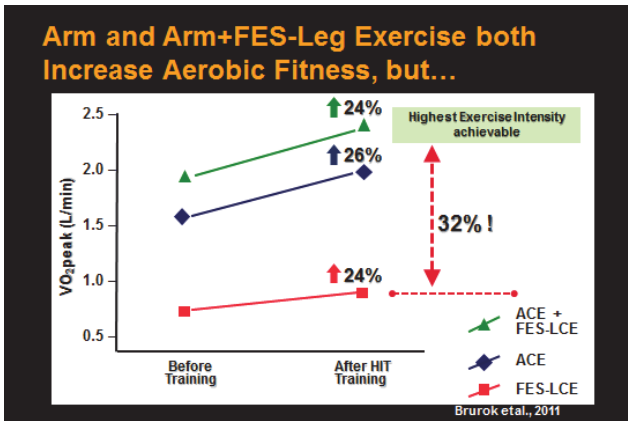

Fig. 4. Arm + FES-leg exercise increases arm and leg peak metabolism, but leg peak is only 32% of whole body aerobic fitness [5]

A recent study by Brorok and colleagues [5] demonstrated that 8-weeks of high-intensity arm+leg ("hybrid) interval training increased arm, leg and hybrid peak aerobic fitness by 24-26% (Fig. 4). However, closer examination of these findings showed that the highest leg VO_2peak after training achieved only 32% of the peak arm+leg value – too low to be considered even "moderate" intensity.

Hettinga and Andrews [6] undertook a thematic review of FES studies containing 171 observations and the authors observed that arm+leg cycling or FES-rowing produced greater aerobic metabolism that leg exercise alone. When this author inspected their data, it became apparent that peak FES-leg exercise achieved only 50-60% of whole-body aerobic fitness – and rarely is this leg exercise intensity deployed due to high fatigue rates (Fig.5)

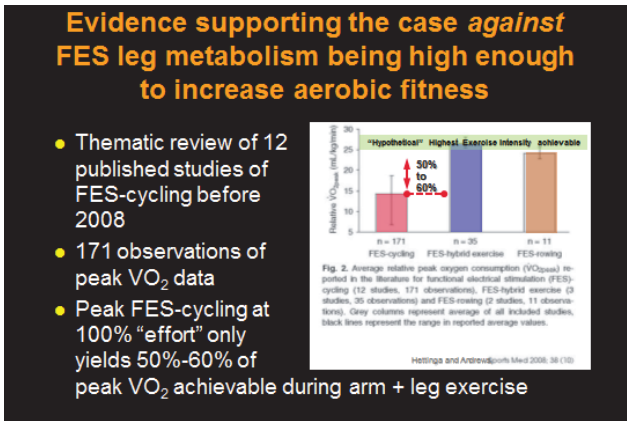

Fig 5. Thematic review suggesting that leg exercise alone is less 'dose-potent' to improve aerobic fitness than arm+leg hybrid exercise

Discussion

This study reviewed key studies that either supported or refuted the notion that FES exercise can improve aerobic fitness and reduce cardiovascular risk. Some key findings of this review were that randomized, controlled, or quasi-experimental evidence of different modes of FES-evoked exercise cautiously support the view that FES leg exercise promotes positive leg metabolic responses during exercise but rarely *by itself* enhances peak aerobic fitness in people with SCI.

For FES-evoked leg exercise to be clinically effective to promote peak aerobic fitness *by itself*:

- Intensive FES cycling training must achieve sufficient 'dose-potency' of at least "moderate" exercise intensity evidenced by greater than 40% heart rate reserve for at least 150 minutes per week.

- The beneficial effects of the FES cycling to promote aerobic fitness and reduce the risk of cardiovascular disease become more evident with increased intensity and duration of training.
- The beneficial cardiovascular effects from the adoption of exercise diminish once the FES cycling has ceased.

However, longer durations of FES cycling than 150 min per week, may have an important role to control weight gain, improve blood glucose tolerance and insulin resistance and reduce obesity in the SCI population. These are a separate cardiovascular risk factors than low aerobic fitness. It is recommended that when exercise intensities below "moderate" are achieved during FES cycling, that at least 240 min of such exercise per week be achieved.

Bibliography

[1] Garber CE. (2011). Quantity and quality of exercise for developing and maintaining cardiorespiratory, musculoskeletal, and neuromotor fitness in apparently healthy adults: Guidance for prescribing exercise. Med Sci Sports Exerc. 43:1334-1359

[2] Hooker S et al. (1995)Peak and submaximal physiologic responses following electrical stimulation leg cycle ergometer training. J Rehabil Res Develop, 32:361-366.

[3] Hamzaid NA and Davis GM (2009). Health and fitness benefits of Functional Electrical Stimulation-evoked leg exercise for spinal cord injured individuals: A position review. TSCIR 14:88-121.

[4] Griffin L et al (2009). Functional electrical stimulation cycling improves body composition, metabolic and neural factors in persons with spinal cord injury. J Electro Kinesiol, 19: 614–622.

[5] Brurok B et al (2011). Effect of Aerobic High-Intensity Hybrid Training on Stroke Volume and Peak Oxygen Consumption in Men with Spinal Cord Injury. APMR. 90:407-414

[6] Hettinga DM and Andrews BJ. (2008) Oxygen consumption during functional electrical stimulation-assisted exercise in persons with spinal cord injury: implications for fitness and health. Sports Med. 38:825-38

High-Intensity Virtual-reality Arm plus FES-leg Interval Training in Individuals with Spinal Cord Injury

Hasnan N[1], Engkasan JP[1], Husain R[2] and Davis GM[3]

[1]Department of Rehabilitation Medicine, University of Malaya, Kuala Lumpur, Malaysia
[2] Department of Physiology, University of Malaya, Kuala Lumpur, Malaysia
[3]Clinical Exercise and Rehabilitation Unit, University of Sydney, Sydney, Australia

Glen.Davis@sydney.edu.au

Abstract: *This study investigated the effect of high-intensity arm and FES-leg cycle training in a virtual reality environment on power output, aerobic fitness and blood biochemistry in persons with spinal cord injury (SCI). Eight individuals with chronic SCI undertook 6 weeks of high-intensity (80-90% HRpeak) interval training using an arm+FES-leg tricycle. As a result of the virtual reality interval training program, subjects increased their peak aerobic fitness by 20% ($p<0.05$). Their body mass-adjusted VO_2 peak also significantly increased from 19.3±3.4 $mL•kg^{-1}•min^{-1}$ to from 23.2±3.4 $mL•kg^{-1}•min^{-1}$. Arm+ leg peak power output during "hybrid" exercise was raised from 52.5±10.4 W to 70±12.0 W ($P<0.05$). Total cholesterol, HDL, LDL and oral glucose tolerance results were unchanged after training.*

Keywords: *arm+leg exercise, virtual reality, hybrid exercise*

Introduction

Upper body exercise (e.g. wheelchair propulsion, arm cranking) is often recommended for people with spinal cord injury (SCI) to maintain or enhance their aerobic fitness and upper-body muscular endurance, but due to the relatively small muscle mass in their arms such exercise may not be as beneficial as leg exercise. However, FES-evoked leg exercise (e.g. cycling, stepping) is by itself not sufficient stimulus to promote cardiorespiratory fitness if the leg muscles are atrophic and de-trained [1].

Recently, Hasnan and colleagues [2] have demonstrated that combined voluntary arm and FES-evoked leg exercise ("hybrid") elicited a higher oxygen uptake and greater cardiovascular demand compared to arm exercise or FES cycling alone. Commercially-available hybrid exercise devices have enabled outdoor arm+leg cycling as well as indoor virtual reality (VR) hybrid exercise for people with SCI. VR-enhanced exercise (Fig. 1) allows the participant to interact within a virtual environment mimicking outdoor overground cycling, and may provide a sense of participation and exercise motivation. Hasnan and co-workers [3] demonstrated that mean oxygen uptake and energy expenditure of indoor virtual reality hybrid exercise were no different from outdoor overground arm+leg exercise, even though "steering" and "gearing" differences contributed to different limb movements over 30-min of exercise.

The purpose of this study was to investigate the effect of high-intensity "hybrid" (arm and FES-leg cycling) interval training in a virtual reality environment on aerobic fitness, power output, lipid profiles and glucose tolerance in persons with SCI.

Methods

Eight individuals with chronic SCI undertook 6 weeks of hybrid high-intensity interval training (HIT) using an arm+FES-leg tricycle. Training sessions were either 32 min, three times per week or 48 min, two times per week. For the thrice-weekly programme, the subjects were instructed to perform four 8-min exercise intervals of high intensity training (80-90% of predicted HRmax) interspersed with four 8-min intervals of low intensity training (LIT; FES-stimulated legs only at 40% of predicted HRmax). For the twice-weekly programme, the subjects were instructed to undertake six 8-min intervals of HIT interspersed with six intervals of LIT. For both training regimes, all subjects completed 96 min of HIT and 96 min of LIT per week.

Fig 1: 'Hybrid' Virtual Reality Indoor Exercise

The recumbent tricycle (BerkelBike®) was positioned on Tacx i-Magic VR Trainer®, indoors in front of a flat panel monitor displaying simulated outdoor overground cycling. All training incorporated VR technology whereby the subjects trained to a pre-selected VR programme. Voluntary arm cranking was at a cadence selected by the subjects to achieve their desired exercise intensity. Computer-controlled electrical stimulation was applied bilaterally to the quadriceps, hamstrings and

glutei to evoke leg cycling. The subjects were encouraged to cycle to their best effort within safety limits and increase/ramp up their leg stimulation intensities based on their comfort and tolerance level to a maximum stimulation intensity of 150 mA at 35Hz.

The participants were assessed for their peak cardiorespiratory responses and power output before and following completion of the six-week training programme. Heart rate and cardiorespiratory parameters were measured continuously breath-by-breath by open-circuit spirometry with a metabolic gas analysis system at rest and during the maximal effort assessments. Lipid profiles, cholesterols and oral glucose tolerance were also measured before and after the training.

Analysis of variance was utilised to investigate pre-training versus post-training differences of all variables, whereby the level of statistical significance was set to the 95% confidence limit ($p<0.05$). Data are presented as mean ± standard deviation. Statistical analyses were performed using the SPSS 21 statistical package.

Results

As a result of the hybrid HIT program, the subjects increased their arm+leg peak power output from 52.5±10.4 W to 70±12.0 W ($P<0.05$). Their peak aerobic fitness was increased by 20% (Fig. 2; $p<0.05$). Their body mass-adjusted VO_2peak also increased from 19.3±3.4 $mL \cdot kg^{-1} \cdot min^{-1}$ to 23.2±3.4 $mL \cdot kg^{-1} \cdot min^{-1}$ $p<0.05$). No other resting or peak exercise cardiorespiratory variables were changed as a result of hybrid HIT training. Leg girths and volumes were also unchanged after hybrid HIT. Blood biochemistry markers of cardiovascular risk, including total cholesterol, HDL, LDL and oral glucose tolerance results were unchanged after training, although modest improvements were observed in some subjects.

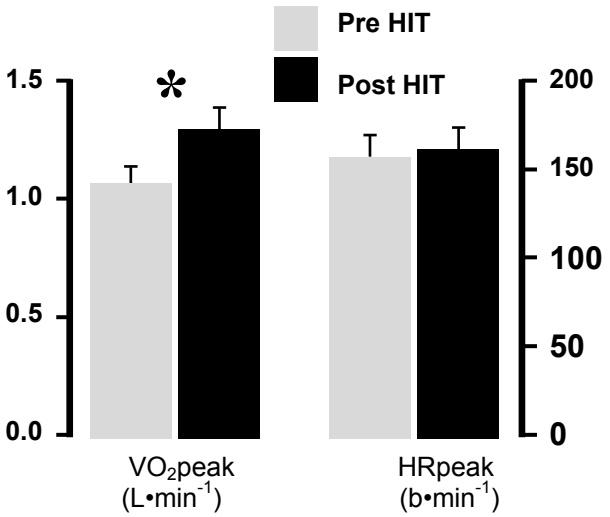

Fig. 2. Changes of Aerobic Fitness following 6-weeks of hybrid HIT. * denotes $p<0.05$. Data and mean ± SD

Discussion

This study investigated indoor virtual-reality "hybrid" exercise training in individuals with SCI. Traditionally, FES cycling has been clinically recommended to individuals with SCI for its ability to recruit the large musculature of the legs. Yet, Vrellen and co-workers [1] and Hasnan et al [2] have shown that the metabolic responses during an acute bout of leg cycling exercise alone may not be sufficient to promote cardiorespiratory fitness in this population.

Numerous authors have recommended "hybrid" (e.g. arm+leg) exercise during rehabilitation as potentially more dose-potent to induce physiological adaptations within the cardiorespiratory system after SCI. Our 20% increase of aerobic fitness and 33% higher peak power output was more than twice that observed by Heesterbeek and colleagues [4] for a similar BerkelBike® training program. The larger increases of the current study were likely due to a longer training period and our use of high-intensity interval training (HIT) for this relatively de-conditioned population.

There are no previous studies that have investigated changes of lipid profile and oral glucose tolerance following "hybrid" exercise training in SCI. The lack of changes in these biochemical measures suggests that six weeks of twice- or thrice-weekly training, even at a high intensity, may be too short to modify these biochemical markers of cardiovascular risk in the SCI population.

Acknowledgement

This work comprised a portion of the PhD studies of the primary author under a University of Sydney – Universiti of Malaya Cotutelle agreement. Partial financial support was provided by the University of Sydney internal grants schemes and partial financial support was provided by Universiti of Malaya UM.C/HIR/MOHE/ENG/39 Program Grant.

Bibliography

[1] Verellen J et al. Cardiorespiratory responses during arm ergometry, functional electrical stimulation cycling, and two hybrid exercise conditions in spinal cord injured. *Disabil Rehabil Assist Technol*. 2:127-132, 2007.

[2] Hasnan N et al. Exercise Responses during FES Cycling in Individuals with Spinal Cord Injury. *Med Sci Sports Exer*. doi: 10.1249/MSS.0b013e3182805d5a [ePub ahead of print] , 2013

[3] Hasnan N et al. Virtual Reality Hybrid Cycling Versus Outdoor Hybrid Cycling In Individuals With SCI: A Pilot Study. Proceedings of the 17th Annual International Functional Electrical Stimulation Society Conference, 144-146, 2012.

[4] Heesterbeek PJC et al. Increased physical fitness after4-week training on a new hybrid FES-cycle in persons with spinal cord injury. *Technol Disabil*., 17:103–110, 2005.

PREVENTION OF ORTHOSTATIC HYPOTENSION WITH ELECTRIC STIMULATION IN PERSONS WITH ACUTE SPINAL CORD INJURY

Tesini S[1], Frotzler A[1], Bersch I[1], Tobón A[1]

[1]Swiss Paraplegic Centre Nottwil, Switzerland

stefanie.tesini@paraplegie.ch

Abstract:
The impact of three different types of electric stimulation (ES) (ES of the abdominal muscles versus ES of lower limb muscles versus simultaneously ES of abdominal and lower limb muscles versus control) on blood pressure stabilization and verticalisation-degrees between 0° and 70° in nine patients with acute spinal cord injury positioned in a tilt-table was investigated. Data analysis revealed that blood pressure did not differ significantly between the types of ES and the control at any verticalisation-degree ($p>0.05$). Although statistical significance was missed, a clear tendency towards a stabilization of blood pressure using any type of ES up to a verticalisation-degree of thirty was found.

Keywords: *orthostatic hypotension, spinal cord injury, functional electrical stimulation, tilt-table, redistribution of blood volume*

Introduction

The Consensus Committee of the American Autonomic Society and the American Academy of Neurology defined orthostatic hypotension (OH) as a decrease in systolic blood pressure of at least 20mmHg, or a reduction in diastolic blood pressure of at least 10mmHg, upon the change in body position from a supine position to an upright posture, regardless of the presence of symptoms.
The presence of OH as a consequence of blood volume redistribution during verticalisation in persons with spinal cord injury (SCI) is a common condition that affects 74% of these patients [1,2]. An OH may discourage SCI individuals from participating in the early stage of rehabilitation [3]. The management of OH in the early stage of SCI using electric stimulation (ES) of lower limb muscles was found to be effective in stabilizing blood pressure during verticalisation [4,5,6]. However, the impact of ES of the abdominal muscles on blood pressure during verticalisation in patients with SCI is unknown. Therefore, the aim of the present study was to compare the impact of three different types of ES methods on blood pressure stabilization and on the incidence of OH.

Methods

Design: Prospective interventional study.
Setting: Swiss Paraplegic Centre, Nottwil (Switzerland).
Patients: Women and men, at least 18 years of age, following an acute and traumatic SCI, with a lesion level above T6, an American Spinal Injury Association (ASIA) Impairment Scale A/B/C and a diagnosis of OH (by tilt table test) were eligible for the study.

Intervention: Each patient underwent randomly three different types of ES sessions while being positioned on a tilt-table. The following sessions were planned within 10 consecutive days:
A) ES of the abdominal muscles
B) ES of the lower limb muscles (Mm. gastrocnemii, hamstrings, Mm. quadriceps,)
C) Combination of A and B
D) Control session (=diagnostic session)
For the ES session "B" lower limb muscles were stimulated to produce a milking mechanism from the distal to proximal part of the limb to pump the venous blood from the peripheral to the central part of the body [7]. ES was applied with surface electrodes and fixed stimulation parameters (biphasic rectangular, 35Hz, 300µs pulse width) with individual mA, depending on each patients´ sensibility. In each session, tilting progressed in 15° increments every three minutes, from 0° to 70°, except from 60° to 70°. Therefore, the patients were verticalised on a tilt table to 0°, 15°, 30°, 45°, 60° and 70°. Within each interval, blood pressure (systolic, diastolic, mean arterial pressure) was measured and the Perceived Presyncope Scale (0=no symptoms, 1=mild symptoms, 2=moderate symptoms, 3=severe symptoms, 4=syncope) was collected to assess the patient's well-being. If the PPS was ≥ 3 the tilting trial was discontinued and the patient returned to supine position (0°).

Table 1: Characteristics of the patients.

Gender	Age [years]	Time post injury [days]	Level SCI	AIS score
F	46.9	112	C4	A
M	31.2	135	C8	A
F	24.2	34	C6	C
F	26.7	53	C4	B
M	20.5	45	T2	A
M	31.0	30	T4	A
M	18.1	33	C4	A
M	57.6	28	C6	A
M	30.1	20	C5	A
Median	**30.1**	**34**		
25;75 Quartile	**22.3;39.1**	**29.0;82.5**		

Abbreviations: M, male; F, female; SCI, spinal cord injury; AIS, American Spinal Injury Association Scale

Results

A total of nine patients (three women, six men, median age: 30.1 years [22.3;39.1], median lesion duration: 34.0 d [29.0;82.5] and a lesion level between C4 and T4 were recruited (Tab.1).
Blood pressure (systolic, diastolic, mean arterial pressure) did not differ significantly between the interventions A, B, C or D at any verticalisation-degree ($p>0.05$). Although statistical significance was missed, blood pressure was more stable (up to 30% at a verticalisation-degree of 30°) within the sessions A, B, or C compared to D (Fig. 1). In addition, independent of the type of stimulation, i.e. A, B or C, patients reached a higher degree of verticalisation with ES compared to the intervention D.

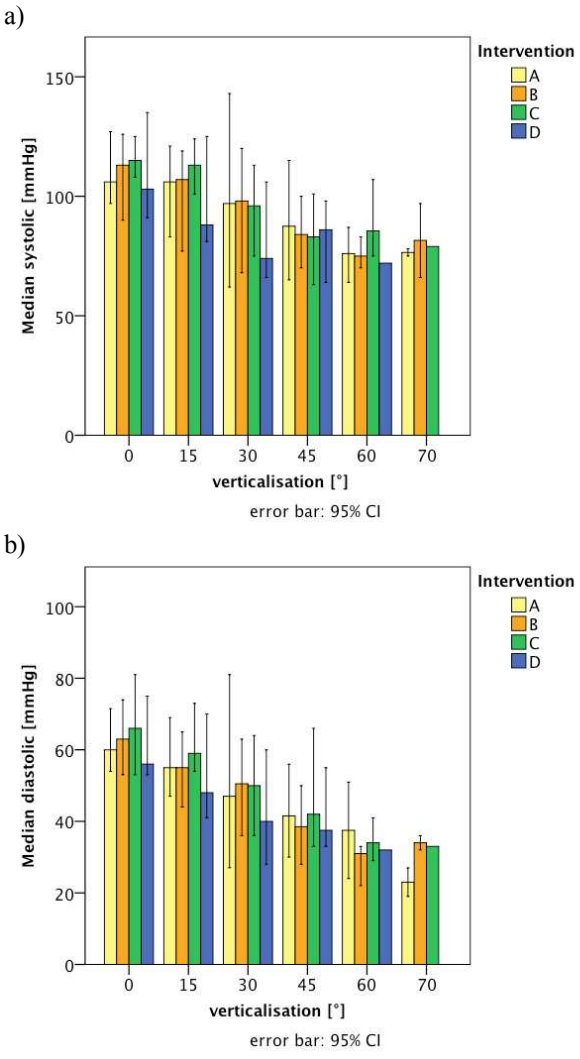

Figure 1: Median a) systolic and b) diastolic blood pressure for each verticalisation-degree and type of ES session (A, B, C) and control session (D).

Discussion

There seems to be a tendency to a clinical benefit of ES for the treatment of OH in individuals with SCI. With respect to limited time resources in clinical daily routine, ES of the abdominal muscles might be most feasible.

Acknowledgement

We would like to thank all patients as well as Kathrin Hartmann (research assistant), Trudy Röösli (MTA Neurology), and Andrijana Maric (MTA Neurology) who contributed to this study.

Bibliography

[1] Ten Harkel AD, van Lieshout JJ, Wieling W. Effects of leg muscle pumping and tensing on orthostatic arterial pressure: a study in normal subjects and patients with autonomic failure. *Clin Sci (Lond)* 1994;87:553-558.
[2] Claydon VE, Steeves JD, Krassioukov A. Orthostatic hypotension following spinal cord injury: understanding clinical pathophysiology. *Spinal cord.* Jun 2006;44(6):341-351.
[3] Illman A, Stiller K, Williams M. The prevalence of orthostatic hypotension during physiotherapy treatment in patients with an acute spinal cord injury. *Spinal Cord* 2000;38:741-747.
[4] Elokda AS, Nielsen DH, Shields RK. Effect of functional neuromuscular stimulation on postural related orthostatic stress in individuals with acute spinal cord injury. *J Rehabil Res Dev* 2000;37:535-542.
[5] Faghri PD, Yount J. Electrically induced and voluntary activation of physiologic muscle pump: a comparison between spinal cord-injured and able-bodied individuals. *Clin Rehabil* 2002;16:878-885
[6] Sampson EE, Burnham RS, Andrews BJ. Functional electrical stimulation effect on orthostatic hypotension after spinal cord injury. *Arch Phys Med Rehabil* 2000;81:139-143.
[7] Glenn MB, Berman SB. Cardiovascular changes following spinal cord injury. *Topics in Spinal Cord Injury Rehabil 1997;2:47–53.*

Functional Electrical Stimulation in Spinal Cord Injury: Clinical Evidence versus Daily Practice

Bersch I[1], Frotzler A[1], Baumberger M[1]

[1]Swiss Paraplegic Centre Nottwil, Switzerland

ines.bersch@paralpegie.ch

Abstract: *Functional electrical stimulation (FES) has clinical evidence in the rehabilitation of patients with spinal cord injury. Nevertheless, looking into daily clinical practice, the use of FES is poor. Expenditure of time, complexity of technical equipment and compliance and acceptance of therapists and patients should be discussed as limiting factors.*

Keywords: *spinal cord injury, functional electrical stimulation, rehabilitation, daily practice*

Introduction

Functional electrical stimulation (FES) is an inherent part of rehabilitation in spinal cord injury. It is amongst others used for preserving and increasing muscle mass [1,2,3], contracture prophylaxis [4], treating and preventing pressure ulcers [5,6,7,8] neuromodulation [9], motor-learning [10,11] improve and support coughing [12], improve and support function of upper and lower extremities [13,14] as well as reducing spasticity [15,16,17]. However, the findings of the above-mentioned effects were proved in research settings. Therefore, the aim of this study was to verify the evidence, acceptance and feasibility of FES in clinical and domestic setting.

Methods

Design: Retrospective observational study
Setting: Swiss Paraplegic Centre Nottwil (Switzerland)
Patients: Woman and men aged at least 16 years, following an upper or lower motor neuron lesion due to a traumatic or non-traumatic spinal cord lesion with an American Spinal Injury Association (ASIA) Impairment Scale A/B/C/D.
Data extraction: Number of patients, focus as well as amount of stimulation in either a clinical or a domestic setting were extracted from patient charts of the years 2011 and 2012. Data of stimulation sessions focused on preserving and increasing muscle mass, contracture prophylaxis of upper and lower limbs, treating pressure ulcers, preventing pressure ulcers, neuromodulation, motor learning, support coughing, improve and support function of upper limbs, improve and support function of lower limbs and management of spasticity by using FES were included. The number of patients who continued stimulation after rehabilitation in domestic setting was separately evaluated.
Assessments: 6 min. walking test, WISCI II, British medical council scale, Canadian occupational performance measure (COPM), Goal attainment scale (GAS), Ashworth scale, Spasm frequency scale, power output measure of the MotionMaker®.

Tab. 1: Number of patients and amount of stimulation

	2011	2012
Number of IN Patients	113	153
Number of Stimulation sessions for IN Patients	2941	2071
Number of OUT Patients	29	32

Results

Data of a total of 266 inpatients and 61 outpatients were extracted (Tab. 1). In the clinical setting, EMG-triggered FES with visual or acoustic feedback for motor learning and the stimulation of single muscles or muscle groups to improve function was mostly used. The number of patients using FES for treating and preventing pressure sources increased in the last year. Only a few number of spinal cord injured patients used stimulation for preserving muscle mass, coughing and reducing spasticity (Tab.2). Clinical relevant improvements following FES interventions were found in 6 min. walking test, WISCI II, British medical council scale, (COPM) and power output measure of the MotionMaker®. Individual different effects were observed in the Ashworth and Spasm frequency scale.

Table 2: Number of patients and focus of stimulation

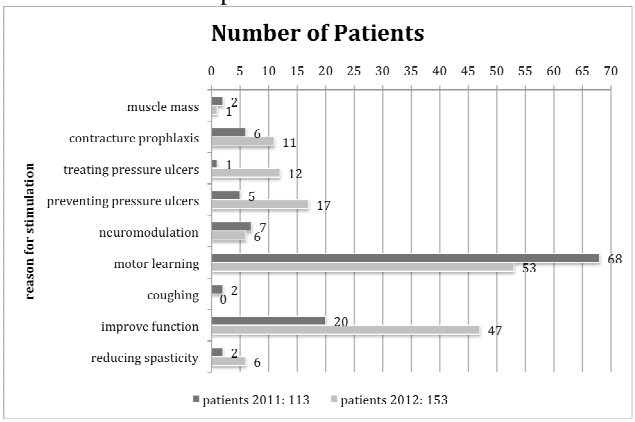

Discussion

FES seems to be accepted by the patients as an inherent part of rehabilitation. Furthermore, FES interventions

seem to be implementable in daily clinical practice. In persons with spinal cord injury the main focus lies on motor learning. Regarding outpatients, FES-interventions are much less conducted. It is assumed that the time consuming aspect might be one reason to discontinue FES-interventions at home. The expenditure of time for each training is about 30 min to one hour, including preparation. Indeed, stimulation should be done regularly in order to benefit from its effect [18]. A noticeable effect is not always seen after the first treatment and the impact is not long lasting. To reach long term effects treatment needs to be continued over weeks and months. Unfortunately Swiss insurances do not pay for the equipment although some patients would effort the expenditure of time. Coughing, in case of tetraplegia with surface electrodes seems to be an easy method to cough efficiently. It would be easily possible to integrate into daily physiotherapy treatment.

Success of FES is limited by expenditure of time, complexity of technical equipment, acceptance of therapists and financing.

Acknowledgement

We would like to thank Anna Müller (PT) to collect and review the stimulation protocols.

Bibliography

[1] Tessa Gordon and Jian Mao Muscle Atrophy and Procedures for Training After Spinal Cord Injury *PHYS THER.* 1994; 74:50-60.

[2] Scelsi, R. (2001). Skeletal Muscle Pathology after Spinal Cord Injury. *Basic Appl Myol*, *11*, 75–85.

[3] Mahoney, E. T., Bickel, C. S., Elder, C., Black, C., Slade, J. M., Apple, D., Jr, & Dudley, G. A. (2005). Changes in Skeletal Muscle Size and Glucose Tolerance With Electrically Stimulated Resistance Training in Subjects With Chronic Spinal Cord Injury. *Archives of physical medicine and rehabilitation*,*86*(7),1502–1504.

[4] Rayegani, S. M., Shojaee, H., Sedighipour, L., Soroush, M. R., Baghbani, M., & Amirani, O. B. (2011). The effect of electrical passive cycling on spasticity in war veterans with spinal cord injury. *Frontiers in neurology*, *2*, 39.

[5] C A J Smit, G L G Haverkamp, S de Groot, J M Stolwijk-Swuste, and T W J Janssen, Effects of electrical stimulation-induced gluteal versus gluteal and hamstring muscles activation on sitting pressure distribution in persons with a spinal cord injury, Spinal Cord 50, 590 (2012)

[6] Mittmann, N., Chan, B. C., Craven, B. C., Isogai, P. K., & Houghton, P. (2011). Evaluation of the Cost-Effectiveness of Electrical Stimulation Therapy for Pressure Ulcers in Spinal Cord Injury. *Archives of physical medicine and rehabilitation*, *92*(6), 866–872.

[7] Kim, J., Ho, C. H., Wang, X., & Bogie, K. (2010). The use of sensory electrical stimulation for pressure ulcer prevention. *Physiotherapy Theory and Practice*, *26*(8), 528–536.

[8] Houghton, P. E., Campbell, K. E., Fraser, C. H., Harris, C., Keast, D. H., Potter, P. J., et al. (2010). Electrical Stimulation Therapy Increases Rate of Healing of Pressure Ulcers in Community-Dwelling People With Spinal Cord Injury. *YAPMR*, *91*(5), 669–678.

[9] Estigoni, E. H., Fornusek, C., Smith, R. M., & Davis, G. M. (2011). Evoked EMG and Muscle Fatigue During Isokinetic FES-Cycling in Individuals With SCI. *Neuromodulation: Technology at the Neural Interface*, *14*(4), 349–355.

[10] Lo, H.-C., Hsu, Y.-C., Hsueh, Y.-H., & Yeh, C.-Y. (2012). Cycling exercise with functional electrical stimulation improves postural control in stroke patients. *Gait & posture*, *35*(3), 506–510.

[11] Kapadia, N. M., Zivanovic, V., Furlan, J., Craven, B. C., McGillivray, C., & Popovic, M. R. (2011). Functional Electrical Stimulation Therapy for Grasping in Traumatic Incomplete Spinal Cord Injury: Randomized Control Trial. *Artificial Organs*, *35*(3), 212–216.

[12] Stanic, U. (2000). Functional Electrical Stimulation of Abdominal Muscles to Augment Tidal Volume in Spinal Cord Injury. *IEEE TRANSACTIONS ON REHABILITATION ENGINEERING, 8, 1–5.*

[13] Takuya Watanabe, Yoshihiko Tagawa, Member, IEEE, Eiichiro Nagasue and Naoto Shiba, Surface Electrical Stimulation to Realize Task Oriented Hand Motion, Minneapolis, Minnesota, USA, September 2-6, 2009

[14] Mirbagheri, M. M., Ladouceur, M., Barbeau, H., & Kearney, R. E. (2002). The effects of long-term FES-assisted walking on intrinsic and reflex dynamic stiffness in spastic spinal-cord-injured subjects. *IEEE Transactions on Neural Systems and Rehabilitation Engineering*, *10*(4), 280–289.

[15] Rayegani, S. M., Shojaee, H., Sedighipour, L., Soroush, M. R., Baghbani, M., & Amirani, O. B. (2011). The effect of electrical passive cycling on spasticity in war veterans with spinal cord injury. *Frontiers in neurology*, *2*, 39.

[16] P. Métrailler, R. Brodard, R. Clavel, R. Frischknecht, Closed loop electrical muscle stimulation in spinal cord injured rehabilitation, 6th Mediterranean Forum of PRM, 18-21 October, Villamura, Portugal.

[17] Sköld, C., et al., Effects of functional electrical stimulation training for six months on body composition and spasticity in motor complete tetraplegic spinal cord-injured individuals. *J Rehabil Med*, 2002. 34(1): p. 25-32.

[18] Petrofsky, J.S., R. Stacy, and M. Laymon, The relationship between exercise work intervals and duration of exercise on lower extremity training induced by electrical stimulation in humans with spinal cord injuries. *Eur J Appl Physiol*, 2000. 82(5-6): p. 504-9.

Modelling a BCI system to estimate FES stimulation intensity for individual stroke survivors in foot drop cases

Mahadevappa M[1], Shendkar C[1], Lenka P[2], Biswas A[2], Kumar R[3]

[1]School of Medical Science & Technology, Indian Institute of Technology Kharagpur, India
[2]National Institute for the Orthopaedically Handicapped, Kolkata, India
[3] Department of Disability Affairs, Ministry of Social Justice and Empowerment, New Delhi, India

mmaha2@smst.iitkgp.ernet.in, shendkar.shekhar@gmail.com

Abstract: *This work provides a model to estimate stimulation level required for hemiplegic patient to achieve foot dorsiflexion using BCI approach. The model's input is EEG from motor cortex of hemiplegic patient. The model's output is estimation of stimulation strength. The delta mean and alpha peak frequencies are found to be suitable as EEG features to establish the relationship between EEG parameters and stimulus strength for this model. This model is self-adaptive in nature. As therapeutic procedure continues, the model uses a feedback loop, so that it can fine tune the stimulus strength to optimum value for individual patients. The model is prepared by using analysis of EEG feature from all the frequency bands and stimulus strength as observed clinically in 15 stroke patients while achieving dorsiflexion.*

Keywords: *BCI, Foot drop, Modelling, Functional Electrical stimulation, Stimulation strength*

Introduction

Conventional approach used for setting functional electrical stimulation (FES) therapy parameters in neurorehabilitation of stroke survivors is to adjust it by a trained physiotherapist. Brain-computer interface (BCI) technology in association with assistive devices has already shown the potential to restore lost motor function in stroke survivors. However use of BCI for estimating the amount of stimulus needed by stroke patient is limited. There is need to correlate the manually set stimulus strength and information obtained through bio-signals such as EEG. Work in this area is lacking. We tried to work in direction of using BCI approaches to actually understand the condition of patient for accessing the possibility of subjective treatment to each patient to achieve desirable movement. BCI system based on EEG feedback for training stimulator device could improve efficacy of stimulation therapy through optimized feedback [1].

We evaluated the model for BCI based estimation of strength of stimulation required for stroke patient to achieve foot dorsiflexion suitable for comfortable walking. Our system adapts itself as therapeutic use of FES continues. Patient needs the new level of stimulation due to plasticity of the brain. We used EEG from Cz point of motor cortex as a decision making parameter for estimating approximate value of stimulation current necessary for the particular hemiplegic patient [2]. The system extracts information from EEG signal for controlling the stimulator device[3].

Methods

Recording of EEG signal and stimulation strength

EEG data from 15 hemiplegic patients was acquired from Cz point of motor cortex of stroke subjects. EEG signal was recorded using EEG acquisition device (Thought Technology; Biograph Infiniti; Canada). Subjects performed foot dorsiflexion at interval of every 5 seconds. for five minutes. Then EEG data was processed to get temporal and spectral information about all EEG bands. For each subject, stimulation was applied using single channel stimulator (Cefar Compex;Step II; UK) and value of stimulation intensity was recorded for which appropriate dorsiflexion was attained. Then regression analysis was done to find correlation between features from different EEG bands (alpha, beta, delta, gamma, sensorimotor rhythm band information) and stimulation requirement of each patient.

Stimulus strength estimation model using BCI:

Figure1 shows our BCI based model for calculating optimal stimulus strength to achieve appropriate foot drop dorsiflexion. For this, model used prior data from the pool of subjects recorded at clinical setup. The model was prepared by analysing actual clinical data (EEG and stimulation strength requirement) of 15 subjects. Model comprised of the following steps:

- Acquiring a person's EEG signal and Processing it
- Extraction of important features from EEG signal for estimation of stimulus strength
- Subject dependent model relating important EEG features with stimulation strength requirements
- Feedback module for calibrating the estimation model which detects motor execution ability of patient
- Stimulation element for providing stimulation to the person according to the BCI feedback information

Sample EEG of stroke patients motor cortex and the features selected after analysis of EEG are presented in the Figure 2. We have designed low weight, miniaturized, portable embedded system (Figure 3) for implementing the proposed model. It consists of microprocessor (Texas Instruments Inc.; USA) in association with integrated analog front end. For acquisition of the EEG data, processing it and implementing the relation presented in this paper. The hardware will be tested in future work as per the model proposed in this paper.

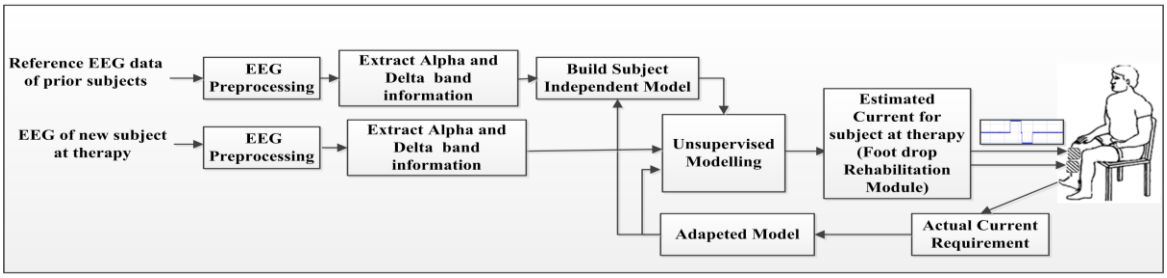

Figure1: BCI system and method for optimising FES therapy parameters (ex. stimulation strength requirement) of stimulating element used in motor rehabilitation of stroke survivors

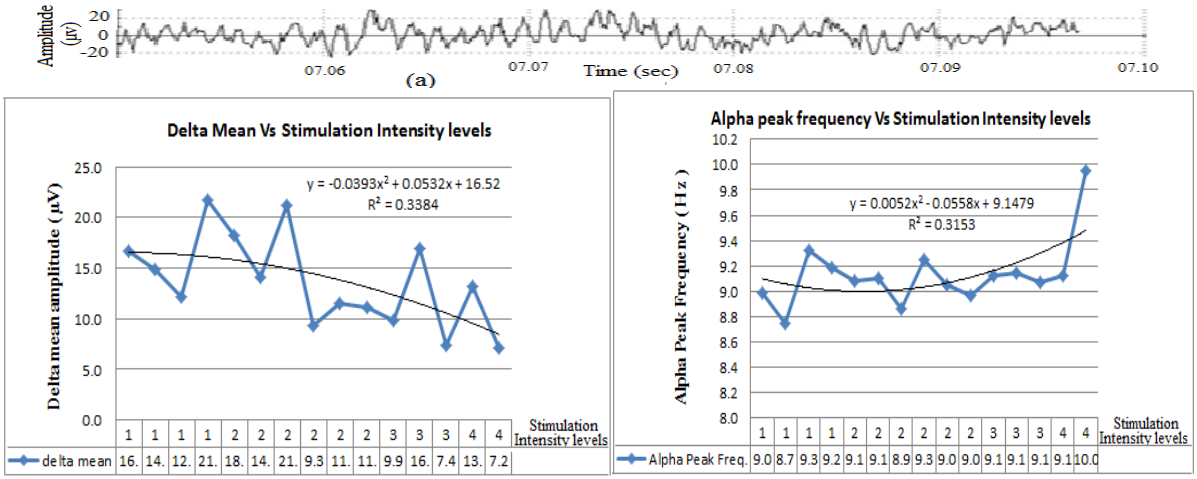

Figure2. EEG Feature selection for modelling stimulation strength requirement of individual stroke patient (a) EEG signal acquired from motor cortex by positioning electrode at Cz location according to 10-20 electrode placement system and IFCN standard (b) Relation between Delta mean amplitude and stimulus intensity levels (Level 1 corresponds to 50mA, 2→ 40mA, 3→35mA and 4→30mA) applied to 15 subjects (c) Relation between Alpha peak frequency and stimulus intensity levels (Level 1 corresponds to 50mA, 2→ 40mA, 3→35mA and 4→30mA) applied to 15 subjects. [Delta mean was computed using cumulative average of amplitude values throughout the recording and alpha peak frequency was computed using frequency value of the highest frequency bin in the alpha range (8-12 Hz) of the FFT spectrum.]

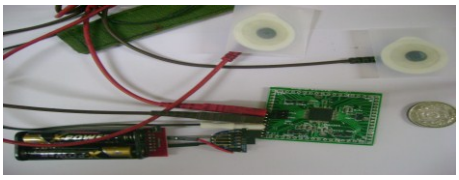

Figure3: Embedded system (Microprocessor and analog front end) for acquisition and processing of EEG data to produce decision about stimulation requirements**.**

Results

We found that the delta mean amplitude and the alpha peak frequency are the best features for estimating the stimulus strength. Regression model for these parameters and stimulation strength could be expressed by 2nd degree polynomial as shown in Figure 2.These features correlate moderately with stimulation strength and having coefficient of determination (R^2) up to 0.34 and 0.31 respectively for these features. The R^2 values are seems to be quite lower and suggest moderate correlation. Reason is, features correlations were evaluated independently and noise prone nature of EEG signal. Better correlation could be obtained if multiple features are used simultaneously. All other EEG band amplitudes and frequency parameters are not found significant (R^2 <0.1) and hence are not used in estimating the required current strength in this model.

Discussion

We suggested a BCI model and provided the relationship for estimating stimulus strength required for individual stroke subject using delta mean amplitude and alpha peak frequency from their EEG recordings. This BCI model is suitable to be implemented using low cost, portable embedded system and could act as important point of care (POC) technique to derive the command signal to control the stimulator device. We provided the suitable EEG features and mathematical relationship to achieve this. This is an intelligent system developed for identifying individual stroke patient's stimulus strength requirement without the assistance of the physiotherapist. Future work could be attempted to study the combination of EEG features towards better estimation model and testing it on more number of patients.

Acknowledgement

Authors thank Indian Council of Medical Research, New Delhi for sponsoring this project and NIOH Kolkata for clinical support. We thank to the subjects participated in this study.

Bibliography

[1] H. Gollee, I. Volosyak, A. J. McLachlan, K. J. Hunt, and A. Graser, "An SSVEP-based brain–computer interface for the control of functional electrical stimulation," Biomedical Engineering, IEEE Transactions on, vol. 57, pp. 1847-1855, 2010.

[2] G. R. Müller-Putz, V. Kaiser, T. Solis-Escalante, and G. Pfurtscheller, "Fast set-up asynchronous brain-switch based on detection of foot motor imagery in 1-channel EEG," Medical and Biological Engineering and Computing, vol. 48, pp. 229-233, 2010.

[3] A. H. Do, P. T. Wang, C. E. King, A. Abiri, and Z. Nenadic, "Brain-computer interface controlled functional electrical stimulation system for ankle movement," Journal of NeuroEngineering and Rehabilitation, vol. 8, pp. 1-14, 2011.

ESTABLISHMENT OF AN *IN VITRO* MODEL FOR STRESS TESTING OF VAGAL NERVE CUFF ELECTRODES

Katja Prystaz[1, 2], Christoph Ulmer[3] , Karin H. Somerlik-Fuchs[1,4] , Thilo B. Krueger[2]

[1] Animal Physiology / Neurobiology, Faculty of Biology, Albert-Ludwigs-University Freiburg, Germany
[2] inomed Medizintechnik GmbH, Emmendingen, Germany
[3] Department of General and Visceral Surgery, Robert-Bosch-Hospital, Stuttgart, Germany
[4] Bernstein Center Freiburg (BCF), Albert-Ludwigs-University Freiburg, Germany

k.prystaz@inomed.com

Abstract: In thyroid surgery cuff-electrodes for stimulation of the vagal nerve are used in order to prevent recurrent laryngeal nerve damage. The aim of this study was to illustrate resulting forces at application of cuff-electrodes at the vagal nerve as well as to determine electrical characteristics with impedance spectroscopy and simulation of the electrical field of cuff- electrodes. The final goal is to assure save application of cuff-electrodes at the vagal nerve for continuous stimulation by describing the physical parameters with the suggested in vitro model.

Keywords: *cuff electrode, vagal nerve stimulation, mechanical characterization, electrical characterization*

Introduction

For continuous intraoperative neuromonitoring in thyroid surgery, surgeons often use cuff-electrodes for stimulation in order to notice physical stress to the nerve that is responsible for the voice (Recurrent laryngeal nerve) [1, 2]. The investigated cuff-electrodes consist of a biocompatible silicone shape and stainless steel electrode contacts in varied forms and compositions. Requirements of such electrodes are a stable electrical contact to the tissue while at the same time sudden tearing forces may not result in nerve stretching. This paper describes and compares different geometries and materials for such cuff-electrodes (see Fig. 1). A mechanical model was established, which simulates the vagal nerve within the operation field to determine acting forces. Additionally,

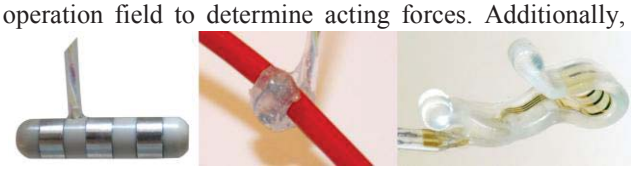

Figure 1: Characterized electrodes: V3-electrode (left), C-electrode (middle) and polyimide electrode (right)

stimulation electrodes were studied by an impedance spectroscopy and the electrical field distributions of the different electrodes were simulated. Experiences of the mechanical model and the electrical characterization for safe application of cuff electrodes in humans were transferred to the designs.

Methods

Mechanical properties

For mechanical characterization of the stimulation cuff-electrodes, we built up a measurement setup simulating the operation field of the vagal nerve. As an artificial nerve, silicone copper cables (3868-9017, Sab Bröckskes Gmbh & Co.Kg, Viersen and comparable cables) with different diameters (A) were hold between two Plexiglas columns by alligator clips (B). The spring scale (C) was attached to an aluminium cube (D) which is also bolted in the middle of the aluminium plate (E). The electrode (F) is fixed with a string to the attached spring scale (see Fig. 2). For measurement the electrode was applied to the artificial nerve and the electrode was raised by means of a microdrive (G) until the electrode slipped off. The measurement series were performed in a dry environment. For investigation of the mechanical properties of the electrode we determined the remove force of the electrode, measured the stretch length of the nerve (H) and the opening angle of the electrode (I). Additionally we analyzed the reproducibility. The aim of this measurement was to examine the application of varied electrode types and designs at different nerve diameters.

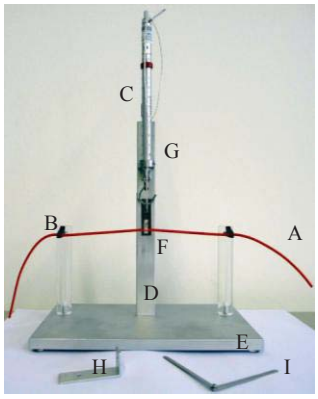

Figure 2: Description of the mechanical model

Electrochemical measurement

For electrochemical characterization we performed an impedance spectroscopy of different electrode types with an electrochemical interface (Solartron 1287, Farnborough Hampshire, UK) and a frequency response analyzer (Solartron 1260, Farnborough Hampshire, UK). We used a three-electrode configuration with a platinum electrode as counter electrode, a silver-silver chloride electrode as reference electrode and the cuff-electrodes as working electrodes. We measured electrodes in a ringer solution over a frequency range from 1 Hz until 10^6 Hz with an amplitude of 10 mV. Collected data were analysed in the software ZView (Farnborough Hampshire, UK).

Field distribution simulation

For electrical characterization of the cuff-electrodes we simulated the electrical field distribution of varied spherical electrode compositions. The 3D simulations were performed with FlexPDE 5.0.8 Professional Version (PDE Solutions Inc, Spokane Valley, WA 99206, USA), a partial differential equation solver software based on the finite element method. For obtaining meaningful results we simulated the polyimide electrode of the IKONA project [4] form with spherical contacts and mono-, bi-

and tripolar electrode compositions. The electrode metal stainless steel was simulated with $1.4 \cdot 10^6$ $(\Omega mm)^{-1}$. For a surrounding medium we chose a 0.9% NaCl solution and simulated it with a conductivity of 0.0033 $(\Omega mm)^{-1}$. The insulation material of the electrode consists of silicone and was simulated with 4.2 $(\Omega mm)^{-1}$. The simulation current was 1 mA.

Results

Based on the mechanical model we could measure the resulting forces, which appeared at the application of the different cuff-electrodes at the vagal nerve. The simplest cuff electrode, the C-electrode (inomed Medizintechnik GmbH, EW0023/EWPJ09-11), showed the lowest maximal remove force at every nerve diameter and its highest remove force is 325 mN at a nerve diameter of Ø 2.5 mm. While the more complex designs of the polyimide electrode [4] produced higher remove forces. The highest maximal median remove force were measured at the polyimide electrode with a broad silicone body and has the value 1040 mN at a nerve diameter of Ø 0.6 mm. The analysis of the parameter nerve diameter resulted in the fact that the maximal remove force was independent of the nerve diameter. The evaluation of the opening angle of different electrode types and the stretch length of the artificial nerve increased with larger nerve diameter, but at the thickest nerve the opening angle and the stretch length decreased again. The polyimide electrode with a narrow silicone form exhibited the maximal opened angle at 96° at a nerve diameter of Ø 2.5mm. The reproducibility of the C-electrode was lower in contrary to evident higher reproducibility of the designs of the polyimide electrode.

For the electrochemical characterization the real (resistive) component of the impedance response and the imaginary (mainly capacitive) component of the impedance response were plotted for each frequency. The V3-electrode (inomed Medizintechnik GmbH, P/N 522 200, [3]) with its ring contacts shows the lowest impedance modulus |Z| across all frequencies (100 Ω at 1 kHz) and the electrodes of the polyimide electrode with its spherical and cylindrical electrode form has the highest impedance modulus |Z| across all frequencies (2 kΩ at 1 kHz). While the spherical electrode contact of the C-electrode has an impedance modulus |Z| across all frequencies between the ring contact and the cylindrical electrodes (1 kΩ at 1 kHz). The simulation of the electrical field distribution is presented of a mono-, bi- and tripolar polyimide electrode. The simulation of the monopolar electrode could be characterized by an unselective electrical field. Until a bipolar electrode composition the electrical field showed a selective spatial resolution. The highest field strength and also the highest selective electrical field can be achieved with the tripolar polyimide electrode design. While the leak currents were very high at a monopolar electrode showed the tripolar not so much.

Discussion

In summary the mechanical characterization showed that the design of the polyimide electrode has a greater remove force independent of the nerve diameter, a larger stretch strength of the nerve and also an obvious higher reproducibility like the C-electrode. The C-electrode is the most flexible cuff-electrode and but does not have an as well-defined structure like the other electrodes. Moreover the broad polyimide electrode has the most rigid material properties. The remove forces could be reduced if the environment is wet like the operation field, because then the adhesion force is lower. Improvements of our mechanical model will be to assemble the columns on rails so that you could easy reconstruct the length of the free prepared vagal nerve.

Within the electrical characterization the results of the impedance spectroscopy showed that the C-electrode and the designs of the polyimide electrode had higher impedance like the V3-electrode. Additionally, the simulations confirmed that the tripolar electrode had the most selective and highest electrical field and different electrode designs generate different field strength to stimulate the nerve. Earlier research demonstrated with a direct application of the electrode around the nerve the stimulation results will be the best [5]. Although the V3-electrode has lower impedance than the C-electrode and the polyimide electrode, the higher impedance of the C-electrode and the electrode designs of the polyimide electrode are negligible because finally the C-electrode and the polyimide electrode insure through their direct stimulation at the nerve better impedance and so a better stimulation. To sum up, the electrode geometry and design is crucial for the best stimulation results of the vagal nerve. Our mechanical model could even reduce animal experiments for testing electrodes and raise the quality standard of developing cuff-electrodes for the vagal nerve. With the usage of our mechanical model we could prove and measure the high safety of our electrode in human application with mechanical and electrochemical parameters. It could be useful to characterize the electrodes using the mechanical model in a wet environment and to modify the measurement setup with a pressure sensor [6]. In the next step we want to characterize the maximum stress limits of a nerve with the help of animal experiments in the pig to improve our mechanical model. Also we will take in hand further improvements and automations of our mechanical model to construct a realistic and useful tool for development of electrodes.

Acknowledgement

The authors gratefully acknowledge the valuable assistance of the technicians in the workshop of inomed, especially Wolfgang Heer. We wish to express our thanks to the Laboratory for Sensors, IMTEK, University Freiburg.

Bibliography

[1] Ulmer, C., et. al.: Impact of continuous intraoperative neuromonitoring on autonomic nervous system during thyroid surgery, *Head Neck. 2011*

[2] Plachta, D.T., et. al.: Detection of baroreceptor activity in rat vagal nerve recording using a multi-channel cuff-electrode and real-time coherent averaging, *Conf Proc IEEE Eng Med Biol Soc. 2012*

[3] Jonas, J., et. al.: Signal evaluation of continuous vagal nerve stimulation for recurrent laryngeal nerve protection in thyroid surgery, *Zentralbl Chir. 2010*

[4] Joint project: Continuous intraoperative neuromonitoring as a microtechnological navigation instrument for surgical procedures with subproject of medical and scientific investigations in the minor pelvis (IKONA).BMBF Project. FKZ:01EZ0723

[5] Koch, K.P., et. al.: Intraoperative neural electrode for continuous monitoring of nerve function, *IFMBE Proceedings Vol. 25,* Trier, 2009

[6] Durand, D.M. et. al.: Measurement of external pressures generated by nerve cuff electrodes, *IEEE T Rehabil Eng Vol. 8, NO.1, 2000*

Expected Effects of Auricular Vagus Nerve Stimulation in Dystonia

Stefan Kampusch[1], Eugenijus Kaniusas[1], Jozsef Constantin Széles[2]

[1]Institute of Electrodynamics, Microwave and Circuit Engineering, Vienna University of Technology, Austria
[2]University Clinic for Surgery, Vienna General Hospital, Medical University Vienna, Austria

stefan.kampusch@tuwien.ac.at

Abstract: *Punctual electrical stimulation of the auricular branch of the vagus nerve is a potentially effective, minimal-invasive treatment in primary dystonia. This is due to electrical stimulation effects on brain structures involved in the genesis of dystonia. Preliminary experimental data from stimulation with fixed patterns of three vagal points in the auricle reveals significant improvements in motility in cervical dystonia. Based on theoretical considerations, specific stimulation patterns are proposed here which account for the identified signal transduction pathways, neural plasticity and adaptation processes.*

Keywords: *Vagus Nerve Stimulation, Neuromodulation, Adaptation, Cervical Dystonia, Electromyography*

Introduction

Dystonic symptoms (ICD-10 G24) such as torticollis and retrocollis are observed as abnormal, involuntary and sustained contractions of cervical muscles. As an extrapyramidal, hyperkinetic movement disorder the main focus of dysfunction is located in the so called cortico-striatal-pallidal-thalamic-cortical (CSPTC) circuit (Fig. 1) [1], [2]. However, the pathophysiology of primary cervical dystonia (CD) is not fully understood yet, leading to only symptomatic treatments in clinical practice, such as botulinum toxin injections often associated with highly impaired motility of the patient [3]. Deep brain stimulation of CSPTC structures was proven to alleviate dystonic symptoms [2]. Besides these established methods, vagus nerve stimulation may be an asset in treating such movement disorders, provided the corresponding encouraging evidence in the invasive stimulation of the left cervical vagus nerve [4]. In order to avoid the drawback of highly invasive surgical procedures, punctual auricular vagus nerve stimulation (AVNS) may be an effective treatment [5]. This is supported by brain activation studies for transcutaneous AVNS [6] as well as by AVNS-based alleviation of symptoms in Parkinson's disease (unpublished data).

Methods

Two major signal transduction pathways may be involved in modulating the symptoms of CD (torticollis and retro-

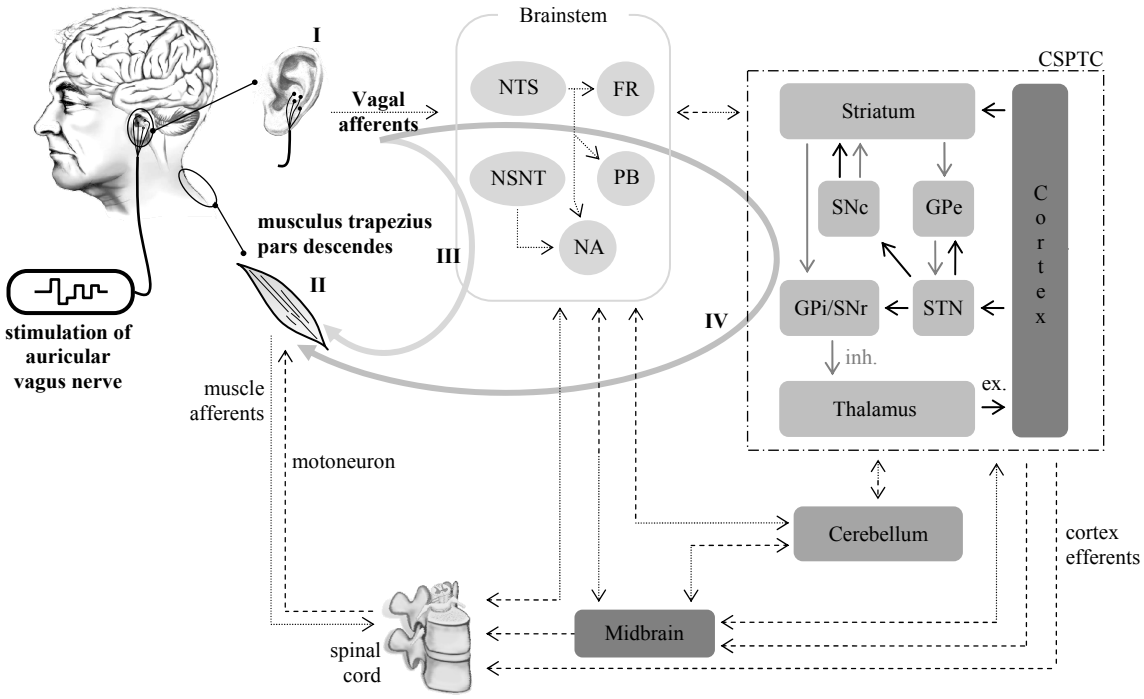

Figure 1: Schematic stimulation setup with affected structures and signal transduction pathways [1], [2], [7]. I – stimulation region; II – affected muscles; III – projection from the auricle to brainstem structures with direct feedback to the considered muscles; IV – projections of the brainstem to the cortico-striatal-pallidal-thalamic-cortical circuit (CSPTC). NTS – nucleus tractus solitarii; NSNT – nucleus spinalis nervi trigemini; FR – formation reticularis; PB – parabrachial nucleus; NA – nucleus ambiguus; SNc,r – substantia nigra compacta, reticularis; GPi,e – globulus pallidus internus, externus; STN – sub-thalamic nucleus; inh. – inhibition; ex. – excitation.

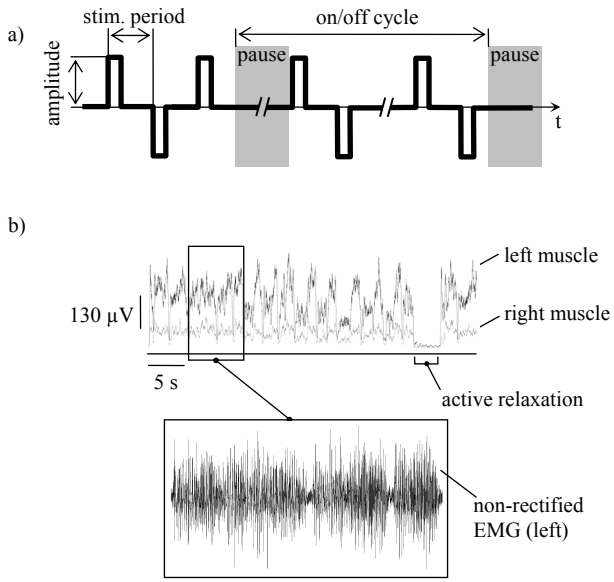

Figure 2: Schematic stimulation pattern with electromyography (EMG) signals from the left (black) and right (grey) musculus trapezius. (a) Fixed stimulation pattern. (b) Rectified EMG with zoomed raw data (left muscle).

collis). The corresponding symptoms include the involuntary activity of cervical muscles and especially of the musculus trapezius pars descendes (Fig. 1, see II).
The stimulation of vagal afferents (Fig. 1, I) in the auricle is forwarded via the ganglion jugulare to the two sensory brainstem nuclei of the vagus nerve, i.e. the nucleus tractus solitarii (NTS) and the nucleus spinalis nervi trigemini (NSNT) [8]. A possible direct feedback to the musculus trapezius (Fig. 1, III) may be established via afferent projections from the NSNT to the nucleus ambiguus [1]. A second pathway (Fig. 1, IV) is build by projections of the formatio reticularis (FR) and the parabrachial nucleus to CSPTC, cerebellum and midbrain structures. This pathway modulates the complex control loops therein and thus the function of the motor cortex [1], [9]. Finally, pyramidal (gyrus praecentralis) and extrapyramidal (CSPTC, midbrain, FR) efferents are send to the muscles.
The minimally-invasive AVNS is mediated via a small, wearable stimulation device P-Stim (Biegler GmbH, Austria). The P-Stim stimulates three vagally innervated regions of the auricle via inserted needles. The stimulation patterns comprise mono-phasic voltage impulses with changing polarity (Fig. 2a). The stimulation rate is 1Hz, the impulse amplitude 4V, the impulse duration 1ms, and the on/off cycle is 3/3 hours. AVNS was applied for about one month on one female patient (49 years) who has suffered from CD for about three years and was resistant to any other therapy. For controlling aims, muscle activity at the left and right musculus trapezius was assessed after this AVNS therapy via electromyography (EMG) using a MP36 acquisition system (BIOPAC Systems Inc., USA).

Results

Preliminary outcome of the AVNS therapy showed significant subjective improvement in motility of the patient with CD. A typical EMG is shown in Fig. 2b with residual and non-symmetric contractions of the left and right musculus trapezius.
However, our experimental evidence and the discussed transduction pathways (Fig. 1) indicate that therapeutic effects are subjected to significant neural plasticity in the brain. Likewise, the brain adapts to almost non-varying stimulation patterns, which disadvantageously diminishes therapeutic effects over extended periods of time.

Discussion

The presented investigations give novel evidence that AVNS is a possible alternative treatment for CD. However, we expect that adopted stimulation patterns and their variability in the course of the stimulation may even overcome adaptation processes in the brain and thus may significantly fortify therapeutic effects. Initial stimulation amplitude should be appropriate to produce comfortable, tingling sensation and thus to excite (only) thick afferent vagal nerve endings. On the other hand, varying stimulation frequency and/or pulse width can be expected to overcome adaptation processes and to maintain therapeutic effects in CD during long-term stimulation. Future studies will involve AVNS applications in CD (or other extrapyramidal movement disorders) with the proposed dynamics of the stimulation patterns, aimed at balanced and reduced non-symmetric muscle contractions.

Bibliography

[1] Kandel, E.R., Schwartz, J.H. and T.M. Jessell: *Principles of Neural Science*, McGraw-Hill, 2000

[2] Oluigbo, C.O. and A.R. Rezai: Addressing Neurological Disorders with Neuromodulation, *IEEE Transactions on Biomedical Engineering*, vol. 58, pp. 1907-1917, 2011

[3] Delnooz, C.C.S. and B.P.C. van de Warrenburg: Current and Future Medical Treatment in Primary Dystonia, *Therapeutic Advances in Neurological Disorders*, vol. 5, pp. 221–240, 2012

[4] Amar, A.P., Levy, M.L. et. al.: Vagus Nerve Stimulation, *Proceedings of the IEEE*, vol. 96, pp. 1142-1151, 2008

[5] Szeles, J.C. and G. Litscher: Objectivation of Cerebral Effects with a New Continuous Electrical Auricular Stimulation Technique for Pain Management, *Neurological Research*, vol. 26, pp. 797-800, 2004

[6] Frangos, E., Ellrich, J. et. al.: Activation of Human Vagus Nerve Afferent Projections via Electrical Stimulation of External Ear: fMRI Evidence, *42nd Annual Meeting of the Society for Neuroscience*, New Orleans, 2012

[7] www.alzheimer-forschung.de, stefan.ganz.priv.at

[8] Napadow, V., Edwards, R.R. et. al.: Evoked Pain Analgesia in Chronic Pelvic Pain Patients Using Respiratory-Gated Auricular Vagal Afferent Nerve Stimulation, *Pain Medicine*, vol. 13, pp. 777-789, 2012

[9] Dietrich, S., Smith, J. et. al.: A Novel Transcutaneous Vagus Nerve Stimulation Leads to Brainstem and Cerebral Activations measured by functional MRI, *Biomedizinische Technik*, vol. 53, pp. 104-111, 2008

DYNAMIC ECHOMYOGRAPHY SHOWS THAT FES IN PERIPHERAL DENERVATION DOES NOT HAMPER MUSCLE REINNERVATION

Zanato R[1], Stramare R[1], Boato N[2], Zampieri S[2,3], Kern H[3,4] , Marcante A[5], Masiero S[5], Carraro U[2]

[1]Radiology, Dept. of Medicine, University of Padua, Italy
[2]Laboratory of Translational Myology, Dept. Biomedical Sciences, University of Padua, Italy
[3] Ludwig Boltzmann Institute of Electrical Stimulation and Physical Rehabilitation,
[4]Dept. Physical Medicine and Rehabilitation, Wilhelminenspital Wien, Austria
[5]Physical Medicine and Rehabilitation, Dept. Neurosciences, University of Padua, Italy

ugo.carraro@unipd.it

Abstract: *Permanent denervated muscles were evaluated by ultra sound (US) to monitor changes in morphology, thickness, contraction-relaxation kinetics and perfusion. In a case of monolateral lesion of the sciatic nerve (due to a surgical neurotomy during the removal of hyperplastic lifenodes in the pelvis) morphology and ultrasonographic structure of the denervated muscles changed during a period of electro stimulation from a pattern typical of complete denervation-induced muscle atrophy to a pattern which might be considered "normal" when detected in an old patient. Despite the higher than normal energy of the delivered electrical stimuli of Vienna home-based Functional Electrical Stimulation (h-b FES) the muscles shown electromyografic and ultrasonographyc signs of re-innervation during the years of training.*

Keywords: *Reinnervation, skeletal muscle, FES*

Introduction

Beside standard clinical RISE testing [1,2], in the Rise2-Italy project we are submitting the enrolled patients with peripheral muscle denervation to a new protocol of quantitative ultrasonography (we named it Dynamic Echomyography to stress the dynamic components of the analyses [3-5]) to evaluate changes in Tibialis Anterior (TA) muscle undergoing home-based electric stimulation according to the Vienna strategies [1,2]. Gross morphology and ultrasonographic structure, thickness, dynamic properties of either voluntary or electrical stimulation-induced contraction-relaxation cycle, and short-term/long-term modifications of the arterial perfusion in response to voluntary and electrical stimulation-induced contractions were monitored. We are, indeed, extending to these patients the training strategies designed in collaboration with the Ludwig Boltzmann Institute of Electrical Stimulation and Physical Rehabilitation, Department of Physical Medicine and Rehabilitation, Wilhelminenspital Wien, Austria that designed and implemented the new standard for long-term muscle denervation by means of the European Project RISE [1,2].

Here we report the case of Rise2-Padua-BN (Female; 27/03/1962) which (due to an injury to the sciatic nerve after surgical removal of a pelvic mass, 05/10/2006), presented loss of sensitivity at the anterior-medial aspect of the leg and the dorsal medial aspect of the foot, lack of elevation of the right leg and no sign of muscle activation to attempts of dorsiflexion of the right foot.

Figure 1: Clinical appearance of the denervated and innervated legs. Self-evident muscle atrophy of the right leg.

Methods

Electromyography and Dynamic Echomyography, according to [3-5], were performed to evaluate ecogenicity, thickness, contraction/relaxation kinetics, perfusion and denervation/reinnervation of leg muscles before and during h-b FES [1,2].

Results

Rise2-Padua-BN: EMG (25/10/2006): … at rest spontaneous activity is not present at the tibialis anterior and extensor digitorum longus muscles of the right leg, nor activity at attempts of voluntary movements. No motor response is derivable from the right tibialis n. to stimulation of the lateral popliteal nerve at the knee. No motor response can be derived from the right pedidius muscle to stimulation of the lateral popliteal nerve at knee and ankle. In 2007 the subject started a 5 day-per-week treatment with electrostimulation for denervated muscles of the right Tibialis Anterior by triangular exponential currents (pulse duration 150 ms, intensity 25 mAmp, pause 300 msec) using a Neuroton (Philips) stimulator and then a Muscular Stimulator for denervated muscles DEMITALIA Model SM1, Leinì (TO) Italy (pulse duration 50 ms, intensity 28 mAmp, pause 2000 msec).

	October 8, 2008		April 7, 2009		September 10, 2009	
	24 months from n. lesion		30 months from n. lesion		35 months from n. lesion	
	12 months of h-b FES		18 months of h-b FES		23 months of h-b FES	
	right	left	right	left	right	left
Proximal third	14	21	14	19	15	20
Medial third	10	24	14	23	16	22
Distal third	11	15	12	16	12	16
EMG	EMG right leg 25.2.2008 Compared to 21.7.2007: Reinnervation of thigh posterior muscles. No reinnervation of T.A.		EMG right leg 5.9.2009 Compared to 25.2.2008: Normal C.V. of tibial nerve. Abnormal reinnervation of T.A. by tibial nerve axons			
In electromyography of 18.10.2010 "The picture is slightly improved compared to the previous 9.9.2009 as are observed in some parts of the tibialis anterior and extensor digitorum longus muscles signs of motor activity (action potentials) in response to attempts of foot and toes extension. There are in the muscles of the antero-external loggia motor unit potentials in response to foot flexion, as result of abnormal innervation by the tibial nerve.						

Figure 2: Follow-up of TA muscle thickness (mm) of Rise2-N.B. patient.

EMG (18/10/2010) right lower limb: Signs of neurogenic pain (mild to medium) to the gluteus medius, gluteus maximums and biceps femoris muscles. Compared to the previous EMG assessment, minimal signs of motor activity are observed in some points of tibialis anterior and extensor digitorum longus muscles that responded with minimal extension of the foot and toes to attempts of voluntary movements. At attempts of foot flexion motor unit potentials are recorded in the muscles of the antero-external loggia, as the result of abnormal reinnervation by fibers of the tibial nerve. The subject is continuing since 5 years the ES treatment and at 25/02/2013 she is able to slightly dorsi-flect the denervated right foot by triangular impulses, using the Muscular Stimulator for denervated muscles DEMITALIA Model SM1.

Discussion

In this case of monolateral sciatic lesion, ultrasonographic structure of the denervated muscle changed during the period of stimulation. Thickness improved more in the middle third of the denervated muscle, reaching almost the same value as the contralateral innervated muscle (Figure 2). The denervated muscles analysed with Echo Doppler showed at rest a low resistance arterial flow that became pulsed during and after electrical stimulation. Despite the higher than normal energy of the delivered electrical stimuli of Vienna h-b FES the muscles shown echomyographic signs of re-innervation during the training (Fig. 2). Dynamic Echomyography shows that among the hyperechogenic atrophic denervated T.A., hypoechogenic stretches of innervated muscle fibers contracts during both volitional and ES attempts of foot extension and dorsiflexion. See Movie in BAM On-Line at: http://www.bio.unipd.it/bam/bam.html.

This case study demonstrates: 1. usefulness of Dynamic Echomyography in the follow-up; 2. the positive effects of h-b FES of denervated/reinnervating muscles; and 3. evidence that h-b FES does not hamper nerve growth and synaptogenesis.

Bibliography

[1] Kern, H., Carraro, U., et al., Home-based Functional Electri-cal Stimulation (h-b FES) recovers permanently denervated muscles in paraplegic patients with complete lower motor neuron lesion, *Neurorehab. Neur. Rep.*, vol. 24, pp. 709-721, 2010

[2] Kern, H., Hofer, C., et al., European Project RISE: Partners, protocols, demography, *Basic Appl Myol/ European Journal of Translational Myology*, vol. 19, pp. 211-216, 2009

[3] Zanato, R., Martino, L., Stramare, R., Functional Echomyography of the human denervated muscle: first results, *European Journal Translational Myology - Basic Applied Myology*, vol. 21, pp. 3-29, 2011

[4] Pillen, S., Skeletal muscle ultrasound. *European Journal of Translational Myology/Basic Applied Myology*, vol. 20, pp. 145-156, 2010

[5] Zanato, R., Martino, L., et al., Functional Echomyography: thickness, ecogenicity, contraction and perfusion of the LMN denervated human muscle before and during h-b FES. *European Journal of Translational Myology/Basic Applied Myology,* vol. 20, pp.33-40, 2010

INVESTIGATING THE INFLUENCE OF 3D CELL MORPHOLOGY ON NEURAL RESPONSE DURING ELECTRICAL STIMULATION

Jörg Encke[1], Heval Benav[2], Paul Werginz[1], Eberhart Zrenner[2] and Frank Rattay[1]

[1]Institute for Analysis and Scientific Computing, Vienna University of Technology, Austria

[2]Institute for Ophthalmic Research, University Hospital Tuebingen, Germany

e1127969@student.tuwien.ac.at

Abstract: *Neuronal compartment models are a basic and often used method to investigate the effect of electrical stimulation on the cell. As the outcome of the model heavily depends on the cells morphology and its position relative to the electrode, a realistic representation of the cell structure and its variations is of great importance. A method is presented which allows the quick and easy creation of a three dimensional neuron morphology on the basis of a single two dimensional image. Basic properties of this morphology like local diameters, cell size or the amount of branching can easily be changed.*

Keywords: *electric stimulation, neuron morphology, computer simulation, compartment model*

Introduction

Many modelling studies of external cell stimulation are concerned with recruitment order and how this order depends on the shape of target neurons and their position relative to the stimulating electrode. From the activation function concept it is known that axons are the most excitable elements and therefore they are in most cases the first candidates to be stimulated [1]. The following features are important indicators for spike initiation sites: (i) spatial change of the electrical field, (ii) large fibre diameter and (iii) strong fiber curvature.

The distance of the neuronal segment to the tip of a microelectrode and the curvature of the neuron are examples where thresholds of different morphologies can essentially differ. One example where this might be of importance are electrically stimulated skin receptors where strong changes of the electric field are located below the edges of surface electrodes. Because of the curvature feature (iii), receptors in the hairy and glabrous skin are stimulated in a different way as the course of the nerve fibers is sinuous and winding in glabrous skin, but straight and stretched in the hairy skin (comp Fig. 5. in [2]).

Another example are microelectrodes in retinal implants where the high resolution needed for visual perception requires relatively small electrode dimensions and close proximity to the cells [3] [4]. Three dimensional cell structures are normally acquired by applying one of the several 3D tracing methods. While creating very realistic morphologies these methods are time consuming and require a high amount of expertise and laboratory equipment. When building a neuron compartment model, one is faced with the question whether morphological variations in the stimulated neuron population might influences the outcome of the model or not.

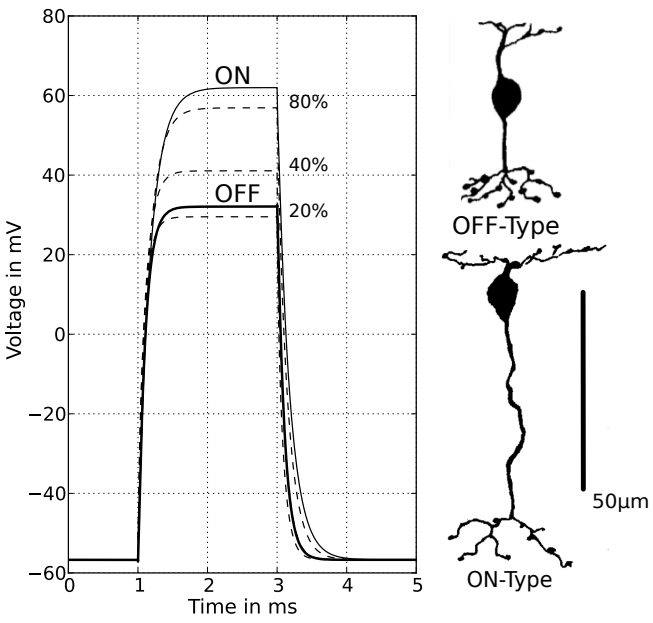

Figure 1: The same electrical stimulation results in a higher depolarization of the synaptic terminals in On bipolar cells than in OFF type cells. The axon length of the ON type cell was stepwise reduced to 80%, 40% and 20% of its original size resulting in a decrease in depolarization.

Methods

Several sources on the internet provide a variety of three dimensional neuron geometries. But these databases still only cover a relatively small amount of different neuron types and seldom a greater number of neurons of one type. In many cases one either has to settle for completely artificial morphologies or 2D-geometries based on images gained by immunostaining or similar methods.

We developed a program in Matalab which allows us to generate a 3D cell geometry based on a 2D image (publication in preparation). For this, the position and size of the compartments is defined on basis of the 2D image. The missing third dimension is then computed using confined, normally distributed random values. This method enables us to create a variety of different cell morphologies while keeping the characteristics included in the 2D image. This makes it

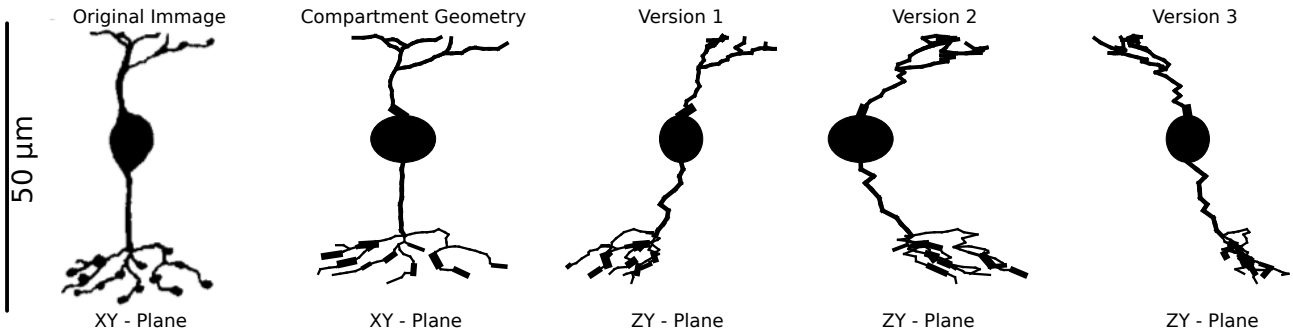

Figure 2: Examples for a randomized 3D morphology of a type 2 OFF retinal bipolar cell. (Image taken from [5]) Depicted are, starting from left, the original image, the simplified compartment geometry and three different versions of the randomized model component.

possible to quickly analyze the impact a change in a certain feature would have. The approach is demonstrated by using a passive model of the electrically stimulated cone bipolar cell which is found in the retina. The electrical potential during stimulation was calculated using the finite element method (FEM). In a second step the cells membrane potential was calculated using a compartment model implemented in Matlab [6].

Results

Retinal bipolar cells (BPC) and their structure have been studied thoroughly [5] [7] but little 3D-data has been made available. In spite of their very simple structure, 9-12 different BPC have been identified in the mammalian retina. To investigate the impact of different synaptic and dendritic branching, multiple cell structures with a randomized third dimension where generated and only little change in the model outcome was found. Figure 2 shows the structure of a typical BPC and three variations of the randomized third dimension. Variations of the axon diameter resulted in slightly slower depolarization for thicker axons. While a change in soma size by +20% to -20% did not result in any changes. The main morphological difference in between BPC types is the axon length and with that, the location of branching in the inner nuclear layer [5]. The shorter cells being OFF type and the longer ON type cells. Figure 1 shows the difference in the outcome of a ON and OFF type cell model. The length of the ON type axon was stepwise reduced. At 20% of it's original size, the model output closely matched that of an OFF type cell resulting in the conclusion that the difference in activation is caused by the different axon length. This might be of interest for the development of retinal implants where a selective activation of ON and OFF cells is desirable.

Discussion

The influence of morphological changes on the response of an electrically stimulated retinal bipolar cell is discussed as an example for the approach of reconstructing 3D cell geometries on the basis of a 2D image. In this example, the difference in depolarization of synaptic terminals between ON and OFF type cells is found to be caused by the difference in axon length. Other structural variations have also been considered and found to have only a minor impact on the model outcome. While only demonstrated on one type of cell this approach should offer a quick and easy way to qualitatively analyze the influence of morphological parameters or variations found in 2D representations of any cell.

Bibliography

[1] F. Rattay, "The basic mechanism for the electrical stimulation of the nervous system.," *Neuroscience*, vol. 89, pp. 335–346, Mar 1999.

[2] V. Provitera, M. Nolano, A. Pagano, G. Caporaso, A. Stancanelli, and L. Santoro, "Myelinated nerve endings in human skin.," *Muscle Nerve*, vol. 35, pp. 767–775, Jun 2007.

[3] D. Palanker, A. Vankov, P. Huie, and S. Baccus, "Design of a high-resolution optoelectronic retinal prosthesis.," *J Neural Eng*, vol. 2, pp. S105–S120, Mar 2005.

[4] A. Butterwick, P. Huie, B. W. Jones, R. E. Marc, M. Marmor, and D. Palanker, "Effect of shape and coating of a subretinal prosthesis on its integration with the retina.," *Exp Eye Res*, vol. 88, pp. 22–29, Jan 2009.

[5] T. Euler and H. Wässle, "Immunocytochemical identification of cone bipolar cells in the rat retina.," *J Comp Neurol*, vol. 361, pp. 461–478, Oct 1995.

[6] H. Benav, *Modelling effects of extracellular stimulation on retinal bipolar cells*. PhD thesis, Eberhard-Karls-Universitaet Tuebingen, 2012.

[7] K. K. Ghosh, S. Bujan, S. Haverkamp, A. Feigenspan, and H. Wässle, "Types of bipolar cells in the mouse retina.," *J Comp Neurol*, vol. 469, pp. 70–82, Jan 2004.

Author Index

P

Q

R

S

T

U

V

W

X

Z

Official Journal of the Vienna FES Workshop:

Artificial Organs

Edited by:
Paul S. Malchesky, D. Eng.
http://www.wiley.com/bw/journal.asp?ref=0160-564X

Sponsors and Exhibitors (in alphabetic order):

DR. SCHUHFRIED MEDIZINTECHNIK GMBH

Dr. Schuhfried Medizintechnik GmbH
Van Swieten-Gasse 10
A-1090 Wien
Austria

GRAZ

Graz
www.graz.at

Das Land Steiermark

Land Steiermark
www.steiermark.at

MED EL

Medel
Fürstenweg 77a
6020 Innsbruck
Austria

ottobock.

Otto Bock Healthcare Products GmbH
Kaiserstraße 39
1070 Wien, Austria